UNIVERSITY OF CINCINNATI

DATE: ***February 26, 2003***

I, ***PENPAN SAIYASOMBATI*** **,**

hereby submit this as part of the requirements for the degree of:

DOCTOR OF PHILOSOPHY

in:

PHARMACEUTICAL SCIENCES

It is entitled:

MATHEMATICAL MODEL FOR PREDICTING PERCUTANEOUS ABSORPTION OF FRAGRANCE RAW MATERIALS

Approved by:

Gerald Kasting, Ph. D., Chair

Frank Gerberick, Ph. D.

Latif Shenouda, Ph. D.

Marty Visscher, Ph. D.

Randall Wickett, Ph. D.

MATHEMATICAL MODEL FOR PREDICTING PERCUTANEOUS ABSORPTION OF FRAGRANCE RAW MATERIALS

A dissertation submitted to the

Division of Research and Advanced Studies
of the University of Cincinnati

in partial fulfillment of the
requirements for the degree of

DOCTOR OF PHILOSOPHY

in the Division of Pharmaceutical Sciences
of the College of Pharmacy

2003

by

Penpan Saiyasombati

B.S. in Pharmacy
Chulalongkorn University, Bangkok, Thailand, 1995

Committee Chair: G. B. Kasting, Ph.D

ABSTRACT

Due to their potential for inducing contact allergy if used improperly, fragrances are carefully assessed for dermal safety prior to incorporation into cosmetic products. Currently, there is no accurate tool for estimating the skin absorption rates and tissue concentrations subsequent to topical exposure of fragrances. This report describes an improved method to estimate the absorption and evaporation of fragrance ingredients from skin, based on their physico-chemical properties. This was accomplished using a first-order kinetic approach expected to be applicable for small topical doses. The rate constants for each compound are functions of temperature T, surface airflow v, and three physico-chemical properties: vapor pressure $P_{vp,}$ molecular weight MW and lipid solubility S_{lip}. The latter is taken to be the solubility of *n*-octanol, expressed as the product of octanol/water partition coefficient K_{oct}, and water solubility S_w. Three kinetic models were developed and tested with published fragrance evaporation data on human skin. One of these models was the one-compartment model, in which all dissipation occurs from a skin compartment that rapidly incorporates a topically-applied ingredient. Two alternative models explicitly consider the vehicle layer present in the early stages post-application. Skin disposition of fragrance ingredients in a controlled *in vivo* study could be satisfactorily correlated with key physico-chemical properties. All three models provided an adequate description of the evaporated fractions. However, the evaporation rate profiles of fixed fragrances were better described by the two-compartment models which yield a biexponential decay. The kinetic models were also tested with the *in vitro* absorption and evaporation data for benzyl alcohol. Modified Franz diffusion cells fitted with a vapor trap were used to obtain these data. Airflow over the skin surface was controlled in the experiment and accounted for in the model. A linear

dependence between airflow and evaporation rate constant(s) was found over the working range of the system, 10-100 mL/min. All three models satisfactorily correlated cumulative absorption and evaporation results. Nevertheless, further details of the evaporation and absorption profiles could be described by means of two-compartment models. Further development of this work may lead to a useful model for dermal exposure assessment for contact allergens.

ACKNOWLEDGEMENTS

I wish to express love and thanks to Dr. Jerry Kasting for seeing me through my PhD. He has been a constant source of inspiration. His guidance, patience and support are always appreciated. I want to thank Dr. Randall Wickett for giving me the opportunity to join UC cosmetic science program and for teaching me very useful knowledge of skin sciences. I wish to acknowledge with great thanks Dr. Latif Shenouda, Dr. Marty Visscher, and Dr. Frank Gerberick for their invaluable inputs and involvement in my project. I thank the University of Cincinnati for the Distinguished Dissertation Fellowship in the year 2002. I also acknowledge with thanks the financial support on my project from the Procter and Gamble Company's International Program for Animal Alternatives, the University of Cincinnati, and NIOSH grant 1 RO1 OH007529-01. I express my appreciation to Dr. Johannes Nitsche for his guidance in UNIFAC/UNIQUAC calculations and his help during my stay in Buffalo, NY. I would like to thank the following people for providing their technical expertise in the development of the vapor trapping methodology: Dr. Pete Rodriguez, Mike Burchfield, Cindy Eddy, and Christa Pelfrey. Thanks also to Dr. Ray Guerry for bringing the IFF published data to our attention. I am grateful to Bill Pickens for everything he did for me in the past few years. Special thanks to Donna Taylor and Marcie Silver for their friendly assistance. I also want to thank all my friends who made my stay in Cincinnati a pleasant and memorable experience. Among these are Amit, Arjun, Ehab, Eileen, Fair, Hemali, John, Mukesh, Namrata, Pik, Priya, Sunila, Varsha, and Vic. Finally, my never-ending thanks and love to my parents and my brother. Without their encouragement, support and teaching, I would not be the person I am today…

TABLE OF CONTENT

LIST OF TABLES

PAGE

LIST OF FIGURES

PAGE

LIST OF SYMBOLS

P_{vp}	=	vapor pressure
MW	=	molecular weight
K_{oct}	=	octanol-water partition coefficient
S_{oct}	=	octanol solubility
S_w	=	water solubility
T	=	temperature
v	=	airflow rate
D	=	diffusivity
k_n	=	first-order rate constants
f_{evap}	=	evaporated fraction
f_{abs}	=	absorbed fraction

CHAPTER 1

INTRODUCTION

All cosmetic and personal care products are formulated to satisfy certain consumer needs. Some of their ingredients perform specific physical functions, such as cleansing or moisturizing, while others play more subjective roles in helping the product achieve consumer satisfaction. Fragrances are among the latter ingredients. They are extensively used in the formulations for either odor masking or aesthetic purposes. Multiple scented products are used on a daily basis, making exposure to fragrances unavoidable. Occupational exposures to fragrances are also common.

FRAGRANCE CHEMISTRY

Each fragrance is a complex mixture of chemicals, which is carefully blended to produce specific scents. These chemicals are so called "perfume raw materials" or "fragrance ingredients". These terms can be used interchangeably. Some fine fragrances may contain as many as 6,000 individual components. Based on their molecular structures, fragrance raw materials fall into three broad categories: aliphatics, benzenoids and terpenoids.[1] Aliphatic compounds are straight-chain organic chemicals. They can be subclassified into C_6-C_{12} alcohols, C_6-C_{12} aldehydes, esters, ketones and lactones. Benzenoids are compounds whose benzene rings are substituted with some functional groups. Terpenoids are compounds that share a common 5-carbon unit, known as "isoprene". Different numbers of the isoprene unit account for different scents of terpenoids. Representative compounds for each type of fragrance raw materials are shown in Figures 1.1-1.3.

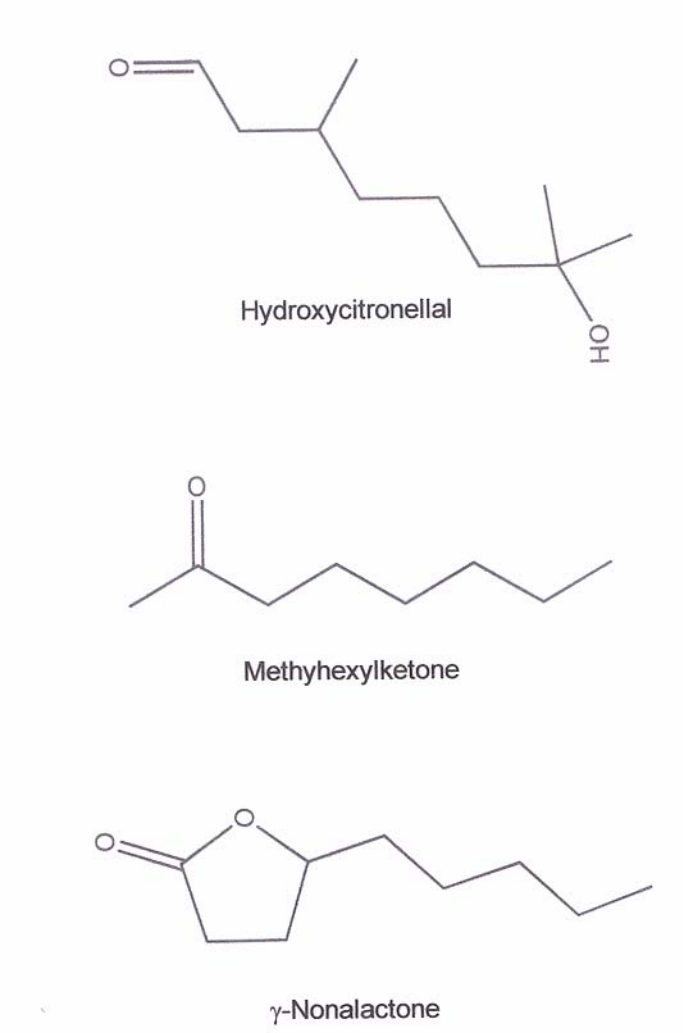

Figure 1.1. Aliphatic fragrance raw materials.

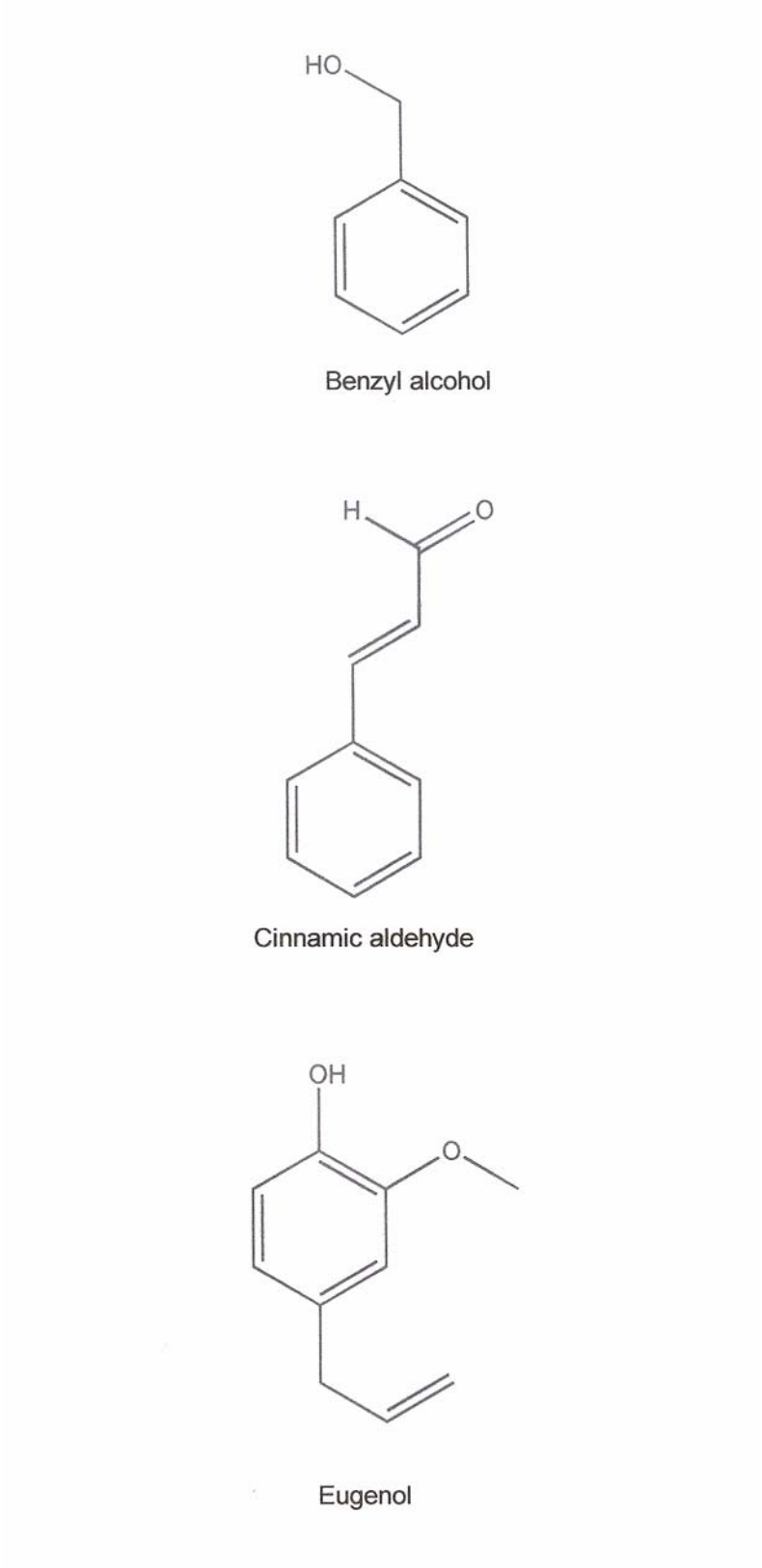

Figure 1.2. Benzenoid fragrance raw materials.

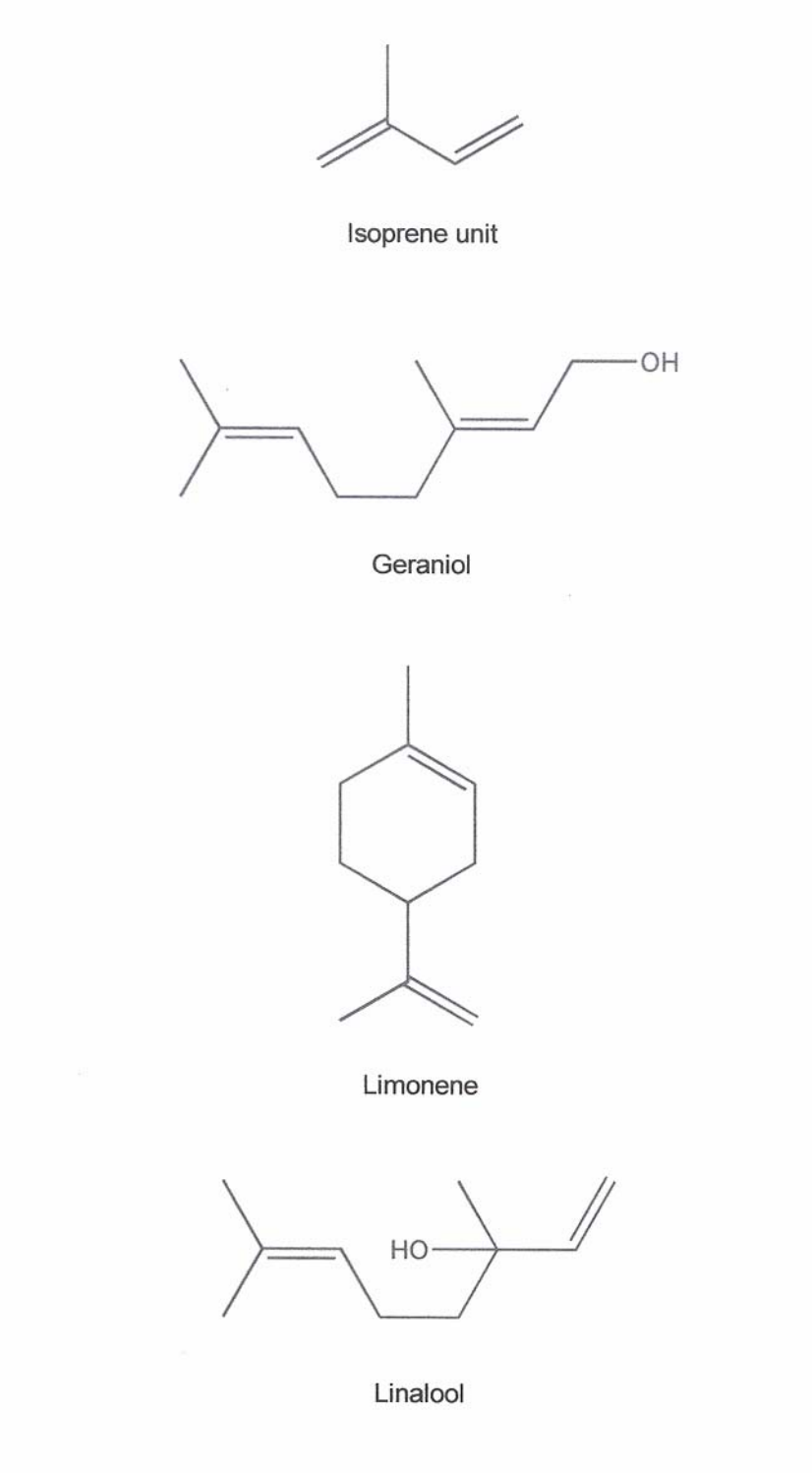

Figure 1.3. Terpenoid fragrance raw materials.

These raw materials can be obtained naturally or synthetically. The natural sources of aromatic chemicals are either plants or animals. Most synthetic raw materials are derived from chemical reactions using crude oil or turpentine oil as the starting materials. The advantages of using synthetic compounds over using natural materials include lower cost, better quality and less supply problems. However, the synthetic compounds, which are mostly single molecules, never perfectly match the multi-component natural ingredients.

Each fragrance has three layers of smell referred to as "notes". The top note, made of the most volatile materials, is the first element sensed when a fragrance is applied. Citrus notes such as limonene are common top note chemicals. The middle (body, heart) note is composed of somewhat less volatile materials. These components come more into play after the top notes have dissipated. Typical middle note ingredients are floral scents. The bottom (end) note is made from the least volatile materials, and it is the longest lasting portion of the fragrance. The bottom note chemicals are often used as fixatives in the fragrance formulation in order to prolong the life and the continuity of the fragrance odor.

FRAGRANCE CONTACT ALLERGY

The most common adverse reaction due to fragrances is contact allergy.[2] Allergic contact dermatitis to fragrance ingredients falls into type IV or delayed-type hypersensitivity reaction, which involves the T-cell mediated immune response. The development of this type of reaction requires two distinct phases: induction and elicitation. In the induction phase, a small molecule contacts and penetrates through the stratum corneum into the viable epidermis, where it

complexes with skin protein. The complex is internalized by antigen-presenting cells in the skin (such as Langerhans cells), then processed and presented along with Class II MHC molecules to T lymphocytes. The activated T cells divide and differentiate into sensitized T cells.

In the elicitation phase, a subsequent exposure to the same inducing chemical activates the sensitized T cells, causing the release of various cytokines (i.e. IL-2, IFN-γ, MIF, TNF-β). The net effect of these cytokines is to cause an accumulation and activation of macrophages, which release lytic enzymes that cause localized tissue destruction. Upon reexposure, the allergenic chemical must first bind to skin protein and be appropriately expressed by the Langerhans cells in the skin to the sensitized T cells before it can activate these cells.

Fragrance raw materials are relatively low molecular weight, highly volatile and have moderate-to-high lipophilicities. These physicochemical properties allow the fragrance ingredients not only to impinge effectively on the olfactory receptors, but also to easily penetrate the skin. From a mechanism standpoint, it is recognized that the potential of fragrance allergens for induction of skin sensitization, as well as for elicitation of clinical manifestation of contact allergy in already sensitized individuals, correlates well with their ability to penetrate the skin and react with skin proteins through their functional groups (i.e. aldehyde, hydroxyl and ketone).

RISK ASSESSMENT FOR FRAGRANCE ALLERGY

It is critical to ensure that existing and newly synthesized fragrance ingredients do not cause allergic contact dermatitis. As aforementioned, the penetration of an allergen into the skin is

required for both the induction and the elicitation of contact allergy. Also, all allergens possess dose-response and threshold characteristics.[3] Thus, the ability to estimate the delivered dose or fraction of the applied dose that will be dermally absorbed is important in skin safety assessment of potential fragrance allergens contained in the products.

Currently, there are several approaches used for predicting dermal absorption of fragrances. The traditional approach is to conduct *in vivo* studies either in animals or in human volunteers. Although this approach seems to be the most accurate way of predicting dermal absorption, it is expensive, time-consuming and involves ethical considerations. Over the past decades, the *in vitro* method has gained recognition as an alternative to the *in vivo* method. Relative to *in vivo*, *in vitro* studies are safer and easier to perform.

For high-risk fragrance allergens (e.g. cinnamic aldehyde) applied in leave-on products, 100% of the applied dose is often assumed for the delivered dose.[4] This assumption is obviously an overestimate for volatile chemicals. Upon application of fragrance-containing products to skin, the higher body temperature aids the volatilization of the fragrance ingredients. Therefore, a substantial portion of the applied dose may evaporate rather than be absorbed into the skin.

In recent years, the percutaneous absorption of selected fragrance ingredients has been evaluated in a number of experiments both *in vitro* and *in vivo*. A summary of the published data is shown in Table 1.1. However, there are thousands of fragrance ingredients that remain unstudied. A number of mathematical models have been developed to extrapolate existing absorption data to unevaluated compounds. Among these models, the prediction method developed by Potts and

Guy[5] appears to be the most widely used for this purpose, since the required input parameters are easily obtained. Potts and Guy have identified, through linear regression analysis, a relationship between skin permeability coefficient, k_p, and the two basic physico-chemical properties– molecular size (which is expressed as the molecular weight) and the octanol-water partition coefficient (a measure of lipophilicity). The permeability coefficient is defined as a ratio of steady-state flux to the concentration of a chemical applied from a large volume of aqueous solution.

The Potts-Guy model is considered to be applicable to chemicals having molecular weight from 18 to 750 Da and a log K_{oct} between -3 and +6. The model focuses on the stratum corneum as the rate-limiting barrier to penetration. The values of the physico-chemical properties of fragrance raw materials fall into the applicable range of the Potts-Guy model. The validity of the Potts-Guy model for fragrance raw materials was demonstrated by Hostynek in 1995. Regression of the observed and calculated permeability coefficients for 24 fragrance ingredients applied from aqueous solution yielded a strong correlation with an r^2 of 0.87.

While the Potts-Guy model may appear to be the obvious choice for predicting skin penetration of fragrance compounds, there are severe limitations to this model that must be addressed. In practice, the amount of perfume ingredients exposed to skin from fragranced products usually falls within the small dose limit where a steady-state is generally not obtained.[6] Furthermore, fragrance ingredients are often not applied from aqueous solutions. Therefore, the commonly used parameter for predicting skin permeability, k_p, in the Potts-Guy model is usually not

Table 1-1. Summary of published data for fragrance absorption.

	Compound	Type of study	Vehicle used	Ref.
1	Acetyl eugenol	e	neat	7
2	AETT[a]	e, h	petrolatum	8
3	AHTN[b]	h, j	ethanol	9
4	Alpha-amyl cinnamic alcohol	e	neat	7
5	Alpha-amyl cinnamic aldehyde	e	neat	7
6	Alpha-hexyl cinnamic alcohol	e	neat	7
7	Alpha-hexyl cinnamic aldehyde	e	neat	7
8	Alpha-methyl cinnamic aldehyde	e	neat	7
9	Anisole	e	butanol, butyl acetate, isophorone, isopropyl myristate, propylene carbonate, toluene	10
10	Benzamide	i	acetone, lotion	11
11	Benzoin	i	acetone, lotion	11
12	Benzophenone	i	acetone, lotion	11
13	Benzyl acetate	i	acetone, lotion	11
		g	neat, ethanol	12
		g	neat, DMSO, ethanol, phenylethanol	13
		e, g	neat	14
14	Benzyl alcohol	g	normal saline	15
		e	neat, butyl acetate, isophorone, isopropyl myristate, propylene carbonate, toluene	11
		e	butanol, butyl acetate, isophorone, isopropyl myristate, propylene carbonate, toluene	10
		e	benzene	16
		e	ethanol, liquid paraffin, propylene glycol, water, cream, lotion, ointment	17
		i	acetone, lotion	11
15	Benzyl aldehyde	e	butanol, butyl acetate, isophorone, isopropyl myristate, propylene carbonate, toluene	10
16	Benzyl benzoate	i	acetone, lotion	11
17	Benzyl propionate	e	neat	7
18	Benzyl salicylate	e	neat	7
19	Cinnamic acid	e, i	acetone	18
20	Cinnamic alcohol	e, i	acetone	18
		e	ethanol	19
21	Cinnamic aldehyde	e	ethanol	19
		e	neat	7
22	Cinnamyl anthranilate	e, i	acetone	18

	Compound	Type of study	Vehicle used	Ref.
23	Coumarin	e, g	ethanol, O/W emulsion	20
		e, f, g	ethanol	7
		e	ethanol	21
		e	ethanol	9
		h	ethanol	22
		h, j	ethanol/water	23
		e, g	ethanol, O/W emulsion	20
24	Diethyl maleate	h, i	acetone, lotion	18
25	Dihydroeugenol	e	neat	7
26	Eugenol	e	neat	7
27	HHCB[c]	h, j	ethanol	23
28	Isoamyl salicylate	e	neat	7
29	Isoeugenol	e	ethanol, liquid paraffin, propylene glycol, water, cream, lotion, ointment	17
		e	neat	7
30	Methyl eugenol	e	neat	7
31	Methyl isoeugenol	e	ethanol, liquid paraffin, propylene glycol, water, cream, lotion, ointment	17
32	Musk ambrette	h	ethanol	24
33	Musk ketone	h	ethanol	24
34	Musk xylol	d, e	isopropyl myristate methanol, O/W emulsion	25
		h	ethanol	24
35	2-Phenylethanol	e	same as Aniline	10
36	Safrole	e, i	acetone	18

a Acetyl ethyl tetramethyl tetralin
b 7-Acetyl-1,1,3,4,4,6-hexamethyl-1,2,3,4-tetrahydronaphthalene
c 1,3,4,6,7,8-hexahydro-4,6,6,7,8,8-hexamethylcyclopenta-2-benzopyran
d *in vitro* studies using hairless guinea pig skin
e *in vitro* studies using human skin
f *in vitro* studies using mouse skin
g *in vitro* studies using rat skin
h *in vivo* studies in human
i *in vivo* studies in monkey
j *in vivo* studies in rat

applicable, since it is a steady-state property. In addition to this, the evaporative loss of ingredients from the skin surface is not accounted for in the Potts-Guy model.

Other predictive models that are presently available are either steady-state models[26] or are transient absorption models based on steady-state data.[27] Neither accurately represents the exposure conditions common to cosmetic and personal care products and neither accounts for evaporation. A more complete model for describing the percutaneous absorption of volatile compounds must express the net effect of two competing processes: evaporation from the skin surface and penetration into the skin. Calculated absorption rates must also reflect the limited quantities of compounds applied to skin under the most common exposure conditions.

There are a number of factors that have significant effects on the extent of percutaneous absorption. Applied dose,[6,28] application site,[29-34] and degree of hydration[35-37] have all been found to affect skin penetration. For volatile chemicals, airflow over the skin surface plays an important role in the volatilization process when transport of vapor across the stagnant air layer (boundary layer) is the rate-limiting step. As the rate of airflow increases, the thickness of the boundary layer decreases and the rate of evaporation increases.[37,38]

The absorption of fragrance ingredients is also dependent upon the vehicle or formulation in which it is contained. In high alcohol-based formulation, e.g., perfumes, colognes, and aftershave products, the evaporation of ethanol increases the relative concentration of the fragrance raw materials, although the fragrance ingredients are also evaporating at the same time. Emulsion systems are widely employed in many types of cosmetics and toiletries. The skin

penetration of some fragrance ingredients applied in an ethanolic vehicle has been found to be significantly different than that following application in an emulsion vehicle.[20,25] The emulsifiers (surfactants) can affect percutaneous absorption of solute by lowering thermodynamic activity and by altering skin permeability.[39,40] The former is a result of the extra solubilizing capacity contributed by surfactant micelles. Friberg and coworkers have found that the change of composition in an emulsion due to the evaporative loss of water causes phase changes in the emulsion and alteration of fragrance vapor pressures.[41-44] The latter reflect the thermodynamic activity of the fragrance ingredients.

Currently, there is no satisfactory tool for estimating the skin absorption rates and tissue concentrations subsequent to topical exposure of fragrances. Such a model is desired, in order to tighten the dermal safety assessment process for fragrance ingredients and to work towards a mechanistical understanding of fragrance contact allergy at a cellular level. An accurate model for predicting fragrance absorption, in combination with human repeat-insult patch test (HRIPT) dose-response data, will streamline the skin sensitization risk assessment of potential fragrance allergens. Such a model should be equally applicable to other non-perfume hazardous materials sharing similar physico-chemical properties to fragrance raw materials. These chemicals include herbicides, insecticides, and pesticides.

This dissertation describes sequential steps in the development of a predictive model for fragrance evaporation and absorption from skin. Both literature data and experimental data from our own laboratory were analyzed. The thesis is organized as follows: Chapter 2 states the objective, hypotheses and specific aims of the project. Chapter 3 focuses on the establishment of

the relationships between the physico-chemical properties of fragrance ingredients and the dermal absorption and evaporation rates of these materials. Chapter 4 describes the compartmental models based on the relationships developed in Chapter 3 and discusses the effect of fragrance fixative on other fragrance components. Chapter 5 and 6 explain the *in vitro* and *in vivo* methodology in skin evaporation/penetration studies. The compartmental models were also tested with the experimental data. Chapter 7 focuses on the application of the physico-chemical properties based model for predicting the evaporation of fragrance ingredients following topical application in fine fragrances and discusses potential ingredient interactions in perfume mixtures.

CHAPTER 2

OBJECTIVE

OBJECTIVE

The long-term objective of this project is to develop a mathematical model for predicting the dermal absorption rate and local tissue concentration of topically-applied fragrance ingredients, in order to streamline the dermal risk assessment process for these compounds.

HYPOTHESES

1. The skin disposition of small topical doses of most materials follows nearly first-order kinetics and can be predicted from physico-chemical properties and environmental factors.

2. Ingredient interactions can affect the thermodynamic activity of fragrance components, thus having a significant impact on the rate of both the absorption and evaporation processes.

SPECIFIC AIMS

1. To establish the relationships between the physico-chemical properties of fragrance ingredients and the dermal absorption and evaporation rates of these materials following application to human skin from an ethanolic vehicle. These relationships will allow the prediction of both absorbed and evaporated fractions of these ingredients following topical application in simple vehicles, including fine fragrance formulations.

2. To determine the effect of ingredient interactions in the perfume mixtures on the skin disposition of the individual components.

CHAPTER 3

A PHYSICO-CHEMICAL PROPERTIES BASED MODEL FOR ESTIMATING EVAPORATION AND ABSORPTION RATES OF PERFUMES FROM SKIN

INTRODUCTION

Perfumes are among the most widely used cosmetic ingredients and are also among the most troublesome. They are composed of low molecular weight, lipophilic compounds (perfume raw materials or PRMs) that readily penetrate the skin. Sensitive individuals may develop allergic contact dermatitis (ACD) following repeated exposures to some PRMs; the incidence of these reactions is known to correlate with chemical reactivity and dermal exposure level of the offending materials.[3,45,46] Consequently, risk assessments for newly developed fragranced products generally include a structural alert search[47] and careful evaluation of the dermal exposure to each PRM relative to known skin sensitization thresholds.[3,45,46] Due to the lack of skin absorption data (usually) or of an accepted model for predicting absorption of volatile compounds, 100% absorption is frequently assumed in exposure assessments.[3] This value is most assuredly an overestimate for fragrance components (or we would not smell them!).

In order to tighten the exposure assessment process for fragranced products and to better understand ACD thresholds at a cellular level, a mathematical model for accurately estimating PRM dermal absorption rates and tissue concentrations subsequent to topical exposure is desired. The present report describes a simple model based on physico-chemical properties of the PRMs and airflow over the exposed skin surface that can potentially fill this need. In this report we present the derivation of the model and its application to fragrance evaporation data from human forearm skin *in vivo* reported earlier in this journal.[48]

THEORY

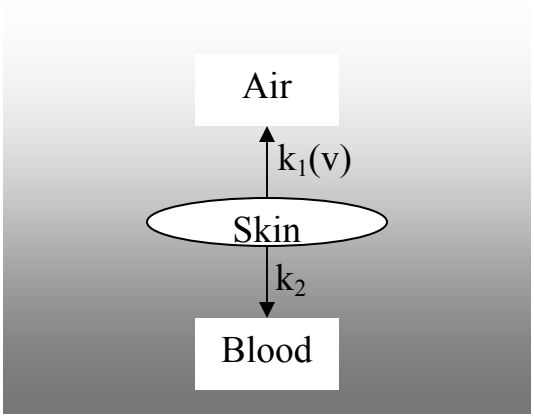

Figure 3.1. Schematic diagram of perfume disposition on skin.

Consider the simple picture of perfume disposition on skin depicted in Fig. 3.1. We assume that, for small doses of topically applied PRMs, absorption and evaporation are first-order processes (limitations arising from this assumption will be discussed later). Thus, for a given set of exposure conditions, we have

$$\frac{dA}{dt} = -(k_1 + k_2)A \tag{3.1}$$

In eq. 3.1, A is the amount of ingredient on the skin surface, k_1 is the evaporation rate constant, and k_2 is the absorption rate constant. The absorption rate is proportional to the product of maximum flux, $J_{\max} = const. \times S_{lip} \times MW^{-b}$,[49] and the fractional saturation of the surface layer, A/A_{max}. Thus,

$$k_2 A = const. \times (A / A_{\max}) \times S_{lip} MW^{-b} \tag{3.2}$$

with b ≈ 2.7 as discussed in the Appendix. In eq. 3.2, we have used the form for J_{max} suggested by Kasting et al.[49] along with the power law dependence for skin permeability on molecular weight first suggested by Anderson and Raykar.[50] For compounds in the narrow molecular weight range of PRMs, this form is interchangeable with the exponential form assumed in Ref. 49 and in related models of skin permeability.[5,26] In fact, eq. 3.2 is quite consistent with the permeability model developed by Potts and Guy,[5] which Hostynek[2] has shown to be effective in correlating PRM absorption from aqueous solution. A_{max} is the amount of an ingredient required to saturate the upper layers of the stratum corneum. For lipophilic ingredients, we expect A_{max} to be proportional to the solubility of the permeant in skin lipids, S_{lip}. Thus, this factor cancels on the right hand side of eq. 3.2, leaving (for $A < A_{max}$):

$$k_2 = k_2^T \times MW_r^{-b} \tag{3.3}$$

In eq. 3.3, molecular weight has been expressed in dimensionless or "reduced" form, MW_r = MW/100 Da, for computational convenience. The parameter, k_2^T, is as yet undetermined. The superscript indicates that its value is a function of skin temperature, T (see Discussion). The value of k_2^T for a room temperature exposure ($T \approx 30°C$) will be determined later by calibration with experimental data.

The model for evaporation of PRMs from skin derives in spirit from an approach developed at Dow Chemicals to describe pesticide evaporation from soil.[51] In direct analogy to the Dow model, evaporation rate at a fixed temperature and airflow velocity may be taken as the ratio of vapor pressure, P_{vp}, to solubility in skin lipids, S_{lip}. We further assume that S_{lip} is proportional to

solubility in octanol, S_{oct} .[49] The latter may be taken as the product of water solubility, S_w, and octanol/water partition coefficient, K_{oct}. Thus,

$$\begin{aligned} k_1 &= const. \times P_{vp} / S_{lip} \\ &= const. \times P_{vp} /(K_{oct} S_w) \end{aligned} \tag{3.4}$$

In practice, it is likely that eq. 3.4 must be modified to account for variable airflow over the skin surface. As wind velocity, v, increases or the turbulence in the flow over the skin increases one expects evaporation rate to increase. Thus, we anticipate that the constant in eq. 3.4 is actually a function of airflow. Thus,

$$k_1 = k_1^v \times P_{vpr} /(K_{oct} S_w)_r \tag{3.5}$$

where the superscript on k_1^v indicates this parameter is dependent on airflow over the skin. The properties $P_{vpr} = P_{vp}/1$ torr and $(K_{oct}S_w)_r = (K_{oct}S_w)/1000$ gL^{-1} are dimensionless values chosen again for computational convenience. Like k_2^T, the value of k_1^v must be determined from experiment. The functional dependence of k_1^v on airflow will be discussed later.

The theory can now be completed. Integration of eq. 3.1 with initial dose A_0 yields

$$A(t) = A_0 \exp[-(k_1 + k_2)t] \tag{3.6}$$

and the fractions of the dose evaporated and absorbed after a long time are, respectively,

$$f_{evap} = \frac{k_1}{k_1 + k_2} \tag{3.7}$$

and

$$f_{abs} = \frac{k_2}{k_1 + k_2} \tag{3.8}$$

Substituting the results from eqs. 3.3 and 3.5 into eqs. 3.7 and 3.8, and expressing the results as a percentage, yields

$$\%\text{evap} = 100 \times \frac{x_r}{k + x_r} \tag{3.9}$$

$$\%\text{abs} = 100 - \%\text{evap} \tag{3.10}$$

In eq. 3.9, k is a parameter depending on v and T, but having the same value for all fragrance ingredients. Its value, equal to the ratio k_2^T / k_1^v, must be determined experimentally. The parameter x_r is the following dimensionless ratio of physicochemical properties of the PRM:

$$x_r = \frac{P_{vpr} MW_r^{2.7}}{(K_{oct} S_w)_r} \tag{3.11}$$

All properties are evaluated at skin temperature, T. Equations 3.9-3.11, which express the percentage of applied material evaporated and absorbed as a function of readily obtained physical properties, are the desired model result for exposure assessment purposes. As a further

step, it is possible to estimate tissue concentrations using eq. 3.2 in conjunction with simple models for epidermal and dermal permeability described elsewhere.[49,52] For the present analysis, however, we will focus only on evaporation and absorption.

METHODS

Fragrance evaporation. Human *in vivo* evaporation data from the study by Vuilleumier et al.[48] were analyzed. The study involved application of two closely related mixtures of PRMs, identified as Vector A and Vector B, to the ventral forearm of a single female subject. Volatiles were collected over a 7.25 h period following dosing by means of a glass trap placed over the 0.6 cm^2 dose site. An airflow rate of 5 Lh^{-1} was maintained during the study. Analysis was by capillary GC. A summary of the dosing and volatile collection data is given in Table 3.1.

Physical properties. Vapor pressures at 30°C were estimated from normal boiling points and molecular weights using a commercially available computer program from Syracuse Research Institute.[53] The algorithm is a weighted average of Antoine's method and the modified Grain method.[54] Normal boiling points were either obtained from the experimental database in the same program[53] or estimated from the chemical structure according to the group contribution method employed therein. Octanol/water partition coefficients, K_{oct}, were taken from the MEDCHEM database (when available) or calculated according to the MEDCHEM CLOGP program.[55] Octanol solubility values at 30°C, S_{oct}, were calculated according to the formula in Ref. 49, which represents a small modification of the original formula proposed by Yalkowski et al..[56] Water solubility values, S_w, were estimated from the ratio of S_{oct}/K_{oct}. In the one case where experimental values of S_w were available (Compound I, Ref. 57), the calculated S_w was

found to be in excellent agreement with experiment. Although values of K_{oct} and S_w are tabulated in this report due to their familiarity among pharmaceutical readers, the fundamental property for the correlations reported is the product of these values, S_{oct}.

Data analysis. The disposition kinetics of each PRM for the study in Ref. 48 were determined using a similar approach to the determination of elimination kinetics from urinary excretion data.[58] The terminal slope of the semilogarithmic evaporation rate vs. time plot represents the total elimination rate constant, $k_1 + k_2$. This may be seen by inserting eq. 3.6 into eq. 3.1 and taking the logarithm. For our analysis, the evaporation rate data for each PRM in Vectors A and B were plotted semilogarithmically versus time. Examples of these plots are shown in Fig. 3.2. The slopes were estimated via linear regression and set equal to $k_1 + k_2$. Area under the evaporation rate curve (AUC) was calculated for each ingredient by summing the experimental values from 0-7.25 h, then applying a correction for the undetermined "tail" using the log trapezoidal rule. This tail represents material that would have evaporated had the experiment been carried out longer. This correction amounted to less than 6% of the total AUC for all compounds except VI (6-13%), XI, and XII.

The two least volatile components, Compounds XI and XII, had nearly constant evaporation rates during the study; hence, the tail could not be estimated. For these compounds, k_1 was calculated by dividing the average evaporation rate by the dose applied to the skin. The values of k_2 and the evaporated fraction, f_{evap}, could not be determined. For the remaining compounds (I-X), f_{evap} was calculated as AUC/Dose, and k_1 was evaluated as $f_{evap}(k_1 + k_2)$ by rearranging

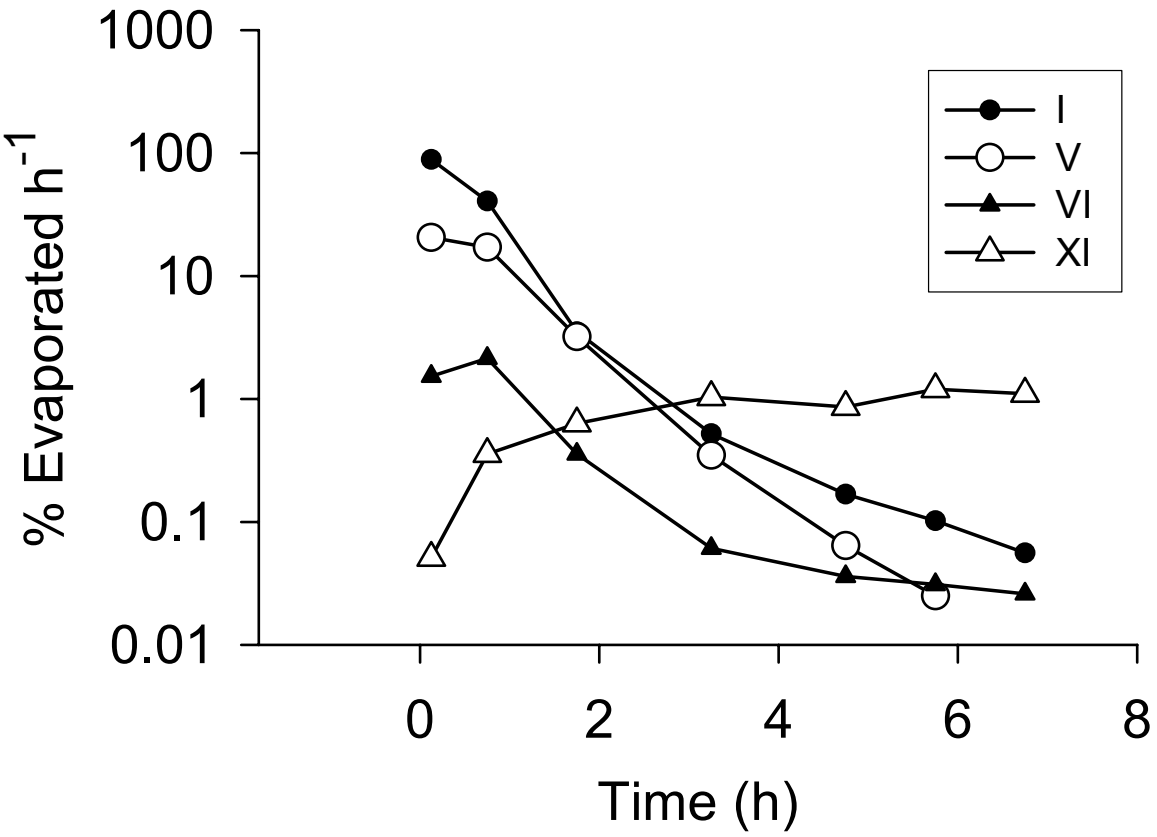

Figure 3.2. Semilogarithmic plots of human *in vivo* perfume evaporation data from Ref. 48. The identities of the compounds are given in Table 3.1. The examples shown were taken from Vector A, Trial 1.

eq. 3.7. The value of k_2 was then calculated by subtracting k_1 from $k_1 + k_2$. Note: Taken together, eqs. 3.1 and 3.6 suggest that the value of k_1 can also be determined from the intercept of the semilogarithmic evaporation rate vs. time plot, this value being equal to log k_1A_0. We found that this method of determination did not yield reasonable estimates for k_1 based on calculated AUCs. This discrepancy implies a breakdown of the first-order absorption and evaporation assumption in the first few minutes following dosing, while the carrier solvent was evaporating and the perfume mixture was absorbing into the upper skin layers. This phenomenon will be discussed later.

The degree of fit of the model to the experimental evaporation data was evaluated by means of the coefficient of determination, r^2, the standard deviation, s, and the χ_ν^2 statistic as defined by Bevington.[59] The former yields the fraction of the experimental variance explained by the model, whereas the latter is a ratio of the unexplained variance to that expected from random errors. A value of χ_ν^2 close to unity with no systematic deviations implies excellent agreement of the model with the data. Statistical significance of the regressions was assessed by the F test and its corresponding p value. The regression analyses were conducted using SigmaPlot (SPSS Inc., Chicago, IL, USA).

RESULTS

The results of the AUC analysis of the fragrance evaporation vs. time plots are shown in Table 3.1. The mean percentage evaporated for the individual components ranged from 4% to 74% for the two perfume vectors. These values and the physical properties in Table 3.1 were used to test the model represented by eqs. 3.1-3.11.

The results of these calculations are shown in Figs. 3.3 and 3.4. Fig. 3.3 shows the percentage evaporated plotted versus the dimensionless parameter x_r defined in eq. 3.11. Significant correlations between the observed values of %evap and the model prediction were obtained for each perfume vector [$r^2 = 0.74$ for Vector A ($p < 0.002$) and $r^2 = 0.52$ for Vector B ($p < 0.02$)]. The standard deviations of the fits were $s = 12\%$ for Vector A and $s = 14\%$ for Vector B. The corresponding χ_ν^2 values were 195 and 16, respectively. These numbers suggest that the

Table 3.1. Physical properties and total percentage evaporated values of perfume ingredients studied in Ref. 48.

ID	Perfume ingredient	MW (Da)	P_{vp}[a] (torr)	log K_{oct}[b]	bp[a] (°C)	S_w[c] (mg/mL)	Total % evaporated (Mean ± SE) Vector A	Vector B
I	linalool	154	0.13	2.55	197[d]	2.3	68.1 ± 0.4	57.5 ± 1.5
II	dihydromyrcenol	156	0.19	3.03	191	0.76	73.5 ± 1.6	65.8 ± 2.2
III	10-undecanal	170	0.093	4.05	235	0.072	59.4 ± 0.4	45.2 ± 6.1
IV	citronellol	156	0.028	3.25	225[d]	0.46	50.0 ± 0.4	41.2 ± 0.7
V	2-phenyl-1-ethanol	122	0.039	1.36[d]	218[d]	35	26.0 ± 0.3	18.6 ± 2.0
VI	(E)-cinnamic alcohol	134	0.0050	1.95[d]	250[d]	8.5	3.9 ± 0.4	3.7 ± 0.6
VII	alpha-damascone	192	0.032	3.62	259[d]	0.16	71.2 ± 0.7	57.0 ± 2.8
VIII	cis-7-p-menthanol	156	0.019	3.33	230	0.38	54.5 ± 1.4	46.9 ± 5.4
IX	2,2,2-trichloro-1-phenylethylacetate	268	0.0029	4.05	288	0.046	42.2 ± 0.4	40.5 ± 3.2
X	M.P.C.C[e]	192	0.010	3.87	278	0.11	33.0 ± 0.5	23.7 ± 2.2
XI	(E)-2-benzylideneoctanal	216	0.00088	4.85	319	0.0090	6.9 ± 0.7[f]	4.3 ± 0.7[f]
XII	15-pentadecanolide	240	0.00010	5.35	364	0.0036	NA[g]	6.6 ± 1.0[f]

[a] Calculated values, Ref. 53 unless otherwise noted
[b] Calculated values, Ref. 55 unless otherwise noted
[c] Calculated as described in text
[d] Experimental values, Ref. 53 or 55
[e] 3-(4-methyl-3-pentenyl)-3-cyclohexene-1-carbaldehyde + 4-(4-methyl-3-pentenyl)-3-cyclohexene-1-carbaldehyde
[f] 0-7.25 h only
[g] Not present in this mixture

accuracy of the present approach will be limited to about 15%. There is considerable room for improving upon this result based on the high values of χ_v^2.

The evaporated fraction for each ingredient was about 30% higher for Vector A than for Vector B, resulting in an average increase in %evap of about 10%. Vector B contained a fragrance fixative – the musk, Compound XII – whereas Vector A did not. We found, as did the original workers,[48] that most of the difference occurred during the first 75 min. This difference is reflected in our analysis by larger values of k_1 and a correspondingly smaller value of k for Vector A ($k = 0.15 \pm 0.06$) versus Vector B ($k = 0.24 \pm 0.14$). Values of k_2 were comparable for the two vectors. The difference in k values was not statistically significant (z test). The presence of the musk in Vector B evidently reduced the volatilization rate of the other ingredients during the dry down period, an interaction that is not taken into account in the present model. This is an area in which an improved analysis may be possible.

Figure 3.4 shows a plot of the average values of the first-order rate constants calculated from the analysis versus the PRM physical properties ratios given in eqs. 3.3 and 3.5. The calculated values of k_1 varied by a factor of 30, whereas those for k_2 varied by a factor of 4. The results of the regression analyses of these data according to eqs. 3.3 and 3.5 are shown in Table 3.2. Both of these regressions were highly significant. The most important factor contributing to the variation in k_1 was P_{vp}; the factors K_{oct} and S_w played only a minor role. This resulted from the fact that they appear together as a product representing lipid solubility, S_{lip} (see eq. 3.4), a property that does not vary greatly for perfume ingredients. If polar or high melting compounds

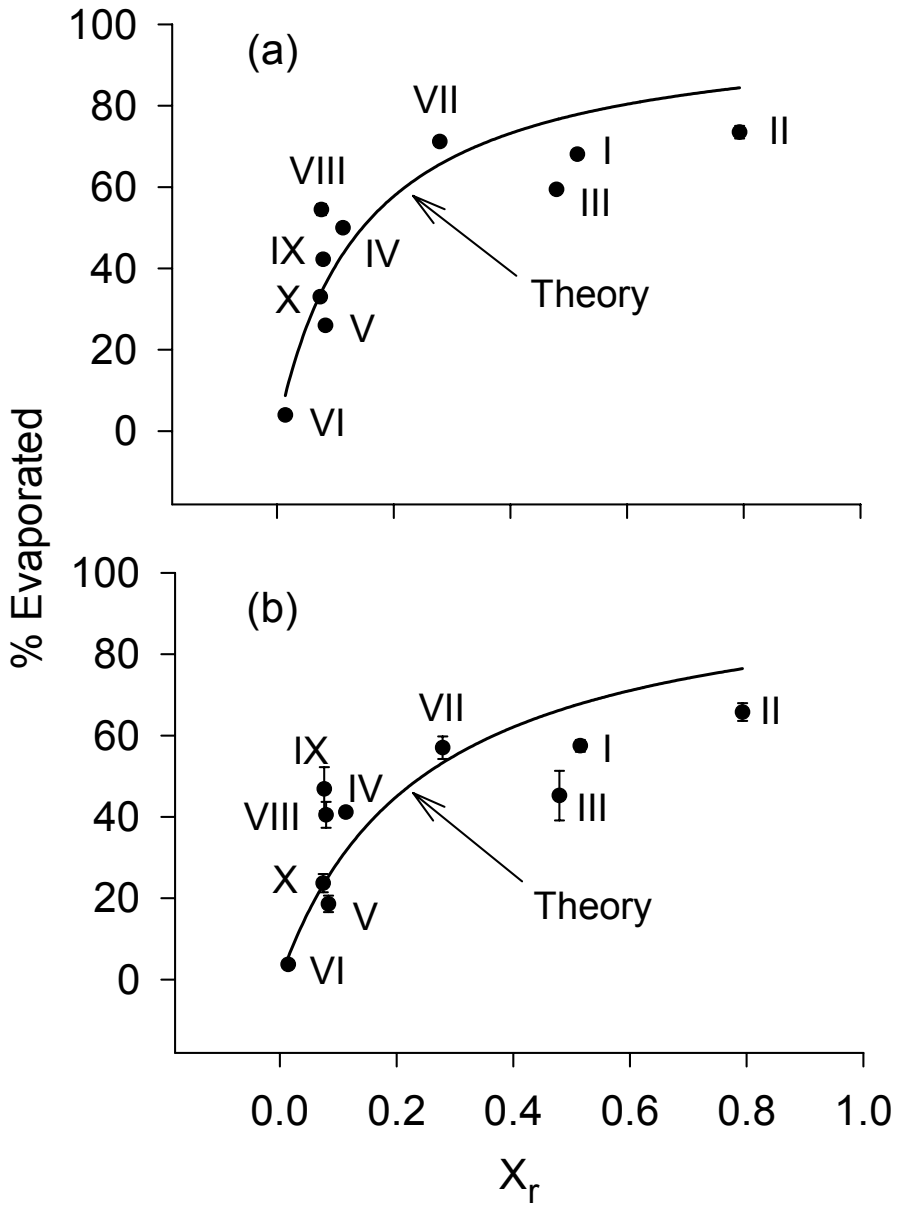

Figure 3.3. Cumulative evaporation of perfume ingredients in Ref. 48 study, plotted versus the ratio of physico-chemical properties defined in eq. 3.11. Each point represents the mean ± SE of two trials. The absence of an error bar indicates the SE was smaller than the size of the symbol. The theoretical curve is the result of fitting eq. 3.9 to these data. (a) Vector A, $k = 0.15$; (b) Vector B, $k = 0.24$.

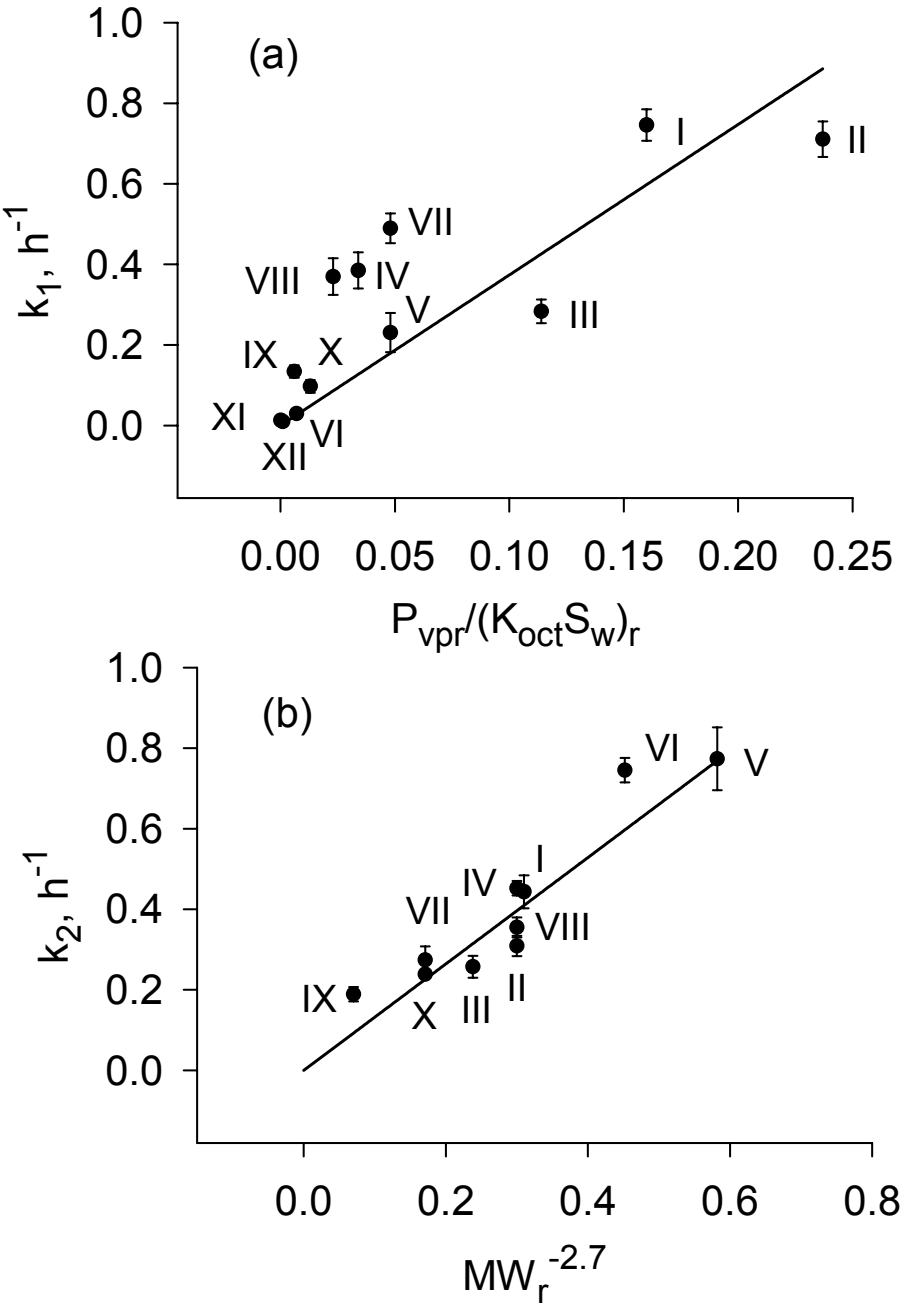

Figure 3.4. First-order rate constants for (a) evaporation and (b) absorption determined from analysis of the Ref. 48 data. Values for Vectors A and B were combined for this analysis, so that each point represents the mean ± SE of four trials. The results are plotted versus the ratios of properties shown in eqs. 3.5 and 3.3, respectively.

were to be included in such an analysis, a larger contribution from these factors would be expected.

Table 3.2. Regression parameters for the correlations shown in Fig. 3.4.

Parameter	k_1 (n = 12) (eq. 3.5)	k_2 (n = 10) (eq. 3.3)
k_1^v, h^{-1}	3.74 ± 0.55	-
k_2^T, h^{-1}	-	1.32 ± 0.18
r^2	0.54	0.87
s, h^{-1}	0.17	0.08
F	13.0	52.1
p	<0.0001	<0.0001

DISCUSSION

The possibility of accurately predicting perfume absorption and evaporation rates from skin – and presumably, those of other volatile compounds – from a small set of readily available physical properties is intriguing. The degree of success with which the present approach can lead to predictions useful for exposure assessment depends on a number of factors, some of which are related to the assumptions inherent in the model and others that are related either to exposure conditions or to consistent estimation of physical properties. These three topics are discussed below.

Model assumptions. To restate briefly, the major assumptions in the present analysis are: (1) absorption and evaporation can be treated as first-order processes; (2) the behavior of each PRM is independent of other ingredients in the mixture including the solvent; (3) skin penetration can be described by the model in Ref. 49; (4) evaporation rates can be calculated from a Henry's Law-like expression with a correction for surface airflow; (5) PRM binding to the stratum corneum is insignificant. While it is possible to remove one or more of these assumptions and still obtain a solution to the problem, the solution becomes more complicated. It seems worthwhile to examine the predictions of this relatively simple model before introducing additional complexity.

First-order rate equations have been successfully used to describe the skin absorption rates of many compounds following small topical applications;[60,61] the key to their utility appears to be the size of the dose. As doses increase there is a gradual transition from first-order to zero-order behavior as the upper layers of the skin become saturated.[62] Based on Ref. 62 and our own experience[63] we would expect first-order kinetics to be a good approximation for perfume doses common to most fragranced products (total PRM load <100 $\mu g/cm^2$). The exception may be heavy applications of fine fragrances, where an extension of the diffusion models described in Refs. 62 and 63 may provide a better description of both absorption and evaporation rates. In order to adequately characterize such a model, a more complete set of experimental data incorporating both absorption and evaporation measurements should be analyzed.

Once the ingredients have absorbed into the upper skin layers, the evaporation of small doses of PRMs is likely to follow first-order kinetics for the same reasons as absorption. The data in Ref.

48, examples of which are shown in Fig. 3.2, generally support this statement. After the first 15 min, most of the semilogarithmic evaporation rate curves are either linear or reasonably so. However, as noted earlier, the evaporation rate constant applicable to this process evidently does not apply in the first few minutes following topical application. Other workers examining these data have also noted this phenomenon and have suggested an explanation in terms of co-evaporation of the PRMs with the ethanol vehicle.[64] It seems that a model refinement of this nature may eventually lead to better predictions than those presently obtained. We have not yet attempted such a refinement.

Ingredient interactions leading to non-independent absorption and evaporation rates are certainly possible and, indeed, are to be expected for high fragrance doses in which the PRM mixture substantially modifies the lipid environment of the skin. Each ingredient modifies the thermodynamic activity of other components according to well-known laws governing liquid-liquid and liquid-vapor mixtures.[65] It would seem possible to incorporate these effects into an improved description of the dry down process by means of an appropriate thermodynamic calculation employing, e.g., UNIFAC or UNIQUAC methods.[65] This type of refinement should be considered as more data become available. For the present analysis we note that after dry down, interaction effects on thermodynamic activity after dry down should have equal impact on both absorption and evaporation rates. Thus, the absolute rates of each process, given by eqs. 3.1-3.5, may be altered by the interaction, but the ratio of these values should be relatively unaffected. Since the final disposition of each PRM is governed by a ratio of the rate constants (see eqs. 3.7 and 3.8), we expect this disposition to be relatively insensitive to the perfume composition. However, departures from this behavior can be generated during the dry down

process, where evaporation rates may be impacted without a corresponding change in absorption rate.

Model assumptions 3 and 4 concern the physical properties dependencies of absorption and evaporation rates. The relationships chosen are drawn from previous models of skin penetration (for the absorption rate) or by analogy with other volatilization processes (for the evaporation rate). These relationships are subject to continuous improvement, as they are derived not from first principles, but rather from correlations of existing data. As more relevant data become available and stronger correlations are obtained, these relationships should be reexamined in order to optimize the predictive power of the model.

Assumption 5 is readily evident from eq. 3.10: 100% of each ingredient is assumed to either evaporate or penetrate through the skin. For chemically or metabolically reactive compounds, this assumption may require modification to allow for covalent binding to stratum corneum constituents. An example would be Schiff's base formation between an aldehyde-containing PRM (e.g., Compounds III, X or XI) and skin keratins. Were such binding to occur in the stratum corneum, the absorbed fraction for exposure assessment could be lowered. However, one recognizes that these compounds are precisely the ones most likely to lead to skin sensitization!

Exposure conditions. The theory presented can, in principle, account for variations in temperature, airflow, intrinsic skin permeability, and degree of occlusion via appropriate adjustment of the model parameters T, k_1^v, and k_2^T. However, it does not provide information as

to the distribution of expected values: the parameters reported here apply to a single subject with a fixed set of exposure conditions. Surface airflow characteristics, in particular, will vary for different exposures leading to variations in the PRM evaporation rate that have not yet been characterized. Optimal application of the model to exposure assessment will entail determination of the airflow effect and estimation of the expected variations in each of the governing factors. This information can then be combined with the deterministic model and incorporated into the exposure assessment by means of a Monte Carlo calculation.[66] The literature provides some guidance as to the anticipated variation of k_1^v and k_2^T with wind velocity and temperature, respectively. The latter is better understood. As the proportionality constant for the skin absorption rate of PRMs, which are moderately to highly lipophilic compounds, k_2^T would be expected to vary with temperature as does the permeability of the stratum corneum lipid pathway. This variation has been extensively characterized; excellent discussions are given by Peck et al.[67] and, much earlier, by Blank et al.[68] For the range of skin temperatures expected in fragrance exposures, an Arrhenius model with an activation energy, E_a, of about 20 kcal mol^{-1} should adequately represent the expected variation in k_2^T. This would lead to an equation of the form

$$\ln\left(\frac{k_2^T}{k_2^{30}}\right) = \frac{E_a}{R}\left(\frac{1}{273+30} - \frac{1}{273+T}\right) \cong 10\left(3.3 - \frac{1000}{273+T}\right) \tag{3.12}$$

where R is the gas constant (1.987 cal deg^{-1}mol^{-1}), T is temperature in °C, and k_2^{30} is the value of k_2^T at 30°C (approximately 1.3 h^{-1} based on the present analysis – see Table 3.2). Equation 3.12 leads to an approximately 3-fold variation in k_2^T for a 10°C change in T.

The variation of k_1^v with airflow is less easily discovered. In general, we would expect a sigmoidal dependence of k_1^v on v, with a plateau in still air determined by convection and a higher plateau under very windy conditions in which the skin surface is maintained effectively at zero concentration.[51] Under the latter conditions, it is possible that evaporation rates will also become independent of vapor pressure,[51] thus departing from the dependence postulated in eq. 3.5. There may be a range between these two extremes where a laminar flow model yielding $k_1^v \propto v$ is appropriate. Because of the range of possibilities and the complexities offered by turbulent airflow, this subject would seem a good candidate for experimental study.

Physical properties estimation. The evaporation data in Ref. 48 can be interpreted differently depending on the values selected for the physicochemical properties.[64] We were impressed with the range of estimated vapor pressure (P_{vp}) values suggested by the original workers,[48] their industrial colleagues,[64] and the SRC computer program.[53] We chose to use the latter method for the analysis because of the extensive documentation and public availability of the SRC program and the fact that we could not find well documented experimental values for this property. As a case in point, consider cinnamic alcohol, Compound VI. Using the calculated P_{vp} value in Table 3.1 of 0.0050 torr, the low percentage evaporation of this compound (<4%) is readily explained on the basis of low volatility and low molecular weight. However, using the Ref. 48 value, P_{vp} =

0.057 torr, the compound becomes an outlier in the present model, and other mechanisms for its low evaporation rate must be invoked.

Similarly, octanol-water partition coefficients (K_{oct}) obtained from other sources may vary substantially from those reported here. We selected a combination of experimental and calculated values from Ref. 55 based on the reputation and widespread use of this database and computational method. In this case, it is important to bear in mind that the theory presented above suggests a dependence of PRM distribution on octanol solubility, $S_{oct} = K_{oct}S_w$, rather than K_{oct} itself, and that S_{oct} does not vary substantially for fragrance ingredients. Consequently, it would seem that the primary requirements for consistent use of the theory for perfume exposure assessment are the determination of the airflow effect, appropriate selection and use of exposure conditions, and agreement among investigators regarding the method of vapor pressure estimation.

CONCLUSIONS

Perfume disposition on human skin in a controlled *in vivo* study could be satisfactorily correlated with the physicochemical properties of the fragrance ingredients using a first-order kinetic model. Further development of this concept may lead to a useful model for dermal exposure assessment for volatile materials contacting the skin.

APPENDIX – Molecular size dependence of diffusivity in skin

The absorption rate constant, k_2, for each permeant is proportional to its effective diffusivity in skin, D, since $J_{max} \propto D$.[49] Numerous reports have discussed the size dependence of D in human stratum corneum.[5,26,49,50,69] Most workers agree there is a steep, inverse dependence of D on molecular weight for compounds ranging in size from water (18 Da) to corticosteroids (350-500 Da). Fragrance ingredients fall in the center of this range, e.g., 122-268 Da for the compounds listed in Table 3.1. Correlations between D and MW have been obtained using exponentials,[5,49] modified exponentials,[26] and power laws.[50]

Since skin permeability coefficients are products of diffusivity, D, and lipid/water partition coefficient, K_{lip}, values of D calculated from steady-state skin permeability data depend sensitively on the model chosen for K_{lip}. Alternatively, for a maximum flux situation, calculated values of D depend on the measure chosen for lipid solubility, S_{lip}. These relationships have been extensively discussed.[5,49,50] In their recent analysis of skin permeability data, Johnson et al.[69] used the functional form $K_{lip} = K_{oct}^{0.76}$ to calculate a consistent set of D values for 120 permeants in human stratum corneum. These values, which are replotted in Fig. 3.5, are the basis for the molecular weight dependence employed in this report. To obtain the working relationship (eq. 3.2), we fit a power law of the form

$$D = aMW^{-b} \qquad \text{(A-1)}$$

to the data in Fig. 3.5.

A linear least squares fit of log D vs. log MW (n = 120) yielded $a = 0.109$, $b = 2.72 \pm 0.13$, $s = 0.52$, and $r^2 = 0.78$. This value of b, while smaller than the value $b = 4.6$ estimated by Anderson and Raykar,[50] still indicates a strong size dependence compared to the values expected for diffusion of small molecules in liquids, $b = 1/3$ to ½.[49] The rounded value $b = 2.7$ was used for the remainder of the analysis.

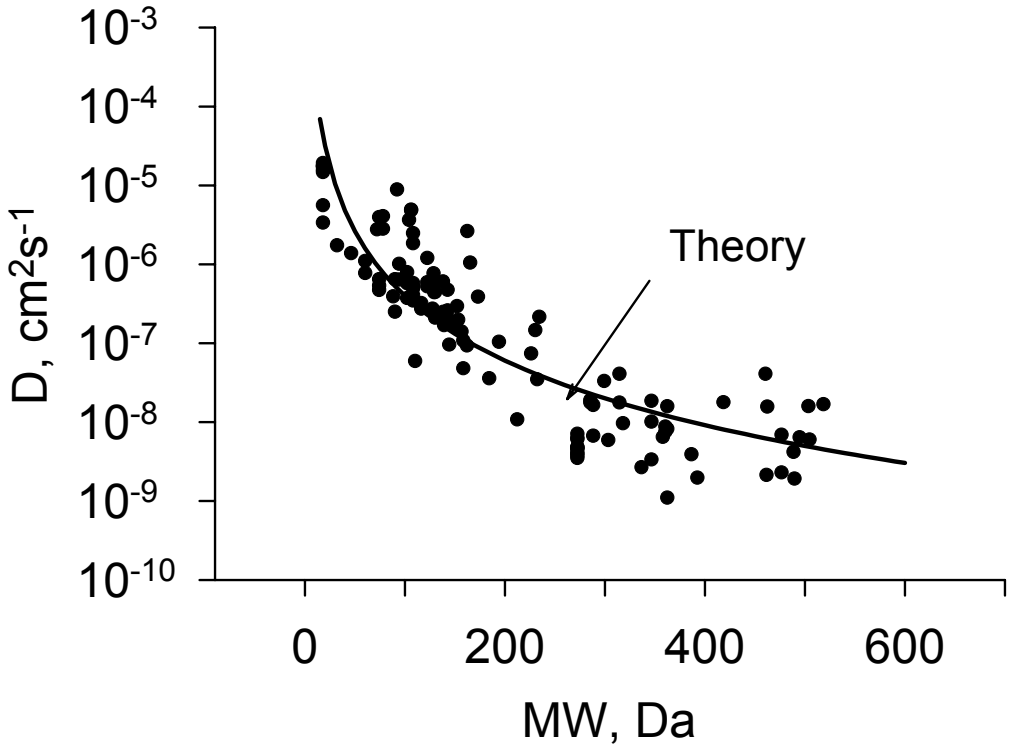

Figure 3.5. Diffusion coefficients for compounds permeating through human skin according to the lipid pathway diffusion model presented in Ref. 69. The data show a strong dependence of D on molecular weight. The theoretical curve is a least squares fit of eq. A-1 to these data yielding the parameters described in the text.

CHAPTER 4

TWO-STAGE KINETIC ANALYSIS OF FRAGRANCE EVAPORATION AND ABSORPTION FROM SKIN

INTRODUCTION

Fragrances are comprised of a complex mixture of ingredients designed to produce a pleasant and/or stimulating aroma following application to the skin. The aroma evolves over time, gradually decreasing in intensity as first the high notes (most volatile compounds), then the middle and low notes (e.g., musks or other fixatives) dissipate through a combination of evaporation and absorption into the skin. A technical understanding of the dissipation process is important for two reasons: (1) it can aid in the design and evaluation of fine fragrances and other fragranced products;[70] and (2) it can aid in the risk assessment process for these products with respect to both skin sensitization and systemic exposure.[71] We have previously described a one-compartment, first-order kinetic approach to modeling the disposition of fragrances on skin (Figure 4.1a – Method 1).[72] The method was used to correlate the evaporated fractions of each component of a 12-component fragrance mixture from human volar forearm[48] with physicochemical properties. More recently, we have extended this approach by explicitly considering the dry-down process immediately following application to the skin.[73] This was accomplished by adding a second compartment to the kinetic model to represent the solution or formulation applied to the skin surface. Two variations were considered (Figure 4.1b – Method 2 and Figure 4.1c – Method 3). The modified models were able to better represent the kinetics of the evaporation and absorption processes for a model fragrance ingredient applied to human skin *in vitro*.[73] In this report we show that the two-compartment models also improve the kinetic description of evaporation rates measured on human skin *in vivo*, using the previously analyzed study of Vuilleumeir et al.[48] as an example. Thus, they may be more useful than the one-compartment model as tools with which to correlate, and eventually predict, the changing

Figure 4.1. Schematic diagrams for compartmental models of skin disposition. a) One-compartment (Model 1); b) Two-compartments with evaporation from vehicle and skin (Model 2); c) Two-compartments with evaporation from vehicle only (Model 3).

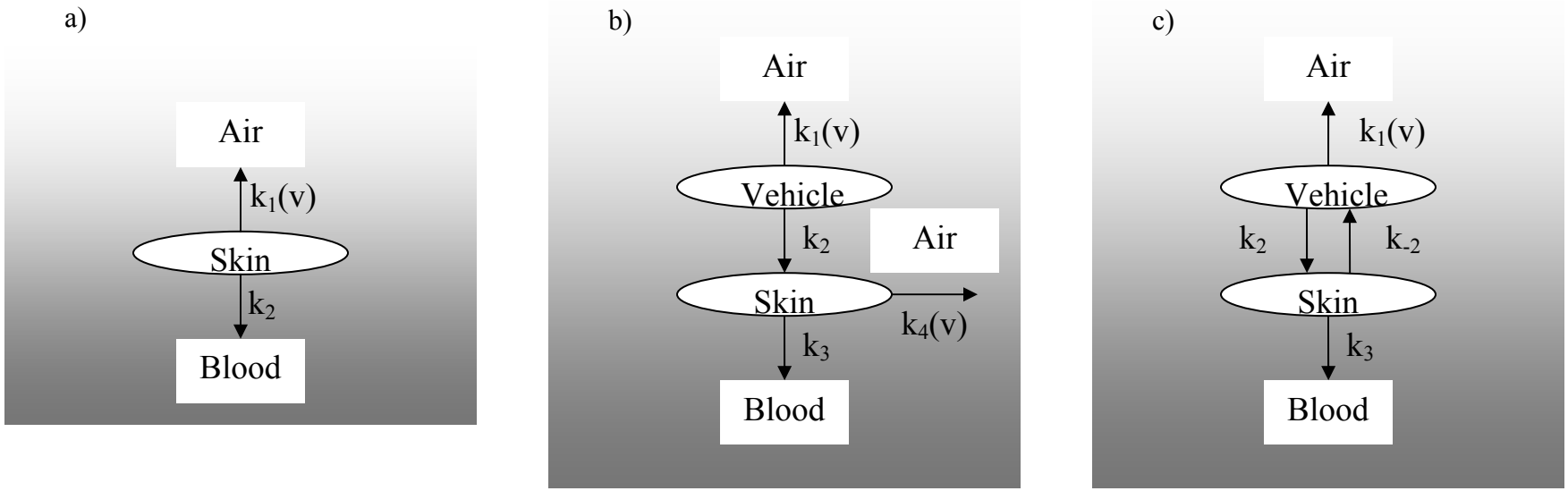

composition of aromas arising from skin following topical application of a fine fragrance or a fragranced consumer product.

THEORY

The compartmental models considered herein have been previously described.[72,73] A brief synopsis is given below.

Model 1 (Fig. 4.1a). The skin is assumed to be a single, well-stirred compartment that rapidly incorporates a topically-applied ingredient. The amount of an ingredient that has evaporated at time t following application of amount A_0 at time zero is

$$A_{\text{air}}(t) = A_0\left(\frac{k_1}{k_1 + k_2}\right)e^{-(k_1+k_2)t} \tag{4.1}$$

where k_1 is the evaporation rate constant and k_2 is the absorption rate constant. The rate constants for each compound are functions of temperature T, surface airflow v, and three physico-chemical properties: vapor pressure P_{vp}, molecular weight MW, and lipid solubility S_{oct}. The latter is taken to be solubility in *n*-octanol, expressed as the product of water solubility S_w and octanol-water partition-coefficient K_{oct}. Each property is expressed in dimensionless, or "reduced", form by dividing by a characteristic value; thus,

$$k_1 = k_1^v \cdot P_{vpr} / \left(K_{oct} \cdot S_w\right)_r \tag{4.2}$$

$$k_2 = k_2^T \cdot MW_r^{-2.7} \tag{4.3}$$

In eqs. 2 and 3, $P_{vpr} = P_{vp} / 1 \text{ torr}$, $\left(K_{oct} \cdot S_w\right)_r = \left(K_{oct} \cdot S_w\right) / 1000 \text{ g/cm}^3$, $MW_r = MW / 100 \text{ Da}$, and k_1^v and k_2^T are proportionality constants dependent on surface airflow and temperature, respectively. The fraction evaporated after a long time ($t \to \infty$) is

$$f_{evap} = \frac{k_1}{k_1 + k_2} = \frac{x_r}{k + x_r} \tag{4.4}$$

where $k = k_2^T / k_1^v$ and $x_r = P_{vpr} MW_r^b / \left(K_{oct} \cdot S_w\right)_r$. The variation of k_1^v and k_2^T with airflow and temperature are discussed in Refs. 73 and 72, respectively. In this report these conditions do not vary, and k_1^v and k_2^T are treated as constants to be determined from the data.

Model 2 (Fig. 4.1b). In this model there are two well-stirred compartments – one representing the surface film (or vehicle), the other representing the skin (e.g., the stratum corneum). All ingredients are initially present in the vehicle only. Evaporation is assumed to occur first from the vehicle, which is rapidly depleted by the combination of this process with partitioning into the skin. Subsequent evaporation and absorption occur from the skin compartment. The amount of an ingredient that has evaporated at time *t* following application of amount A_0 at time zero is

$$A_{air}(t) = \frac{A_0}{\alpha\beta(\beta - \alpha)} \left\{ \left[k_1 \beta (\beta - \alpha) + k_2 k_4 \beta\right] \left(1 - e^{-\alpha t}\right) - k_2 k_4 \alpha \left(1 - e^{-\beta t}\right) \right\} \tag{4.5}$$

where $\alpha = k_1 + k_2$ and $\beta = k_3 + k_4$. After a long time the fraction evaporated is

$$f_{evap} = \frac{1}{\alpha\beta}\left(k_1k_4 + k_1k_3 + k_2k_4\right) = \frac{k_1k_4 + k_1k_3 + k_2k_4}{k_1k_4 + k_1k_3 + k_2k_4 + k_2k_3}. \qquad (4.6)$$

The evaporation rate constants k_1 and k_4 are considered to have the physical properties dependencies shown in eq. 4.2. The vehicle-to-skin rate constant k_2 and the absorption rate constant k_3 are considered to depend on molecular weight as described by eq. 4.3. The rationale for these assumed dependencies is presented in Ref. 72.

Model 3 (Fig. 4.1c). This model is similar to Model 2, except that the vehicle layer persists much longer, remaining as a discrete film until the last of the components has completely dissipated. A situation corresponding to either of these models might occur in practice, with the more volatile and/or skin permeable films dissipating according to Model 2 and less volatile/permeable films dissipating according to Model 3. The amount of an ingredient that has evaporated at time t following application of amount A_0 at time zero is

$$A_{air}(t) = \frac{k_1A_0}{\alpha\beta(\beta-\alpha)}\left[\left(k_3 + k_4 - \alpha\right)\beta\left(1 - e^{-\alpha t}\right) + \left(\beta - k_3 - k_4\right)\alpha\left(1 - e^{-\beta t}\right)\right] \qquad (4.7)$$

where α and β are the roots of the equation $x^2 + (\alpha+\beta)x + \alpha\beta$, $\alpha + \beta = k_1 + k_2 + k_3 + k_4$ and $\alpha\beta = k_1k_3 + k_1k_4 + k_2k_4$. After a long time the fraction evaporated is

$$f_{evap} = \frac{k_1}{\alpha\beta}\left(k_3 + k_4\right). \qquad (4.8)$$

METHODS

Overview. The Vuilleumeir et al. study involved trapping and GC analysis of volatiles arising from the skin following topical application of two closely-related fragrance compositions to the forearm of a single human volunteer.[48] Trapped volatiles were analyzed at eight time points spaced between 0.25 and 7.25 h. The compositions and the physical properties of the ingredients are listed in Table 4.1. Vector A comprised the first 11 of these ingredients. Vector B differed from Vector A in that a musk or fixative agent (Compound XII) was included in the composition. Addition of the musk led to a reduction in the initial evaporation rates of the other components, as noted by the original workers (cf. also Ref. 72). The present analysis focuses on the different kinetic profiles displayed by the two fragrance vectors.

Thus, cumulative evaporation data for each ingredient, normalized by applied dose, were calculated as described previously.[72] Average evaporation rates over each time interval were calculated and plotted semilogarithmically versus time. Examples of these plots are shown in Figures 4.2 and 4.3. The rate constants for kinetic models 1-3 were fit to the data for each ingredient by nonlinear least squares using the two different weighting schemes described below. The physical properties were then deconvolved from the rate constants using eqs. 4.2 and 4.3 (and equivalent expressions for the other rate constants – see Theory section) to give the

Table 4.1. List of fragrance raw materials studied in Ref. 48.

ID	Compound	MW (Da)	P_{vp}^{a} (Torr)	$\log K_{oct}^{a}$	S_{w}^{a} (g/L)	X_r (eq.4)	f_{evap}^{b} Vector A	f_{evap}^{b} Vector B
I	Linalool	154	0.13	2.55	2.3	0.52	0.68 ± 0.00	0.58 ± 0.02
II	Dihydromyrcenol	156	0.19	3.03	0.76	0.79	0.74 ± 0.02	0.66 ± 0.02
III	10-undecanal	170	0.093	4.05	0.072	0.48	0.59 ± 0.00	0.45 ± 0.06
IV	Citronellol	156	0.028	3.25	0.46	0.11	0.50 ± 0.00	0.41 ± 0.01
V	2-phenyl-1-ethanol	122	0.039	1.36	35	0.08	0.26 ± 0.00	0.19 ± 0.02
VI	(E)-cinnamic alcohol	134	0.0050	1.95	8.5	0.01	0.04 ± 0.00	0.04 ± 0.01
VII	Alpha-damascone	192	0.032	3.62	0.16	0.28	0.71 ± 0.01	0.57 ± 0.03
VIII	Cis-7-p-menthanol	156	0.019	3.33	0.38	0.08	0.54 ± 0.01	0.47 ± 0.05
IX	2,2,2-trichloro-1-phenylethylacetate	268	0.0029	4.05	0.046	0.08	0.42 ± 0.00	0.40 ± 0.03
X	M.P.C.C[c]	192	0.010	3.87	0.11	0.07	0.33 ± 0.00	0.24 ± 0.02
XI	(E)-2-benzylideneoctanal	216	0.00088	4.85	0.0090	0.01	0.07 ± 0.01[e]	0.04 ± 0.01[e]
XII	15-pentadecanolide	240	0.00010	5.35	0.0036	0.001	NA[d]	0.07 ± 0.01[e]

[a] For sources of physical properties, see Ref. 72.

[b] Experimental fraction of dose evaporated, extrapolated to $t \rightarrow \infty$ (Ref. 72).

[c] 3-(4-methyl-3-pentenyl)-3-cyclohexene-1-carbaldehyde + 4-(4-methyl-3-pentenyl)-3-cyclohexene-1-carbaldehyde

[d] This ingredient (a musk fixative) was included in Vector B, but not in Vector A.

[e] 0-7.25 h only

compound-independent proportionality constants k_1^v, k_2^T, k_3^T, etc. The latter values were averaged across compounds in a sequential manner (see below) to give the values reported in Table 4.2. Finally, the average values were used to simulate the evaporation profiles for all of the compounds. Thus, in the final step of the analysis, the evaporation rates for 11 compounds (Vector A) or 12 compounds (Vector B) were calculated based on three physico-chemical properties (P_{vp}, S_{oct} and MW) and either two (Model 1) or four (Models 2 and 3) adjustable parameters.

In conducting this analysis, Compounds XI and XII were excluded from the fitting procedure, as the extent of evaporation was not sufficient to allow an unambiguous determination of the rate constants (cf. Ref. 72). However, they were included in the simulation phase of the analysis. Comparison of the calculated and observed evaporation profiles for these compounds is an unbiased, albeit limited, test of the predictive power of the derived models.

Least squares fitting procedure. The parameters in each model were sequentially optimized by the method described previously.[73] The order of optimization was k_2^T followed by simultaneous determination of the other parameters. The sum of squared residuals $SSE = \sum_i w_i \left[y_i(obs) - y_i(fit) \right]^2$ was minimized for two different choices of the dependent variable y_i and the corresponding weights w_i. In the first (cumulative) version, y_i was taken to be the cumulative amount of each ingredient evaporated at time t_i, and $w_i = 1$. This is the fitting procedure used in Ref. 73. In the second (incremental) version, y_i was taken to be the incremental amount evaporated between times t_{i-1} and t_i, and $w_i = 1/y_i^2$. This procedure

minimized the relative errors in Δ(amount evaporated) at each time point; thus, it was much more sensitive to low evaporation rates occuring at later times in the study. For Models 2 and 3, the two weighting schemes gave substantially different parameter values as described below.

RESULTS

Representative semilogarithmic plots of evaporation rates versus time are shown in Fig. 4.2 and 4.3. After the first 15 min, most of the data plotted in this manner were either linear or reasonably so; this was the basis of the one-compartment kinetic analysis presented in Ref. 72. However, closer examination of these data revealed a systematic difference between Vector A (11-component mixture without fixative) and Vector B (12-component mixture with fixative). For most ingredients, the presence of the fixative agent – a musk, Compound XII – depressed the initial evaporation rate and increased the rate after 4-6 h. This led to log linear evaporation rate profiles for these components in Vector B (e.g., Fig. 4.2b) and curvilinear profiles for the same components in Vector A (e.g., Fig. 4.2a). This effect was especially pronounced for compounds having high volatility – the so-called "top notes" like linalool and limonene. Several of the plots also revealed a low evaporation rate for the initial 0-15 min interval. This effect may be attributed to a lag time for vapor collection resulting from the finite headspace between the skin surface and the vapor trap, as discussed elsewhere.[73]

Optimized parameters resulting from the kinetic model data analysis are shown in Table 4.2. Model 1 (one-compartment) was found to adequately represent both the cumulative evaporation and the evaporation rate profiles for the components of Vector B. Examples of such fitted curves

are shown in Figs. 4.2d and 4.2b, respectively. This finding is consistent with our earlier analysis of these data[72] and with the single exponential decay of the evaporation rates in this vector. Models 2 and 3 (two-compartments) offered no improvement in the fit; in fact, it was not possible to obtain unambiguous parameter values for these models when applied to the Vector B data.

Table 4.2. Regression parameters for compartmental models of fragrance ingredients studied in Ref. 48.

Vector A.

		Model		
Parameters	Unit	1	2	3
k_1^v	h^{-1}	14.5±10.5	14.1±9.5	14.3±9.8
k_2^τ	h^{-1}	1.9±0.6	1.3±1.1	1.9±1.8
k_{-2}^τ	h^{-1}	-	-	0.9±1.7
k_3^τ	h^{-1}	-	2.5±0.7	2.4±0.7
k_4^v	h^{-1}	-	1.9±2.5	-
n		170	150	150
χ_v^2		0.02	2.52	2.66

Vector B.

Parameters	Unit	Model 1
k_1^v	h^{-1}	9.1±8.9
k_2^τ	h^{-1}	1.5±0.5
n		160
χ_v^2		0.02

The findings for Vector A were substantially different. Model 1 still provided an adequate description of the cumulative evaporation versus time curves (c.f. Figs. 4.2c-d, Figs. 4.3c-d).

The absorption rate constant k_2^T obtained for Vector A (Table 4.2, Model 1) was significantly higher than that for Vector B (p = 0.013, Student's t-test). However, it was not possible to describe the details of the evaporation rate profiles for Vector A (c.f. Figs. 4.2a-b, Figs. 4.3a-b) using Model 1. The evaporation rates for most Vector A components simply could not be described as a single exponential decay.

The two-compartment models, Models 2 and 3, yielded better descriptions of the Vector A evaporation rates. In order to obtain a suitable match to the "tail" of these plots, i.e., the evaporation rates at times longer than 4 h, it was necessary to use the incremental model fitting procedure described in the Methods section. This may be seen by comparing the theoretical curves in Fig. 4.2a (cumulative fits) with those in Figs. 4.3a-b (incremental fits). The incremental procedure minimized differences in the small amounts evaporated at longer times, with a concurrent sacrifice in describing the cumulative evaporation profiles. However, the loss in the latter area would not seem to preclude the use of Models 2 and 3 in exposure assessment (c.f. Figs. 4.2c and 4.3c). Qualitatively, Model 2 led to slightly better descriptions of evaporation rates than did Model 3 (e.g., Fig. 4.3c), in agreement with a previous report.[73] However, there was no significant difference between the χ_ν^2 values of both the two-compartment models calculated from these approaches (Table 4.2).

By employing the optimized parameters from the analysis of Compounds I-X, we found that all three models could also satisfactorily predict the total evaporated fractions of Compound XI in both Vector A (Fig. 4.4a) and Vector B. However, the evaporation of the musk (Compound XII) was highly underpredicted in this case. Figure 4.5 shows the correlation between the observed and predicted values of the total evaporated fraction for all the compounds in Vector A.

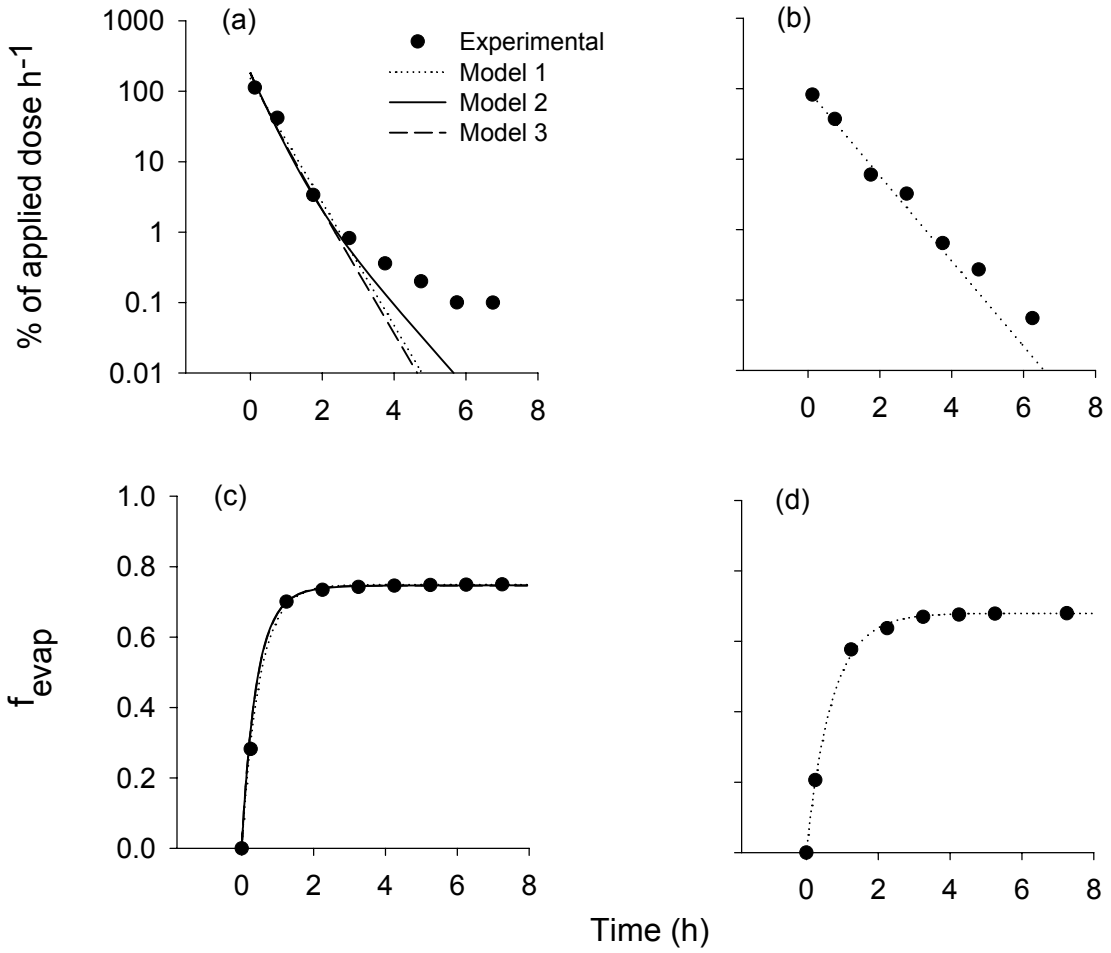

Figure 4.2. Evaporation of dihydromyrcenol from human skin *in vivo* (Trial 2).[4] (a) Evaporation rate, Vector A; (b) Evaporation rate, Vector B; (c) Cumulative evaporation, Vector A; and (d) Cumulative evaporation, Vector B. The model calculations were based on the cumulative fitting procedure.

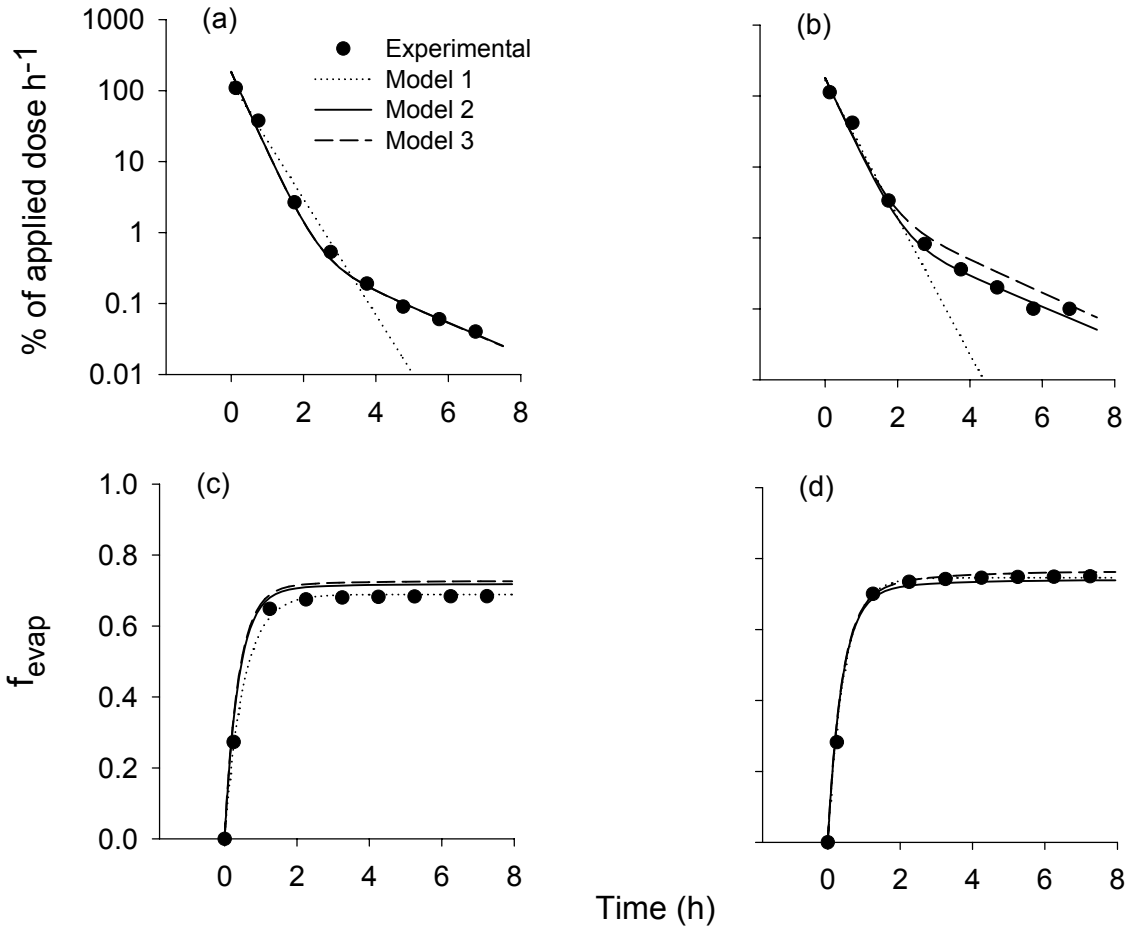

Figure 4.3. Evaporation of linalool (Compound I) and dihydromyrcenol (Compound II) from human skin *in vivo*, following application in Vector A (Trial 2).[4] (a) Evaporation rate, Compound I; (b) Evaporation rate, Compound II; (c) Cumulative evaporation, Compound I; and (d) Cumulative evaporation, Compound II. The model calculations were based on the incremental fitting procedure.

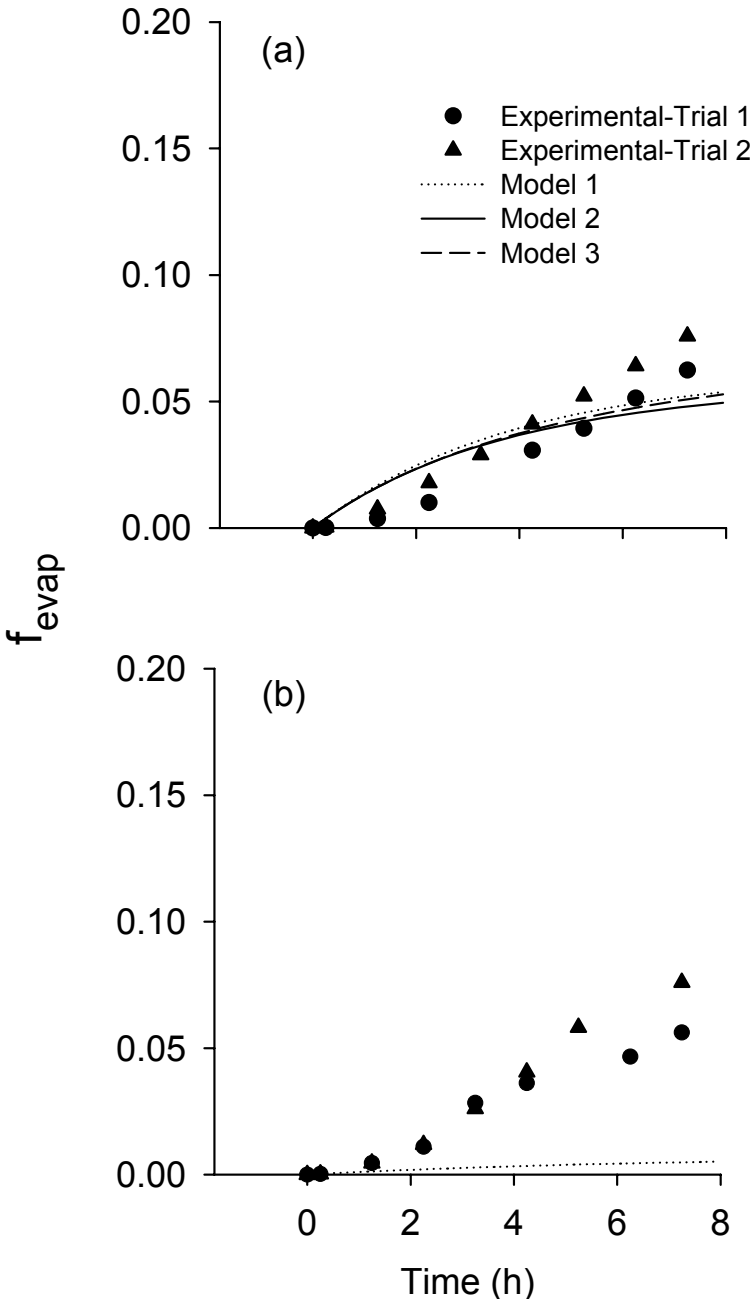

Figure 4.4. Cumulative evaporation of (E)-2-benzylideneoctanal (Compound XI) and 15-pentadecanolide (Compound XII) from human skin *in vivo*.[4] (a) Compound XI, Vector A and (b) Compound XII, Vector B. The model calculations were based on those average parameters reported in Table 4.2.

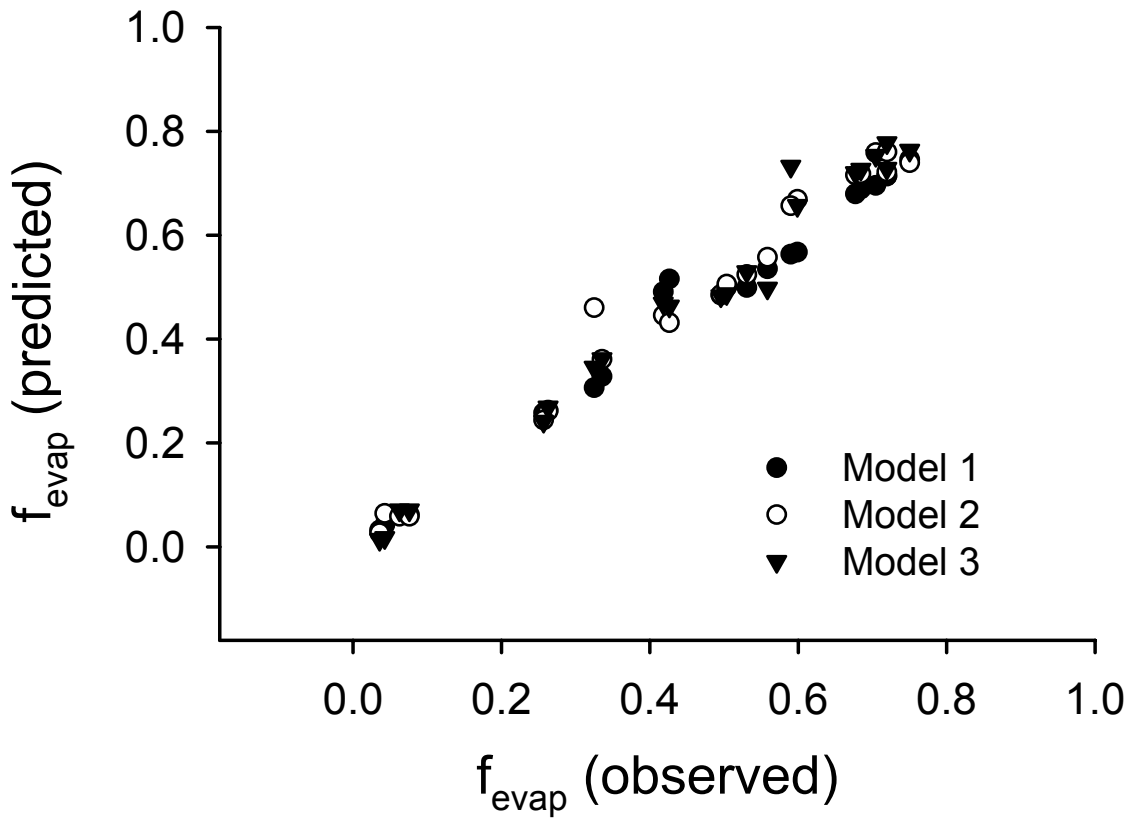

Figure 4.5. Predicted and observed values of the total evaporated fractions of each component in Vector A (both Trials 1 and 2). The model parameters used were those in Table 4.2.

No significant difference was found in the ability of Models 1, 2 and 3 to describe these data ($p >$ 0.6 based on a two-way ANOVA).

DISCUSSION

The above analysis shows a systematic difference of evaporation profiles of two nearly identical fragrance mixtures, which differed only in the presence (Vector B) or absence (Vector A) of the musk fixative, Compound XII. It is generally recognized that a fragrance fixative retards the evaporation of fragrance components in order to increase the life of a perfume on skin.

Quantitative analysis (e.g., Figs. 4.2a and 4.2b, see also Appendix C) supports this notion, as evaporation rates of dihydromyrcenol are sustained longer in Vector B than in Vector A. These findings and chemical intuition suggest that the musk lowers the thermodynamic activity of the other fragrance ingredients, thereby retarding both absorption and evaporation. The effect appears to be greatest for the most volatile components, i.e., the "top notes" of the fragrance.

The kinetic models described here provide a way of quantifying the differences in evaporation rates between fixed and unfixed fragrances. We found a one-compartment model (Model 1) to be adequate for the fixed fragrance, Vector B, whereas two-compartment models (Models 2 or 3) provided a better fit to the data for Vector A. However, none of the present models account explicitly for the ingredient interactions leading to the observed differences. In order to do so, it would seem appropriate to extend the analysis to a true diffusion/evaporation model incorporating activity coefficients to represent the interactions. Using the present dataset, we experimented with this idea by applying activity coefficients calculated by the UNIFAC/UNIQUAC approach[65] as multipliers to the kinetic rate coefficients, as described elsewhere.[73] Consistent with the previous finding, this approach failed to yield an improved description of the results. A longer term goal of our laboratory is to develop a plausible and calculationally manageable way of accounting for such ingredient interactions. This would seem to be critical in order to make accurate predictions for complex fragrance mixtures containing fixatives and for fragranced personal care products.

Both the one-compartment (Model 1) and two-compartment (Models 2 and 3) kinetic models yielded satisfactory correlations with total evaporated fraction of each component, with the

exception of the musk (Compound XII), whose evaporation was underpredicted in this report (c.f. Fig. 4.4b). In the absence of significant chemical reactivity or binding to skin, this correlation implies a similar correlation to fraction of dose absorbed. Thus, all of the models may have use for systemic absorption estimation in dermal risk assessment. Relative to Model 1, Models 2 and 3 yielded improved descriptions of the evaporation rate profiles for the unfixed fragrance vector, and comparable descriptions for the fixed fragrance. Thus, it would seem the latter models may have more utility than the one-compartment approach for product developers interested in quantifying the duration of aromas on skin.

CONCLUSIONS

A kinetic analysis of previously reported fragrance evaporation data on skin has shown both qualitative and quantitative differences between evaporation profiles from fixed and unfixed fragrances. The fixed fragrance (Vector B) led to nearly first-order evaporation kinetics that were well described by a one-compartment model. The unfixed fragrance (Vector A) led to more complex kinetics that could be approximated by a biexponential decay. Two alternative two-compartment models were developed to simulate this behavior. The analysis provides strong evidence for interactions of the more volatile fragrance components with fixative agents that should be explainable on a thermodynamic basis.

CHAPTER 5

DISPOSITION OF BENZYL ALCOHOL FOLLOWING TOPICAL APPLICATION TO HUMAN SKIN *IN VITRO*

INTRODUCTION

Fragrances are extensively used in cosmetics and personal care products for either odor masking or aesthetic purposes. These products are intended for daily contact with the skin. Allergic reactions to fragrance ingredients have become of increasing concern to both dermatologists and the cosmetic and toiletries industry. The penetration of an allergen into the skin is required for both induction and elicitation of skin sensitization.[71] Therefore, it is not surprising that the potential of a chemical to act as a contact allergen is related to its ability to penetrate the skin. One of the critical components in skin sensitization risk assessment is the determination of percutaneous absorption of those chemicals identified as potential allergens. Currently, 100% of the topically-applied dose from the leave-on products is often assumed for final exposure in assessing skin sensitization risk.[3] This is obviously an overestimate for volatile chemicals.

Computational models for dermal absorption are increasingly used in lieu of animal experiments to estimate absorption of new ingredients. However, the predictive models presently available for this purpose are either steady-state models[5,26] or are transient absorption models based on steady-state data.[27] Neither accurately represents the exposure conditions common to cosmetic and personal care products. The absorption rate of an ingredient from a small dose applied to skin differs significantly from absorption of a large dose.[6] For volatile materials the situation is even more complex, as a substantial portion of the dose may evaporate rather than absorb into the skin. A reliable computational model for predicting absorption and skin concentrations under these conditions would have great value in the area of dermatological and personal care product development, dermal risk assessment, and the mechanistic understanding of contact allergy.

The investigators have previously proposed a simple, first-order kinetic model for the absorption and evaporation of small amounts of volatile compounds applied to skin.[72] The model was used to interpret evaporation data obtained following application of fragrance mixtures applied to human volar forearm *in vivo*.[48] This report presents a detailed test of an extended first-order kinetic approach using combined absorption and evaporation data obtained following application of a single fragrance ingredient, benzyl alcohol, to human skin *in vitro*. Benzyl alcohol penetrates skin to a significant extent[7,10,11,16,74] and is one of the more frequently reported contact allergens,[75] possibly due to its widespread use in both fragrance and preservative systems for cosmetic products. However, it is not considered a high risk ingredient.

We show below that the previous one-compartment kinetic model[72] satisfactorily correlates the absorbed and evaporated fractions of benzyl alcohol from human skin *in vitro* with surface airflow over a wide range of airflow conditions. However, the detailed kinetics of these processes are missed by this approach. Two different two-compartment models that are presented provide significant improvements in this area by explicitly considering the surface film present in the early stages of evaporation. Thus, they represent an important step in the understanding and eventual prediction of skin absorption/evaporation phenomena.

THEORY

The absorption of a volatile compound or mixture from the skin surface is a combined diffusion/evaporation process. Immediately after application transport presumably occurs from a surface film, the components of which evaporate and absorb into the stratum corneum at

different rates depending on their physicochemical properties. Highly volatile and skin permeable components like ethanol dissipate rapidly, whereas less volatile, higher molecular weight compounds may reside on the skin surface for a substantial period of time. For mixtures, rapid evaporation of the more volatile compounds may lead to significant surface cooling, delaying the evaporation of other components by depressing their vapor pressure. Ingredients in solution may interact with one another, thereby altering activity coefficients. Hence, a complete description of the evaporation process involves the solution of a combined heat and mass-transport problem involving concentrated solutions with multiple ingredient interactions. Skin absorption makes the problem even more complex, as skin is a heterogeneous membrane comprised of multiple layers of substantial complexity.[5]

In this report, as in the previous one,[72] we have adopted the philosophy of offering the simplest solution to the problem that provides insight into the operative physical processes and has the potential to make useful predictions. We begin by briefly reviewing the one-compartment kinetic model, Model 1.[72] A schematic diagram is shown in Fig. 5.1a. The skin is assumed to be a single, well-stirred compartment that rapidly incorporates a topically-applied ingredient. The amount of the ingredient remaining in the skin at time t following application of amount A_0 at time zero is

$$A(t) = A_0 e^{-(k_1+k_2)t} \qquad (5.1)$$

where k_1 is the evaporation rate constant and k_2 is the absorption rate constant. The rate constants for each compound are functions of temperature (T), surface airflow (v), and three physico-chemical properties: vapor pressure (P_{vp}), molecular weight (MW), and lipid solubility

Figure 5.1. Schematic diagrams for compartmental models of skin disposition. a) One-compartment (Model 1); b) Two-compartments with evaporation from vehicle and skin (Model 2); c) Two-compartments with evaporation from vehicle only (Model 3).

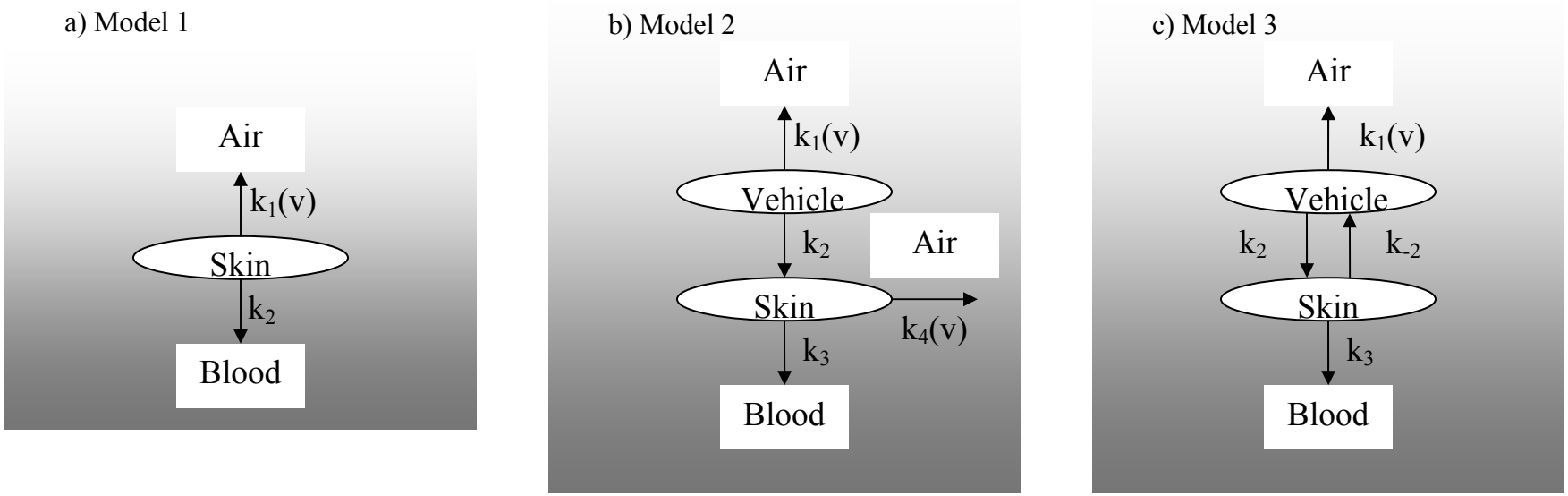

(S_{lip}). The latter is taken to be solubility in *n*-octanol, expressed as the product of water solubility (S_w) and octanol-water partition-coefficient (K_{oct}). Each property is expressed in dimensionless, or "reduced", form by dividing by a characteristic value; thus,

$$k_1 = k_1^v \cdot P_{vpr} / (K_{oct} \cdot S_w)_r \tag{5.2}$$

$$k_2 = k_2^T \cdot MW_r^{-2.7} \tag{5.3}$$

In eqs. 2 and 3, $P_{vpr} = P_{vp} / 1 \text{ torr}$, $(K_{oct} \cdot S_w)_r = (K_{oct} \cdot S_w) / 1000 \text{ g/cm}^3$, $MW_r = MW / 100 \text{ Da}$, and k_1^v and k_2^T are proportionality constants dependent on surface airflow and temperature, respectively. The fractions evaporated and absorbed after a long time are

$$f_{evap} = \frac{k_1}{k_1 + k_2} = \frac{x_r}{k + x_r} \tag{5.4}$$

$$f_{abs} = \frac{k_2}{k_1 + k_2} = \frac{k}{k + x_r} \tag{5.5}$$

where $k = k_2^T / k_1^v$ and $x_r = P_{vpr} MW_r^b / (K_{oct} \cdot S_w)_r$.

Equation 5.4 was used to correlate the evaporation of 10-11 perfume ingredients applied as two different mixtures to human skin *in vivo*.[48] Squared correlation coefficients, r^2, of 0.74 and 0.52 for fits of eq. 5.4 to the evaporated fractions were obtained, with standard deviations of 12 and 14%, respectively. Significant correlations of physical properties to the rate constants k_1 and k_2 were obtained according to eqs. 5.2 and 5.3. However, curvature of the semilogarithmic plots of evaporation rate versus time indicated that the evaporation rates of some ingredients could not be

described by the single exponential decay constant, $k_1 + k_2$, given in eq. 5.1. The curvature was suggestive of higher initial evaporation rates, as might be obtained from a surface film.

The previous analysis and the experimental results presented below suggest that an improved absorption/evaporation model might be obtained by including a surface film. Two ways in of doing this are shown in Figs. 5.1b and 5.1c. Both of these diagrams depict two well-stirred compartments – one representing the surface film (or vehicle), the other representing the skin. If the analysis is restricted to compounds of moderate lipophilicity such as ethanol, benzyl alcohol or most fragrance ingredients, the skin compartment may be considered to be the stratum corneum lipids, which form the primary barrier to penetration of such materials.[5,27] In Model 2 (Fig. 5.1b), evaporation is assumed to occur first from the vehicle, which is rapidly depleted by the combination of this process with partitioning into the skin. During the depletion process the volume of the vehicle layer continuously decreases until the layer finally disappears. Subsequent evaporation and absorption occur from the skin (or stratum corneum) compartment. The characterization of evaporation as two distinct processes makes sense only if the time constant for dissipation of the surface film, $1/(k_1 + k_2)$, is much less than that for the skin compartment, $1/(k_3 + k_4)$. If this is not the case, then Model 3 (Fig. 5.1c) should be considered. In Model 3 (Fig. 5.1c), the vehicle layer persists much longer, remaining as a discrete film until the last of the components has completely dissipated. Either of these scenarios might occur in practice, with the more volatile and/or skin permeable films dissipating according to Model 2 and less volatile/permeable films dissipating according to Model 3. We show below that Models 2 and 3 provide comparable descriptions of the dissipation of benzyl alcohol applied to skin in ethanol, and that these descriptions are more accurate at early times than that provided by Model 1.

It is possible to construct two-compartment models having additional rate constants involving reverse transfer from the blood or skin, or to add an additional compartment representing the viable skin layers.[76] Such additions would almost certainly improve the ability of the models to correlate data. However, unless the parameters associated with the additional features can be independently determined, the predictive power is likely to decrease. In the present analysis, we have forgone these elaborations and focused on the extent to which a four-parameter absorption/evaporation model (Model 2 or 3) can improve upon the description offered by a two-parameter model (Model 1). Of particular interest is the form of the surface airflow dependence for the evaporation rate coefficient k_1^v (eq. 2) and its analogs in the two-compartment models.

The rate equations for Models 2 and 3 are readily solved using standard methods for linear pharmacokinetic models.[77] The solutions are given in the Appendix. The integrated equations representing the amount of compound in air (the evaporated amount, eqs. A-3 and A-11) and in blood (the absorbed amount, eqs. A-6 and A-14) will be used to model the data from the *in vitro* evaporation/penetration studies. The physical properties dependencies of the rate constants (see eqs. 2 and 3) will not be considered in this report, as only one compound was studied. However, the airflow dependence of the parameters $k_1(v)$ and $k_4(v)$ in the *in vitro* diffusion/evaporation cells will be examined. Two simple functional forms are proposed (k_1 and k_4 are treated identically):

$$k_1(v) = k_1' \cdot v \qquad (5.6)$$

and

$$k_1(v) = k_1'' \cdot \frac{v}{v+b} \tag{5.7}$$

Equation 5.6 corresponds to a laminar flow model in which the thickness of the unstirred air layer limiting diffusion from the film is inversely proportional to the air velocity v. Equation 5.7 is an extension of the laminar flow model that allows for a component of the evaporative mass transfer resistance, i.e., a surface resistance $R_1 = 1/k_1''$, that is independent of v. At low airflows, eqs. 5.6 and 5.7 yield equivalent results, with $k_1' = k_1''/b$.

EXPERIMENTAL

Chemicals. 7-^{14}C-benzyl alcohol (55 mCi/mmol; 0.1 mCi/mL in ethanol) and unlabeled benzyl alcohol {CAS No. 100-51-6}; 99% (GC assay) were purchased from Moravek Biochemicals (Brea, CA) and Sigma-Aldrich (St. Louis, MO), respectively. The radiochemical purity of the ^{14}C-benzyl alcohol was stated by the manufacturer to be 98.3%.

The physical properties of benzyl alcohol are as follows: molecular weight (*MW*) = 108.1 Da, vapor pressure (P_{vp}) at 30°C = 0.0847 mmHg,[53] water solubility (S_w) at 30°C = 44.7 g/L[57] and octanol-water partition coefficient (log K_{oct}) = 1.1.[55]

Dose solution. In each experiment, 10 µl of a 1% w/v benzyl alcohol in ethanol (50 µCi/mL) was applied to each 0.79 cm^2 skin sample, giving an applied dose of approximately 127 µg/cm^2.

The low surface tension of the ethanolic solution allowed it to spread uniformly on the skin surface prior to evaporation of the solution.

Evaporation/penetration apparatus. Figure 5.2 shows the modified Franz diffusion cell used in the evaporation/penetration studies. The cells were custom-made by Dana Enterprises (West Chester, OH). The donor compartment (~ 4 mL) was modified by the addition of a side arm which allowed the passage of air through the cell. The top of the cell was connected to a Tenax TA cartridge (Supelco, St. Louis, MO) via a custom-made glass connector (Dana Enterprises) and an Omnifit® large variable connector for 4-11 mm tubing (Alltech Associates, Inc., Deerfield, IL). A PAS-500 micro air sampling pump (Spectrex, Redwood City, CA) was connected to the top of the adsorbent tube via silicone tubing to regulate the airflow through the evaporation cell. Room air was constantly drawn into the inlet of the evaporation cell, over the skin surface, and through the Tenax TA cartridge. The receptor compartment was stirred and maintained at 37°C by means of a thermostatted heating-stirring module, yielding a skin surface temperature of 30-32°C.[78]

Skin membrane. Dermatomed human cadaver skin (300 μm) was obtained from the Ohio Valley Tissue and Skin Center (Cincinnati, OH). The frozen skin was cut into small pieces (1.5 × 1.5 cm^2) and thawed in lukewarm, pH 7.4, Dulbecco's phosphate buffered saline (Sigma-Aldrich) containing 0.02% sodium azide prior to being mounted, epidermal side up, in the evaporation/penetration cell. The receptor compartment was filled with the same buffer solution. The dermal side of the skin was in contact with the receptor solution, and care was taken to ensure that no air bubbles were present.

Skin permeability test. Prior to each study, the integrity of the skin samples was checked using ^3H_2O as described previously.[79] The test involved a 5 min exposure to an excess of ^3H_2O, followed by receptor phase analysis after 1 h. Skin samples used in this study had water permeation values of 0.17 to 0.57 μg/cm^2. The skin surface was allowed to air dry prior to application of the ^{14}C-benzyl alcohol solution, as described below.

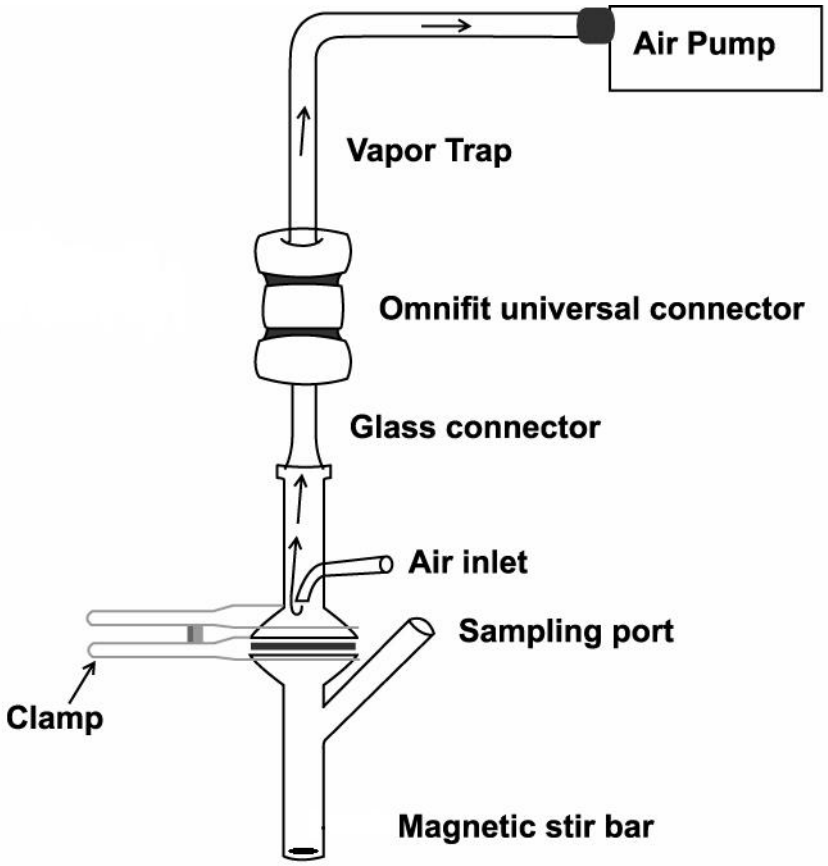

Figure 5.2. Apparatus for measurement of skin absorption and evaporation in vitro.

Evaporation/penetration studies. After the receptor solution was replaced twice to remove any residual ^3H_2O, the vapor trap was fitted to the evaporation cell as shown in Fig. 5.2. The system was then connected to the micro air pump to control the flow of air over the skin. After a one-

hour equilibration period, the glass connector was removed and the dose solution was applied to the epidermal side of the skin using a 10-µL Hamilton syringe. The system was reconnected immediately after dosing. The exact time of application was noted and designated as time zero for the experiment.

The vapor evaporating from the skin surface was entrained in the air and collected in the Tenax TA cartridge. Vapors were collected continuously. The cartridges were exchanged at 0.08, 0.25, 1.25, 2.25, 4.25, 6.25 and 8 h post-dose. Similarly, the receptor solution was removed and replaced at 0.5, 1, 2, 4, 6 and 8 h post-dose. Radioactivity was quantified by liquid scintillation counting (LSC) using a Beckman LS 6500™ multi-purpose scintillation counter (Beckman Coulter, Inc., Fullerton, CA).

After the 8 h samples were collected, the skin was dissolved in 2 mL of Soluene®-350 (Packard BioScience) and analyzed by LSC. The evaporation and penetration cells were separately rinsed with 1 mL of ethanol to remove any residual activity. The rinses were pooled and analyzed by LSC. Studies were conducted at 8 airflow rates ranging from 10-100 mL/min. Two trials were conducted at each airflow, with one diffusion cell per trial.

Vapor collection and desorption. Tenax TA cartridges collected during the study were desorbed directly into scintillation cocktail using flash heating at 180°C for approximately 10 to 15 minutes. During the desorption, ultra pure nitrogen gas at 20 mL/min was purged through the cartridges in the direction opposite to that of sample collection. After the desorption, the tubes

were reconditioned by passage of 40 mL/min ultra pure nitrogen gas and heating at 10-20°C above the desorption temperature for 20 minutes.

Data analysis. The evaporation and absorption rate data were plotted semilogarithmically vs. time. The linear compartmental pharmacokinetic models described earlier (Fig. 5.1) were fit to the cumulative absorption and evaporation data using nonlinear least squares. Prior to these fits the data were normalized by the recovered dose (Table 5.3, right-hand column), so that the total amount of radioactivity recovered agreed with the model prediction (100%) as $t \to \infty$. The normalization factor ranged from 90-105%. The effect of airflow (v) was accounted for by allowing k_1 and k_4 to vary linearly with v (eq. 5.6) or in a saturable manner (eq. 5.7). The parameters in each model were optimized using a computer program of our own design, in the sequence described below. The sum of squared residuals SSR = $\Sigma[y_i(\text{obs}) - y_i(\text{fit})]^2$ was minimized by means of a parabolic extrapolation algorithm.[59] Reduced chi-square values $\chi_v^2 =$ SSR/(n-p), where n is the number of observations and p is the number of adjustable parameters, were used to indicate the goodness of fit of the proposed models to experimental data.

<u>*Model 1*</u>. The optimum values of k_1' (eq. 5.6) or k_1'' and b (eq. 5.7) were determined by fitting the integrated rate equations to each dataset, then averaging the results. The value of k_2 was then redetermined for each dataset using the optimum value of k_1' (or k_1'' and b). The results for k_2 were then averaged across datasets to give values reported in Table 5.4. The logic of this procedure is that the evaporation rate constant (k_1) depends only on physico-chemical properties

of the permeant and the system; hence, it should be less variable than the absorption rate constant (k_2), which depends on skin permeability. By first determining k_1, a better estimate of skin permeability effects on k_2 may be obtained.

Model 2. Parameters were determined sequentially as for Model 1. The order of optimization was k_1', k_2, then (simultaneously) k_3 and k_4'.

Model 3. Parameters were determined sequentially in the order k_1', k_2, then (simultaneously) k_{-2} and k_3.

RESULTS

In vitro skin evaporation and absorption data for ^{14}C-benzyl alcohol at airflows ranging from 10-100 mL/min are listed in Tables 5.1 and 5.2. The mass balance for these studies is given in Table 5.3, and the results of the regression analyses for fits of Models 1-3 to the data are shown in Table 5.4.

The results in Tables 5.1-5.3 show that evaporation and absorption were strong functions of surface airflow. Higher airflow led to more rapid evaporation and a corresponding increase in cumulative percent evaporated, as would be expected from eqs. 5.6 or 5.7. This trend is shown clearly in Fig. 5.3, where cumulative evaporation and absorption over 8 h are plotted vs. airflow. Also shown in this plot are the predicted values from Models 1-3, calculated using the regression parameters in Table 5.4. For these simulations the linear evaporation rate model, eq. 5.6, was used to calculate the evaporation rate constants k_1 and k_4. The use of eq. 5.6 is restricted to

interpolation within the range v = 10-100 mL/min. Departures from this behavior are expected outside of this range, especially at lower values of v, since a finite evaporation rate is anticipated even in the absence of convective flow ($v = 0$).

Except for the lowest airflow rate, most benzyl alcohol evaporation occurred within 15 minutes post-dose (Table 5.1). Absorption was somewhat slower, but most occurred within 2 h (Table 5.2). By 8 h post-dose less than 3% of the applied dose was found in the skin, with one exception (Table 5.3). The overall recovery of radioactivity in these studies ranged from 90-105% of the applied dose, with a mean value of 97% (Table 5.3). Thus, the skin disposition of benzyl alcohol was largely complete within 8 h post-dose, and there was little evidence for binding of the compound to the skin.

Representative semilogarithmic plots of evaporation and absorption rates versus time are shown in Fig. 5.4. Examination of these plots revealed several consistent trends. At low airflow rates (10-30 mL/min) the initial evaporation rate (average rate from 0-5 min) was lower than that observed during the next time period, 5-15 min. An example may be seen in Fig. 5.4a. This may be attributed to a lag time for vapor collection resulting from the finite headspace (~ 4 mL) between the skin surface and the vapor trap. The initial low benzyl alcohol concentration, and correspondingly low chemical potential may also have contributed to this effect. It seemed unwise to attempt to model this effect on the basis of such limited data; hence, the 0-5 min values have been omitted from the regression analysis below. A second trend, also evident in Fig. 5.4, was that the absorption rate plots were nearly log linear following an initial time lag, whereas the evaporation rate plots were concave with respect to the top of the figure. Both of

Table 5.1. Evaporation of ^{14}C-benzyl alcohol from human skin *in vitro*. Values are expressed as the percentage of the applied dose (Table 5.3) that evaporated during each time interval.

Airflow rate (mL/min)	Trial	Percentage of dose						
		0.08 h	0.25 h	1.25 h	2.25 h	4.25 h	6.25 h	8 h
10	I	0.95	26.6	15.4	0.86	0.42	0.17	0.09
	II	0.66	18.6	26.0	0.99	0.47	0.15	0.08
20	I	2.5	46.6	9.2	1.1	0.63	0.29	0.23
	II	1.9	35.4	16.5	1.2	0.62	0.34	0.21
30	I	12.6	49.0	11.4	0.97	0.57	0.30	0.18
	II	18.5	43.5	6.6	0.94	0.63	0.29	0.17
40	I	41.4	26.1	4.7	0.59	0.32	0.17	0.10
	II	33.4	29.5	4.4	1.3	0.77	0.28	0.29
50	I	51.0	27.2	3.5	0.58	0.52	0.29	0.14
	II	40.3	34.5	4.7	0.81	0.39	0.15	0.11
65	I	54.7	11.0	2.3	0.43	0.26	0.19	0.11
	II	56.3	20.9	2.8	0.46	0.39	0.22	0.14
80	I	53.2	24.6	4.1	0.86	0.22	0.23	0.10
	II	62.6	18.9	2.1	0.51	0.23	0.12	0.09
100	I	73.0	8.7	4.0	0.70	0.28	0.25	0.17
	II	66.9	11.8	2.3	0.71	0.29	0.20	0.13

Table 5.2. Skin absorption data for ^{14}C-benzyl alcohol, expressed as in Table 5.1.

Airflow rate (mL/min)	Trial	Percentage of dose					
		0.5 h	1 h	2 h	4 h	6 h	8 h
10	I	15.2	18.8	10.7	2.7	0.60	0.24
	II	11.0	22.8	14.8	5.4	1.1	0.37
20	I	14.9	12.2	5.2	1.3	0.35	0.17
	II	9.9	15.9	9.2	2.6	0.59	0.21
30	I	5.0	7.8	5.7	1.7	0.26	0.09
	II	6.9	8.9	6.4	2.1	0.42	0.12
40	I	5.5	5.9	3.1	1.0	0.18	0.07
	II	7.0	9.1	6.0	2.3	0.43	0.15
50	I	4.2	3.7	2.3	0.65	0.13	0.05
	II	6.1	5.6	2.4	0.62	0.13	0.06
65	I	5.5	4.2	2.0	1.0	0.45	0.27
	II	5.5	4.8	2.7	0.81	0.18	0.07
80	I	3.3	3.9	2.5	0.77	0.16	0.07
	II	5.5	6.1	3.8	1.2	0.25	0.10
100	I	6.0	4.0	2.0	0.51	0.12	0.05
	II	5.5	3.9	1.7	0.54	0.11	0.04

Table 5.3. Mass balance for ^{14}C-benzyl alcohol skin disposition studies.

Airflow rate (mL/min)	Trial	Dose (μg/cm^2)	$^3H_20$ Permeability (μL/cm^2)	% of dose				
				Evaporation	Absorption	Skin	Cell wash	Total recovery
10	I	138.7	0.51	44.5	48.3	2.9	0.5	96.2
	II		0.44	46.9	55.4	1.9	0.4	104.6
20	I	118.1	0.17	60.6	34.0	1.6	0.2	96.4
	II		0.28	56.2	38.4	1.6	0.2	96.4
30	I	127.1	0.17	75.0	20.5	1.1	0.6	97.2
	II		0.40	70.6	24.8	1.3	0.4	97.1
40	I	129.1	0.26	73.4	15.8	0.7	0.3	90.2
	II		0.38	70.0	25.0	1.4	0.4	96.7
50	I	128.7	0.26	83.2	11.1	0.6	0.4	95.2
	II		0.36	81.0	14.9	0.6	0.6	97.1
65	I	120.8	0.29	69.0	13.5	8.7	0.2	91.4
	II		0.24	81.2	14.2	0.6	0.2	96.1
80	I	139.0	0.24	83.4	10.8	0.6	0.4	95.1
	II		0.57	84.5	16.9	0.7	0.6	102.6
100	I	119.1	0.48	87.2	12.7	0.5	0.1	100.5
	II		0.40	82.3	11.8	0.5	0.2	94.7
							Mean ± SD:	96.7 ± 3.6

Table 5.4. Regression parameters for compartmental models of benzyl alcohol skin disposition.

		Model		
Parameters	Units	1	2	3
$k_1'(v)$	$h^{-1}.(min/mL)$[a]	0.141±0.051	0.194±0.058	0.197±0.057
k_2	h^{-1}	1.6±0.8	3.8±1.5	3.5±1.2
k_{-2}	h^{-1}	-	-	0.6±0.4
k_3	h^{-1}	-	0.9±0.2	0.9±0.3
$k_4'(v)$	$h^{-1}.(min/mL)$[a]	-	0.013±0.009	-
n		120	120	120
s	% of dose	4.72	4.66	3.97
r^2		0.9792	0.9807	0.9862
χ_v^2	$(\%\ of\ dose)^2$	22.2	21.6	15.7

[a] Yields h^{-1} when multiplied by v in mL/min (eq. 5.6)

these trends can be qualitatively described using the two-compartment models, Models 2 and 3, as shown below. They cannot be described by Model 1, which leads to a single exponential decay rate for both evaporation and absorption.

Fit of pharmacokinetic models to experimental data. The rate constants for Models 1-3 were fit to the experimental data in Tables 5.1 and 5.2 as described in the Methods section. The results of this analysis are shown in Table 5.4. The linear evaporation model represented by eq. 5.6 yielded slightly better fits than eq. 5.7 and was therefore selected for this analysis. The cumulative percentages of benzyl alcohol evaporated and absorbed after 8 h were adequately described by all three of the pharmacokinetic models. This may be seen by examining the long-time skin disposition plots in Fig. 5.3. There was some evidence of systematic deviations of the model predictions from the experimental data, indicating that the dependence of evaporation rate on airflow may be more complex than that given in eq. 5.6. These deviations were not reduced

by the substitution of eq. 5.7 for eq. 5.6 or by the addition of a second compartment (Models 2 and 3).

Substantial differences were found in the ability of the three pharmacokinetic models to describe the time course of evaporation and absorption. Examples are shown in Fig. 5.4. Model 1, which yields a single exponential decay rate and no time lag for absorption through the skin, clearly missed the details of both the evaporation and absorption processes. The two- compartment models were somewhat better in this respect. Models 2 and 3 lead to a biexponential decay for evaporation rate and a time lag for skin absorption. We found that Model 2 yielded more consistent matches to the evaporation rate plots than did Model 3.

However, both models failed to accurately describe the pronounced "tail" of the evaporation rate plots (and, to a lesser extent, the absorption rate plots) at long values of the time. In other words, the evaporation rate of benzyl alcohol from the skin at long times was higher than predicted by the compartmental models. Although these differences could presumably be reduced by weighting them more heavily in the regression analysis, such improvements would come at the expense of accuracy in the cumulative evaporation and absorption estimates. This may be seen qualitatively by noting that slopes of the evaporation rate curves in Fig. 5.4 change continuously rather than bilinearly with time.

The regression statistics in Table 5.4 (s, r^2, χ_ν^2) indicate that Model 3 yielded slightly better fits to the combined datasets than did Models 1 and 2, using the sequentially determined parameter values reported in the table. The differences are significant ($p < 0.05$ for Model 3 vs. either

Model 1 or 2) based on an F-test of the χ_v^2 ratios.[59] This does not negate the fact that Model 2 more consistently described the evaporation rate data for individual datasets. Each of the three models has certain strengths, yet none of them provided a complete description of the data. Their utility ultimately hinges on their predictive power in other situations.

DISCUSSION

The kinetic analysis for benzyl alcohol disposition on skin presented here builds on an earlier analysis of *in vivo* skin disposition of a multicomponent fragrance mixture.[72] In the previous study only evaporation data were available and the data were collected at a single airflow rate. Thus, it was not possible to verify absorption rates or to test the airflow dependence (eqs. 5.6 and 5.7). The present study focuses on these factors. Since only a single compound was tested, it was not possible here to confirm the physical properties dependencies of the rate constants proposed earlier (eqs. 5.2 and 5.3). A comprehensive model of fragrance disposition on skin must combine these factors along with skin temperature and a defensible range of exposure conditions.[72] Considerable work remains in order to reach this objective. The investigators envision that a deterministic model of the nature described here can be combined stochastically with exposure variables such as wind velocity, temperature, body site and skin condition to produce improved dermal absorption estimates for fragrance ingredients and other volatile organic compounds that transiently contact skin.

The question of ingredient interactions deserves further attention. The present analysis, including the multicomponent mixture analysis,[72] does not consider such interactions; thus, each

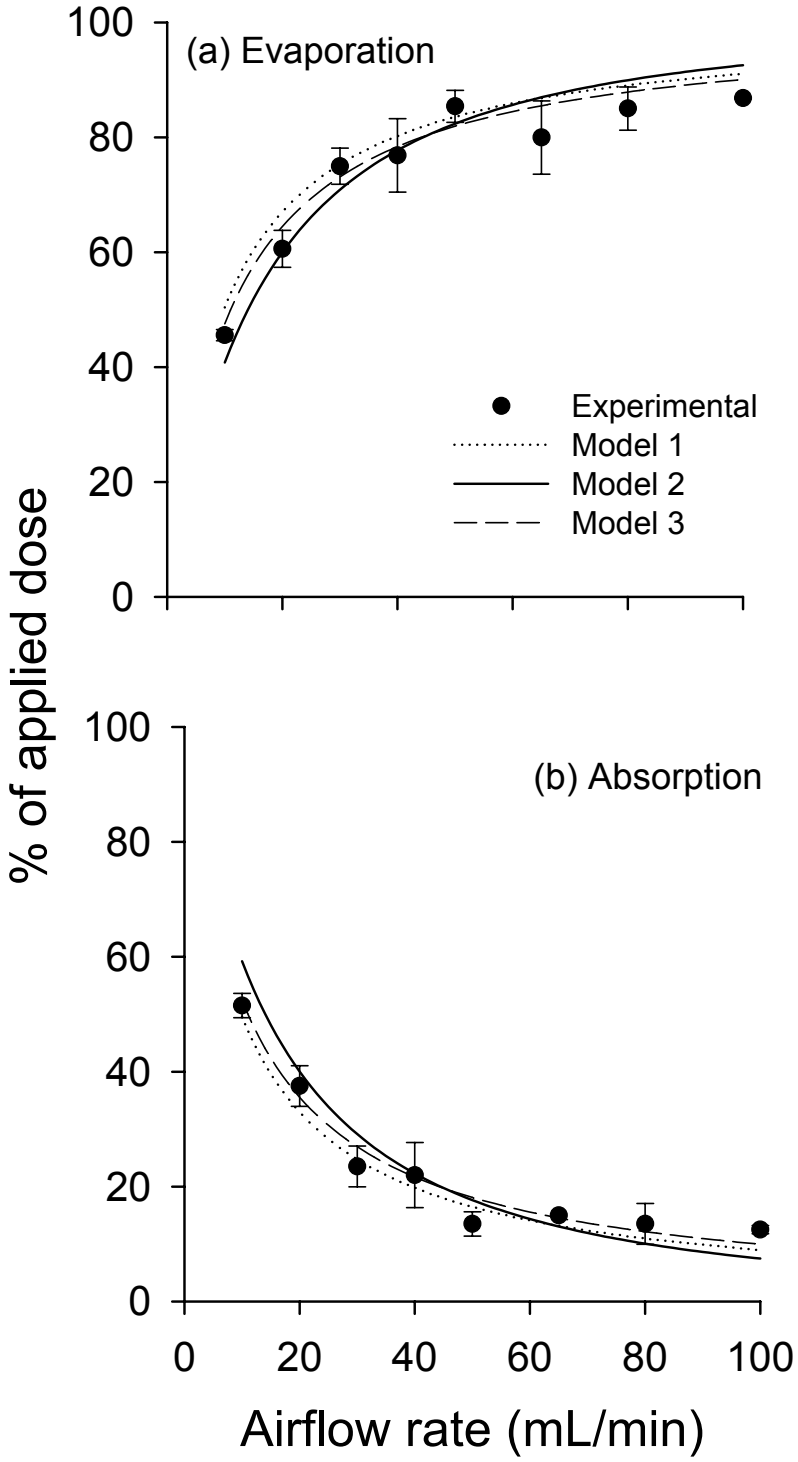

Figure 5.3. Correlations of a) total percentage of benzyl alcohol evaporated; and b) total percentage absorbed vs. surface airflow.

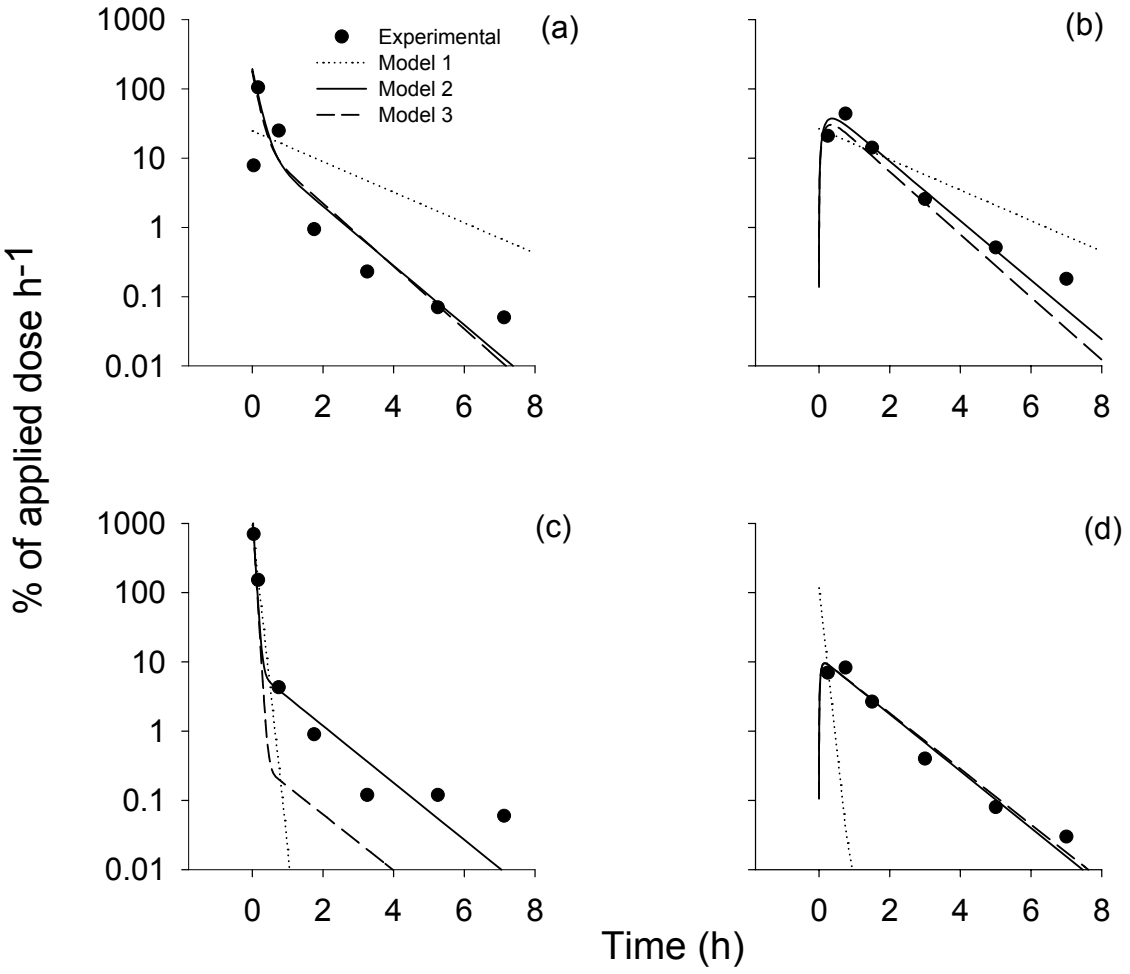

Figure 5.4. Evaporation and absorption rate plots of benzyl alcohol *in vitro* a) Evaporation (10 mL/min); b) Absorption (10 mL/min); c) Evaporation (80 mL/min) and d) Absorption (80 mL/min).

component is assumed to diffuse and evaporate independently. This is clearly an oversimplification of the physical situation, as thermodynamic activity of each component depends on the composition of the milieu in which it resides. In a true diffusion model these activities could be calculated as the product of local concentration and activity coefficient of

each component. Activity coefficients for fragrance ingredients and other small organic compounds in pharmaceutical systems have been successfully estimated using engineering methods such as UNIFAC and UNIQUAC.[65,80]

In anticipation of these developments, we tested one implementation of the activity coefficient correction for the present dataset, in which benzyl alcohol was applied to skin in ethanolic solution (data not shown). Evaporation and absorption rate constants for ethanol were estimated from those of benzyl alcohol using eqs. 5.2 and 5.3 and the appropriate ratios of physical properties. Activity coefficients in the vehicle and skin compartments were estimated from their current composition using the UNIFAC/UNIQUAC method.[65] To do this, the skin compartment was assumed to contain 0.15 mg/cm^2 of a lipid mixture having the chemical properties of *n*-octanol.[5,26] Activity coefficients thus calculated were used as multipliers for the evaporation and absorption rate constants in eqs. A-1, A-2, A-9 and A-10, and the rate equations were integrated numerically to produce corrected values of A_{air} and A_{bl}. These values were then compared to the observed evaporation and absorption values in Tables 5.1 and 5.2, and the rate constants were optimized by least squares.

Despite the considerable expenditure of time and energy, no significant improvements in fits to modeling the benzyl alcohol evaporation and absorption data were obtained by this process relative to the linear model results in Table 5.4. Therefore, this particular approach based on corrections to linear pharmacokinetic models cannot be recommended. However, it seems probable that careful implementation of this methodology in the context of a true diffusion

model, in combination with experimental observations on more than one component, would lead to more satisfactory results. This seems a promising area for further study.

CONCLUSIONS

Benzyl alcohol disposition on skin *in vitro* following topical application in ethanol is significantly influenced by airflow over the skin surface. A one-compartment, first-order kinetic model with an airflow-dependent evaporation rate constant (Model 1) provides a satisfactory description of the evaporated and absorbed fractions several hours post-dose. More details of the absorption and evaporation curves can be accounted for using two-compartment models (Model 2 and 3) that explicitly consider the initial dry down process on skin. With additional calibration from other compounds and *in vivo* exposures, these models may have value for predicting the disposition of volatile chemicals having transient contact with the skin.

APPENDIX: Solutions to two-compartment skin disposition models

The models shown schematically in Fig. 5.1 are analyzed as follows. Ingredient levels are expressed as the amount of material in each compartment, A, at time t.

Model 1 (Fig. 5.1a). See eqs. 5.1-5.5 and Ref.72.

Model 2 (Fig. 5.1b). The rate equations for this scenario are

$$\frac{dA_{veh}}{dt} = -\left(k_1 + k_2\right) A_{veh} \tag{A-1}$$

$$\frac{dA_{skin}}{dt} = k_2 A_{veh} - \left(k_3 + k_4\right) A_{skin} \tag{A-2}$$

These equations are integrated subject to the initial condition $A_{veh}(0) = A_0$; $A_{skin}(0) = 0$. Because A_{veh} does not depend on A_{skin}, eqs. A-1 and A-2 can be solved sequentially and the exponential decay constants for the vehicle and skin compartments are not coupled. This integrated equations are:

$$A_{air}(t) = \frac{A_0}{\alpha\beta\left(\beta - \alpha\right)} \left\{ \left[k_1 \beta \left(\beta - \alpha\right) + k_2 k_4 \beta\right] \left(1 - e^{-\alpha t}\right) - k_2 k_4 \alpha \left(1 - e^{-\beta t}\right) \right\} \tag{A-3}$$

$$A_{veh}(t) = A_0 e^{-\alpha t} \tag{A-4}$$

$$A_{skin}(t) = k_2 A_0 \left[\frac{1}{\beta - \alpha}\right]\left(e^{-\alpha t} - e^{-\beta t}\right) \tag{A-5}$$

$$A_{bl}(t) = \frac{k_2 k_3 A_0}{\alpha\beta(\beta - \alpha)}\left[\beta\left(1 - e^{-\alpha t}\right) - \alpha\left(1 - e^{-\beta t}\right)\right] \tag{A-6}$$

where $\alpha = k_1 + k_2$ and $\beta = k_3 + k_4$.

After a long time (t → ∞), the amount of ingredient in the air and the amount of ingredient absorbed into blood circulation can be expressed as

$$A_{air}(\infty) = \frac{A_0}{\alpha\beta}\left(k_1 k_4 + k_1 k_3 + k_2 k_4\right) \tag{A-7}$$

and

$$A_{bl}(\infty) = \frac{A_0}{\alpha\beta}\left(k_2 k_3\right) \tag{A-8}$$

where $\alpha\beta = k_1 k_4 + k_1 k_3 + k_2 k_4 + k_2 k_3$.

Model 3 (Fig. 5.1c). The rate equations for this model are

$$\frac{dA_{veh}}{dt} = -\left(k_1 + k_2\right) A_{veh} + k_3 A_{skin} \tag{A-9}$$

$$\frac{dA_{skin}}{dt} = k_2 A_{veh} - \left(k_3 + k_{-2}\right) A_{skin} \tag{A-10}$$

and the initial conditions are $A_{veh}(0) = A_0$; $A_{skin}(0) = 0$.

The equations are solved simultaneously using Laplace transforms. The integrated equations are

$$A_{air}(t) = \frac{k_1 A_0}{\alpha\beta(\beta-\alpha)}\left[(k_3 + k_{-2} - \alpha)\beta\left(1 - e^{-\alpha t}\right) + (\beta - k_3 - k_{-2})\alpha\left(1 - e^{-\beta t}\right) \right] \qquad \text{(A-11)}$$

$$A_{veh}(t) = \frac{A_0}{\beta-\alpha}\left[(k_3 + k_{-2} - \alpha)e^{-\alpha t} + (\beta - k_3 - k_{-2})e^{-\beta t} \right] \qquad \text{(A-12)}$$

$$A_{skin}(t) = \frac{k_2 A_0}{\beta-\alpha}\left[e^{-\alpha t} - e^{-\beta t} \right] \qquad \text{(A-13)}$$

$$A_{bl}(t) = \frac{k_2 k_{-2} A_0}{\alpha\beta(\beta-\alpha)}\left[\beta\left(1 - e^{-\alpha t}\right) - \alpha\left(1 - e^{-\beta t}\right)\right] \qquad \text{(A-14)}$$

where $\alpha = \frac{1}{2}\left[\alpha + \beta + \sqrt{(\alpha+\beta)^2 - 4\alpha\beta} \right]$

$$\beta = \frac{1}{2}\left[\alpha + \beta - \sqrt{(\alpha+\beta)^2 - 4\alpha\beta} \right]$$

$$\alpha + \beta = k_1 + k_2 + k_{-2} + k_3$$

$$\alpha\beta = k_1 k_3 + k_1 k_{-2} + k_2 k_{-2}\,.$$

After a long time (t → ∞), the amount of ingredient in the air and the amount absorbed into blood circulation can be expressed as

$$A_{air}(\infty) = \frac{k_1 A_0}{\alpha\beta}\left(k_3 + k_{-2}\right) \qquad \text{(A-15)}$$

and

$$A_{bl}(\infty) = \frac{k_2 k_{-2} A_0}{\alpha\beta} \qquad \text{(A-16)}$$

CHAPTER 6

EVAPORATION RATE OF BENZYL ALCOHOL FROM HUMAN SKIN *IN VIVO*

INTRODUCTION

We have recently constructed three first-order kinetic models[81] for estimating the absorbed and evaporated fractions of potentially volatile compounds applied onto the skin. All three models are based on known or easily obtained properties such as vapor pressure, molecular weight, and skin lipid solubility, in combination with skin temperature and surface airflow. Human *in vitro* skin penetration studies have been conducted using excised human skin and diffusion cells specially modified for volatiles collection, in order to test the above relationships under controlled conditions. However, this *in vitro* system requires calibration versus evaporation from human skin *in vivo*. This report presents a calibration of this nature in which the *in vivo* exposure conditions have been carefully controlled.

The study involved the use of dynamic headspace technology to measure the evaporation of benzyl alcohol from the forearm, using a custom-built volatiles collection system similar to that of Vuilleumier et al.[48] The effect of surface airflow velocity on evaporation was examined.

THEORY

To restate briefly for Model 1, the fraction of applied dose evaporated at time t is

$$f_{evap}(t) = \left(\frac{k_1}{k_1 + k_2} \right) e^{-(k_1 + k_2)\, t} \qquad (6.1)$$

where the evaporation rate constant k_1 is given by

$$k_1 = k_1^v \cdot P_{vpr} / (K_{oct} \cdot S_w)_r \qquad (6.2)$$

with $k_1^v = k_1^{'} \cdot v$ (6.3)

and the absorption rate constant is

$$k_2 = k_2^T \cdot MW_r^{-2.7} \quad (6.4)$$

In eqs. 6.2-6.4, P_{vpr} = vapor pressure (torr) / 1 torr, K_{oct} = octanol/water partition coefficient, S_w = water solubility (g/L), and MW_r = molecular weight / 100 Da. The superscript *r* on the product $K_{oct}S_w$ means the value is to be divided by 1000 g/L.

EXPERIMENTAL

Chemicals. Benzyl alcohol (CAS No. 100-51-6); 99% (GC assay) was purchased from Sigma-Aldrich (St.Louis, MO). A nonanol and GC-grade hexane (Fisher Scientifics) were obtained from Sigma-Aldrich and Fisher Scientifics, respectively, for the GC analysis.

Dose solution. In each experiment, 100 μL of a 1% w/v benzyl alcohol in ethanol was applied to an 8 cm^2 area of the forearm, yielding an applied dose of approximately 125 μg/cm^2.

Volatiles trapping. The sampling system (Fig. 6.1) consisted of a 10 cm^2 demountable glass cell with fittings for two velco straps. The system was custom-made by Dana Enterprises (West Chester, OH). A Tenax TA cartridge (Supelco, St. Louis, MO) was connected to a cell via an Omnifit® large variable connector for 4-11 mm tubing (Alltech Associates, Inc., Deerfiled, IL). A PAS-500 micro air sampling pump (Spectrex, Redwood City, CA) was connected to the top of the adsorbent tube via silicone tubing to regulate the airflow through the cell. Room air was

constantly drawn into the inlet of the trapping apparatus, over the skin surface, and through the Tenax TA cartridge.

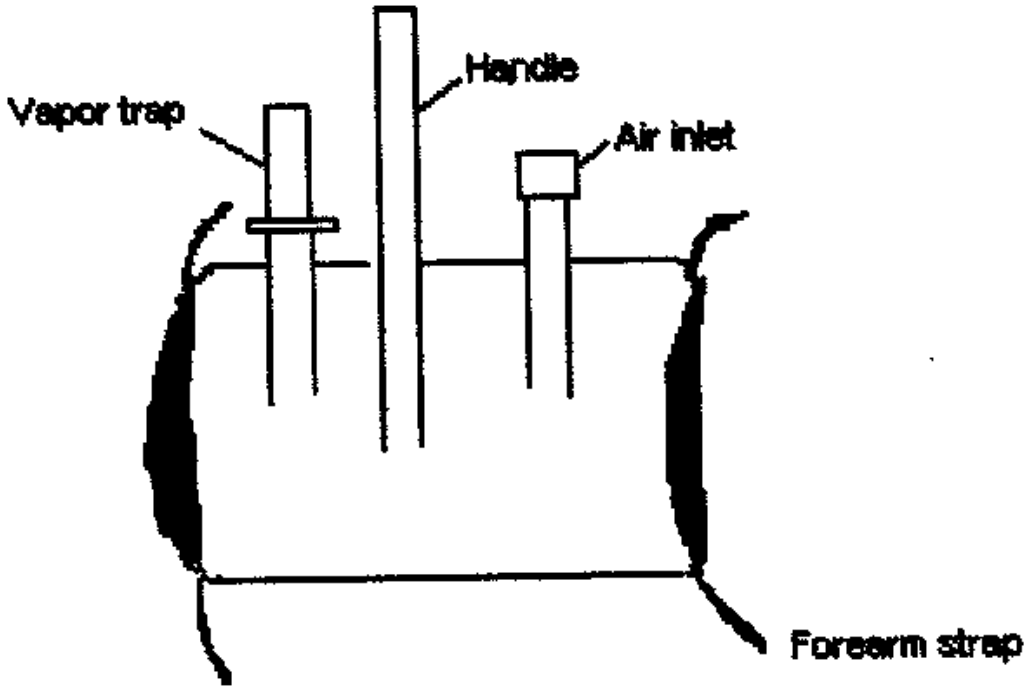

Figure 6.1. *In vivo* volatiles trapping apparatus.

Human subject. To minimize variations due to skin permeability differences, only one subject, a 23-year-old Indian female, was enrolled in the study. Prior to each experiment, the subject was asked to wash her left forearm with a mild, unfragranced detergent (Oil of Olay® Sensitive Skin Foaming Face Wash) and then dry it thoroughly. The subject then waited in the room for 30 minutes with the sleeve rolled up on her left arm.

Evaporation studies. After the subject was equilibrated, the dose solution was applied to the volar forearm of the subject using a 100-μL Eppendorf® pipettor. The trapping apparatus was then strapped onto the forearm immediately and tightly. The exact time of application was noted and designated as time zero for the experiment.

The vapor evaporating from the skin surface was entrained in the air and collected in the Tenax TA cartridge. Vapors were collected continuously. The adsorbent tubes were exchanged at 0.08, 0.17, 0.25, 0.5, 1 and 2 h after application.

Sample desorption. Each Tenax TA cartridge collected during the study was thermally desorbed into a glass wool-packed capillary tube mounted in a cold trap, into which the vapor was condensed. The desorption was performed at 180°C for approximately 15 minutes. During the desorption, ultra pure nitrogen gas at 20 mL/min was purged through the cartridges in the direction opposite to that of sample collection. After the desorption, one end of the capillary tube was sealed with the flame and 20 μL of 0.1% w/v nonanol in hexane was added to extract benzyl alcohol from the glass wool. The other end of the capillary tube was then sealed. The sample was centrifuged at 4°C, 1000 rpm for 3 minutes and kept in the refrigerator prior to the analysis. The desorbed cartridges were reconditioned by passage of 40 mL/min ultra pure nitrogen gas and heating at 10-20°C above the desorption temperature for 20 minutes.

Sample analysis. The samples were analyzed by capillary gas chromatography. The analysis was performed on a Varian 3300 gas chromatograph (Varian Associates, Inc., CA) fitted with 15m × 0.53mm ID Supelcowax 10® column. This type of column is widely used for separation

and purity analyses of many polar compounds, including alcohols, aromatics, flavors, fragrances and other solvents.[82] The flame ionization detector (FID) and the injection port were kept at 280°C. The initial relay for the injector was set at -1 (splitless mode). The column temperature was held at 110°C for 1 min, then raised to 180°C at a rate of 20°C/min and held at 180°C for 1 min. The flow rate of the nitrogen carrier gas through the capillary column was about 20 mL/min at a pressure of 8 psi. The samples were injected quickly into the injection zone using a Hamilton syringe Model 701 (Hamilton Co., NV). The sample injection volume was 1 μL. A Varian 4270 integrator (Varian Associates, Inc.) was used to measure the eluted peak areas. Nonanol (0.1% in hexane) was used as an internal standard for the quantitative analysis. Representative gas chromatograms are shown in Fig. 6.2.

Data analysis. The evaporated fractions of benzyl alcohol were determined from the chromatograms. The evaporation rate data were then plotted semilogarithmically vs. time. The parameters in Model 1 (Ref. 81) were optimized using a computer program of our own design. The sum of squared residuals $SSE = \sum [y_i(obs) - y_i(fit)]^2$ was minimized by means of a parabolic extrapolation algorithm.[59] Reduced chisquare values $\chi_v^2 = SSE/(n-p)$, where n is the number of observations and p is the number of adjustable parameters, were used to indicate the goodness of fit of the proposed models to experimental data. The optimum value of $k_1^{'}$ was determined by fitting the integrated rate equations to each data set, then averaging the results. The results for k_2 were then averaged across datasets to give a value reported in Table 6.3.

a)

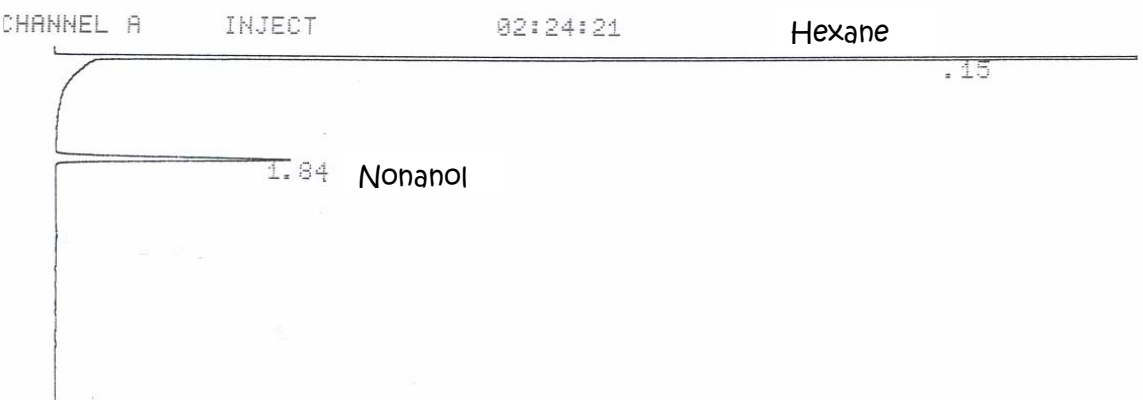

b)

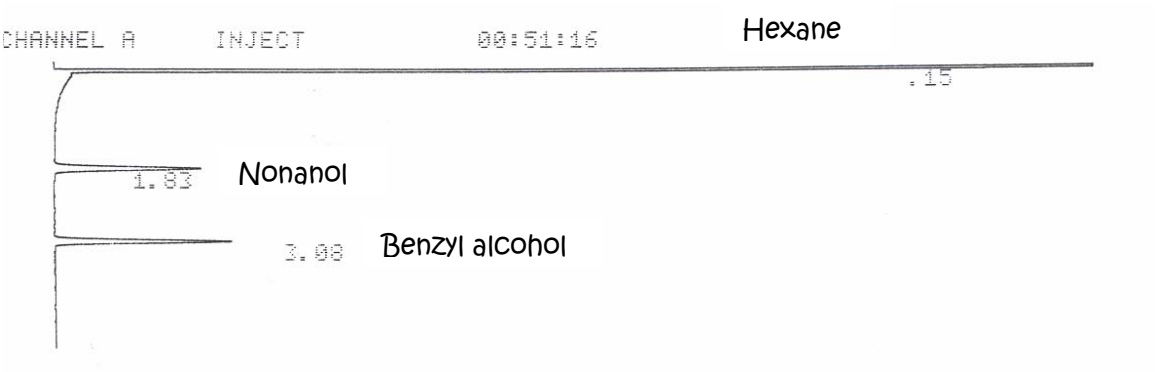

c)

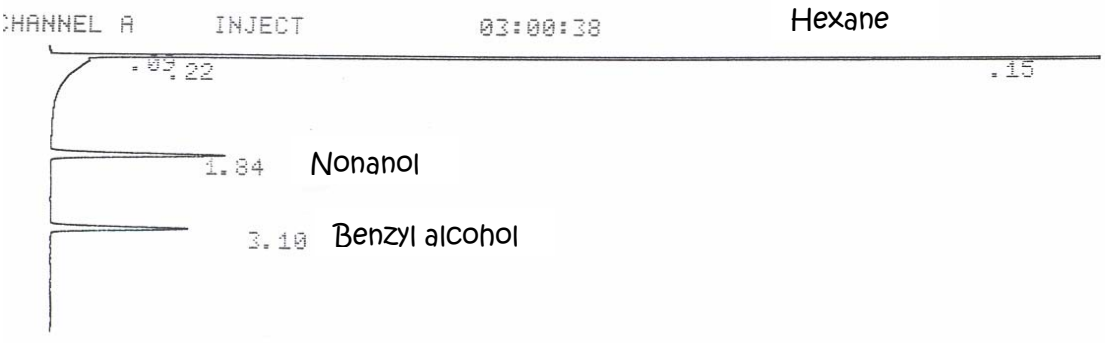

Figure 6.2. Representative gas chromatograms of a) internal standard, nonanol; b) benzyl alcohol standard; and c) benzyl alcohol desorbed sample.

RESULTS

Table 6.1 shows the cumulative evaporation of benzyl alcohol applied onto human skin at different surface airflow velocities. Similar to the findings from the *in vitro* studies, higher airflow led to more rapid evaporation and a corresponding increase in cumulative evaporated fraction.

Representative plots for observed and predicted cumulative evaporated fractions (linear scale) and evaporation rates (semi-log scale) vs. time are shown in Fig. 6.3. The predicted values are from Model 1, based on the parameters in Table 6.3. Examination of these plots revealed that the initial evaporation rates were relatively low. A similar trend was observed in the *in vitro* experiments. It may be attributed to a lag time for vapor collection resulting from the finite headspace between the skin surface and the vapor trap. These low evaporation rate values were omitted from the regression analysis.

Since the evaporation data were obtained only during the first two hours post-dose, we could not determine whether curvature existed at later stages as in the *in vitro* experiments. Only the data at 100 mL/min showed the possibility of a biexponential decay. Thus, we did not fit Models 2 and 3 to these data. Model 1 was found to adequately describe both the cumulative evaporated fractions and evaporation rate data within 2 hours after application.

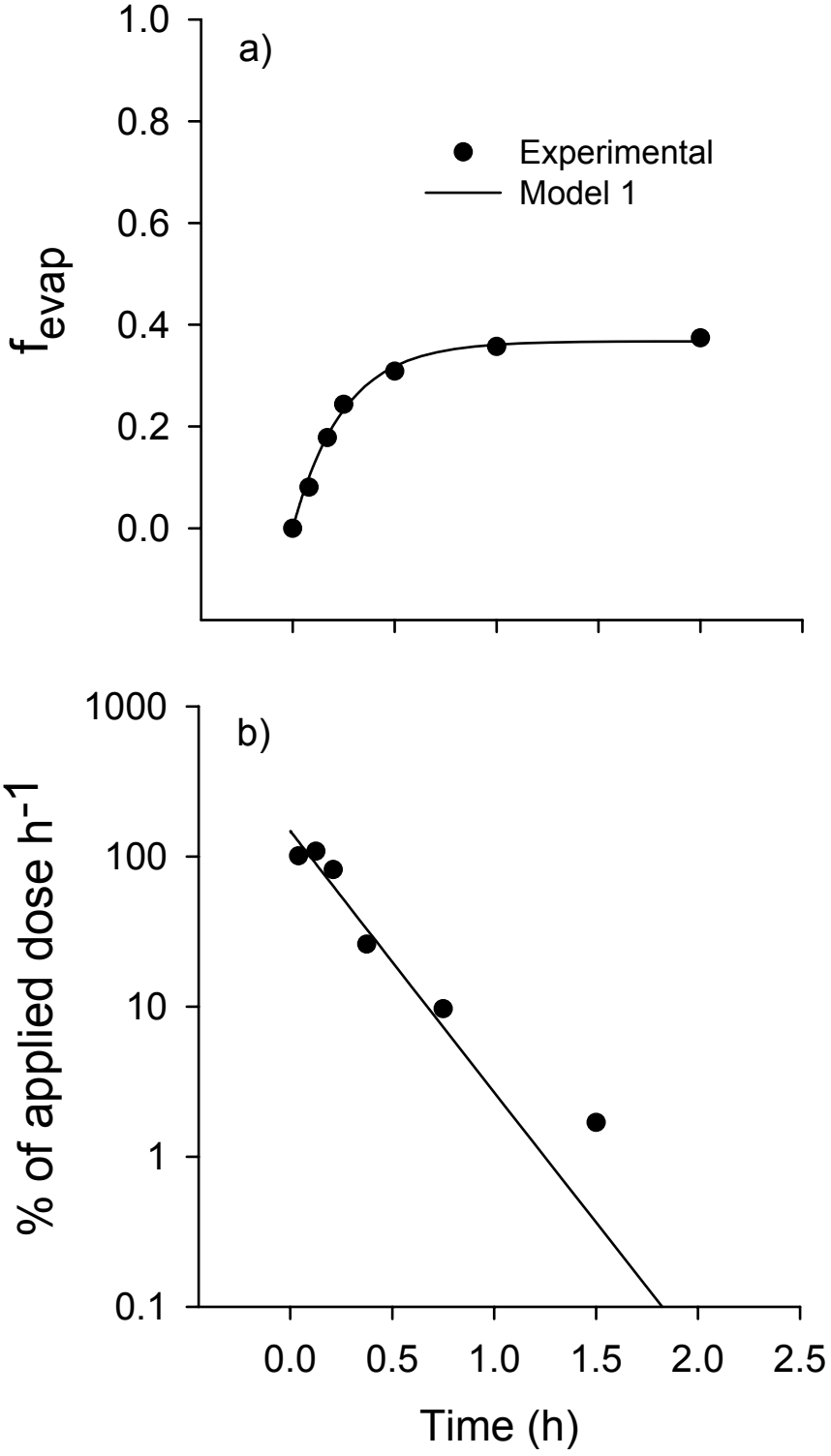

Figure 6.3. *In vivo* evaporation data for benzyl alcohol at 60 mL/min: a) Cumulative evaporated fraction and b) Evaporation rate.

The regression parameters for the fit of Model 1 to the cumulative *in vivo* evaporation data are shown in Table 6.3, in comparison to the results from the *in vitro* studies. The amounts evaporated *in vivo* from 0-2 hours were substantially lower than those evaporated *in vitro* (Table 6.2). The ratio also varied with the airflow rate. For the same applied dose, the *in vivo* data were found to be in a range of 27% (20 mL/min) to 60% (100 mL/min) of the *in vitro* data. The evaporation rate constant $k_1'(v)$ obtained from fitting the *in vivo* evaporation data was significantly lower than that obtained from fitting the *in vitro* evaporation and absorption data., whereas the absorption rate constants k_2 were the same within experimental errors (Table 6.3). This is to be expected because the volume of the *in vivo* dose cell (~32 mL) was much larger than that of the *in vitro* cell (~4 mL). On a volume adjusted basis, the evaporation rate constants were similar, as discussed below.

Due to the absence of absorption and total mass balance data, it was not possible to verify the *in vivo* absorption rates. The lower evaporation amount in the *in vivo* experiments relative to *in vitro* could be due to a variety of reasons. The volume difference of the evaporation chambers is most likely the largest factor. Another possible factor is the sensitivity differences between liquid scintillation counting technique and GC analysis. Based on the calibration results, the recovery from the GC analytical method was in the range of 80 to 90% of that from the scintillation counting analysis. Another factor may be differences in geometry of the *in vitro* evaporation cell versus that of the *in vivo* volatiles trapping apparatus, leading to differences in the airflow pattern within the cells. Other possibilities include loss of material from the apparatus during the study and retention of the applied material in human skin *in vivo*.

Table 6.1. Evaporation of benzyl alcohol from human skin *in vivo*. Values are expressed as the percentage of the applied dose (125 $\mu g/cm^2$) that evaporated during each time interval.

Airflow rate	Percentage of dose					
(mL/min)	0.08 h	0.17 h	0.25 h	0.5 h	1 h	2 h
20	0.03	0.04	1.51	7.59	3.96	2.73
40	0.67	6.69	6.93	9.14	7.20	3.67
60	8.08	9.75	6.54	6.51	4.84	1.69
80	8.96	13.48	6.10	8.08	8.58	3.68
100	11.60	12.60	6.95	10.82	3.93	5.67

Table 6.2. Comparisons of the evaporated fractions at 2 h after application of benzyl alcohol *in vivo* and *in vitro*.

Airflow rate	*in vivo*	*in vitro*[a]	Ratio
(mL/min)			*in vivo/in vitro*
20	0.16	0.59 ± 0.03	0.27
40	0.34	0.76 ± 0.07	0.45
60[b]	0.37	0.79 ± 0.06	0.47
80	0.49	0.84 ± 0.04	0.58
100	0.52	0.86 ± 0.00	0.60

[a]Data from Chapter 5 (Ref. 81)
[b]65 mL/min for *in vitro* experiments

Table 6.3. Regression parameters for one-compartment kinetic model (Model 1) for benzyl alcohol applied to skin in an ethanolic vehicle.

Parameters	Units	*in vivo*[a]	*in vitro*[b]
k_1'	h^{-1}.(min/mL)[c]	1.9 ± 0.4	14.1±5.1
k_2	h^{-1}	1.8 ± 0.3	1.6±0.8

[a]This study
[b]Data from Chapter 5 (Ref.81)
[c]Yields h^{-1} when multiplied by v in mL/min

DISCUSSION

Because the slope of the semilog plot of evaporation rate versus time is proportional to $k_1 + k_2$ and the total fraction evaporated is equal to $k_1/(k_1 + k_2)$ (cf. eq. 6.1), analysis of evaporation data allows the estimation of absorption rates. As shown in Table 6.3, independent analysis of the evaporation rate data for benzyl alcohol *in vitro* and *in vivo* leads to consistent estimates of the absorption rate constant, k_2. This is to be expected if the cadaver skin model studied *in vitro* adequately represents the barrier properties of skin *in vivo*. For the present studies, this appears to be the case.

The multiplier for evaporation rate constant, k_1^v (defined by eq. 6.3) was found to be 7.4-fold lower in the *in vivo* study than in the *in vitro* study (Table 6.3). This ratio is very close to the inverse of the dose cell volume ratio, 4 mL / 32 mL = 1/8. To a first approximation, this is the expected relationship, since the headspace air moved on average 8-fold more slowly in the *in vivo* study and the airflow dependence of k_1 is roughly linear in v (see eq. 6.3 and Ref. 81). Different cell geometries and potentially nonlinear airflow dependencies could lead to a more complicated relationship between *in vivo* and *in vitro* cell parameters. However, it seems that the inverse volume ratio is a good starting point for relating the properties of these two systems.

The current methodology still requires calibration with materials whose evaporation under less controlled conditions is known. This would close the loop between the *in vitro* studies, controlled *in vivo* studies, and common *in vivo* exposure conditions. Experiments of this nature are underway in our laboratory.

CONCLUSIONS

Evaporation of benzyl alcohol from human skin *in vivo* under controlled conditions appears to follow the same (nearly first-order) kinetics as evaporation *in vitro*. A calibration factor relating the two experimental systems has been developed. Further work is required to relate these values to evaporation rates under conditions experienced by fragrance products consumers.

CHAPTER 7

PREDICTION OF FRAGRANCE HEADSPACE CONCENTRATIONS FROM PHYSICO-CHEMICAL PROPERTIES

INTRODUCTION

The amount of fragrance raw materials exposed to skin from fragranced products usually falls within the small dose limit in which nearly first-order absorption is anticipated.[6] On this basis, the authors have described a first-order kinetic model drawing on previous work in skin penetration and environmental engineering.[72] The model allows calculation of absorbed and evaporated fractions of topically applied chemicals based on three key physical properties– vapor pressure, molecular weight and lipid solubility– in combination with skin temperature and wind velocity. The evaporated fraction calculated from this model satisfactorily correlated experimental data on fragrance evaporation from human skin *in vivo*.[48]

However, additional tests are required to validate the first-order kinetic model and to optimize its predictive power. In the present report, the details of an analysis of skin evaporation data presented by Mookherjee and coworkers[70] are given. The study involved the application of different fragrance mixtures on the forearm of human subjects. The volatiles were collected using the SPME (solid-phase micro-extraction) technique.[83] The headspace samples were analyzed by GC/MS.

One of the underlying assumptions of the current model[72] is that the behavior of each fragrance raw material is independent of other ingredients in the mixture. In reality, ingredient interactions affecting both absorption and evaporation are possible, especially when applied doses are high. Each ingredient can modify the thermodynamic activity of other components according to well-known laws governing liquid-liquid and liquid-vapor mixtures.[65] Thus, in the present analysis,

we have included calculations of the activity coefficients in order to determine whether this parameter may improve the accuracy of the model predictions.

DATA ANALYSIS

Theory

- Based on a one-compartment first-order kinetic model,[72] the percentage evaporated of a topically applied compound can be calculated using the following equation:

$$\%evap\,(t) = 100\left(\frac{k_1}{k_1 + k_2}\right)\left[1 - e^{-(k_1+k_2)\,t}\right] \qquad (7.1)$$

In eq. 7.1, k_1 and k_2 represent, respectively, the evaporation and absorption rate constants. They can be calculated using the following equations.

$$k_1 = k_1^v * P_{vpr} / \left(K_{oct} S_w\right)_r \qquad (7.2)$$

and

$$k_2 = k_2^\tau * MW_r^{-2.7} \qquad (7.3)$$

In eqs. 7.2 and 7.3, P_{vp} = vapor pressure in torr, K_{oct} = octanol/water partition coefficient, S_w = water solubility in g/L, and MW = molecular weight. The subscript '*r*' indicates the reduced or dimensionless form of each parameter. The properties $P_{vpr} = P_{vp} / 1\,\text{torr}$, $\left(K_{oct} S_w\right)_r = \left(K_{oct} S_w\right) / 1000\,\text{g/L}$ and $MW_r = MW / 100\,\text{Da}$ are chosen for

computational convenience. Both k_1^v and k_2^τ are constants, which must be determined experimentally. For the present analysis, we used k_1^v and k_2^τ values determined in Ref. 72 by calibration with an earlier experimental study.[48] The product $K_{oct}S_w$ is used, for convenience, to represent octanol solubility, which is a measure of solubility in stratum corneum lipids.[72]

Methods

- Five of the perfumes studied in Ref. 70 were analyzed-- Shalimar, Amarige, Unisex, Feminine and Women's Fragrances. Predicted values of the percentage evaporated after 1 hour were calculated using eq. 7.1. These values were then corrected to represent the predicted concentrations in the headspace samples for direct comparison with the published experimental values. In some cases, the concentrations of each ingredient were corrected in proportion to the activity coefficient parameter, and the predicted headspace concentration values were recalculated using the modified concentrations.

- Vapor pressures at skin temperature (30°C)[53] and octanol-water partition coefficients[55] were estimated using commercially available computer programs. Octanol solubility values were calculated using the formula suggested by Kasting et al.[49] Water solubilities were calculated from octanol solubility values and octanol-water partition coefficients according to the relationship $S_w \approx S_{oct} / K_{oct}$.

Table 7.1. Physical properties and predicted percentage evaporated values of fragrance raw materials studied in Ref. 70.

Component	MW (Da)	P_{vp} (mm Hg)	Log K_{oct}	S_w (mg/ml)	k_1 (h^{-1})	k_2 (h^{-1})	Total %evap	After 1h %evap
Aldehyde AA					NA			
Ambrox	236	0.0069	5.40	0.0017	0.15	0.15	50.4	12.9
Bacdanol	208	0.00015	4.54	0.015	0.003	0.21	1.2	0.2
Benzyl acetate	150	0.28	1.96	8.9	3.10	0.50	86.1	83.8
Benzyl salicylate	226	3.7E-05	3.76	0.024	0.002	0.17	1.4	0.2
Cashmeran	206	0.0071	4.62	0.010	0.15	0.21	42.0	12.9
Cedramber	236	0.016	6.16	0.00036	0.28	0.15	65.6	22.8
Coumarin	146	0.0012	1.39	14.1	0.03	0.54	5.6	2.4
Cyclogalbaniff	198	0.033	2.86	1.1	0.37	0.24	60.8	27.6
Cyclopentadecanolide	240	0.0085	5.35	0.0035	0.10	0.14	41.0	8.7
alpha-Damascone	192	0.032	3.62	0.16	0.43	0.26	62.8	31.3
beta-Damascone	192	0.022	3.77	0.10	0.35	0.26	57.8	26.4
Dihydro myrcenol	156	0.19	2.99	0.83	2.16	0.45	82.8	76.7
Diphenyl ether	170	0.029	4.21	0.050	0.32	0.36	47.6	23.5
Ethyl acetoacetate	130	1.3	0.24	468	14.78	0.74	95.3	95.3
Ethyl linalool	168	0.029	3.08	0.68	0.32	0.37	46.7	23.3
Ethyl vanillin	166	0.00056	1.58	8.6	0.02	0.38	3.9	1.3
Floralozone	190	0.0088	3.60	0.16	0.13	0.26	32.7	10.6
Galaxolide	258	0.00017	6.06	0.00023	0.006	0.12	4.8	0.5
Givescone	210	0.020	4.34	0.031	0.27	0.20	56.9	21.2
Hedione	226	0.00077	2.42	1.6	0.02	0.17	9.2	1.5
beta-Ionone	192	0.069	4.00	0.056	1.11	0.26	81.2	60.5
Iso E Super	234	0.0020	5.23	0.0020	0.05	0.15	26.1	4.8
cis-Jasmone	164	0.036	2.64	1.5	0.48	0.39	55.1	32.2
Limonene	136	2.0	4.57	0.022	22.61	0.65	97.2	97.2
Linalool	154	0.13	2.97	0.87	1.46	0.47	75.8	64.7
Linalyl acetate	196	0.20	3.50	0.26	2.18	0.24	90.0	82.0
Lolitol					NA			
Methyl ionone	206	0.062	4.23	0.030	1.10	0.21	83.9	61.4
Methyl octin carbonate	168	0.16	3.10	0.55	2.03	0.37	84.7	77.0
Methyl phenyl acetate	150	0.23	1.83	12	2.61	0.50	83.9	80.2
Musk xylol	297	1.4E-06	4.04	0.023	0.00005	0.08	0.1	0.005
Passionfruit compound					NA			
Polysantol	222	0.00025	4.61	0.012	0.005	0.17	2.6	0.4
Styrallyl acetate	164	0.26	2.27	4.4	2.96	0.39	88.3	85.2
Tonalid	258	0.032	6.25	0.00038	0.44	0.12	79.3	33.9
Undecavertol	170	0.010	3.69	0.17	0.11	0.36	23.9	8.9

NA = Not Available

- Activity coefficients were calculated using the UNIFAC model.[65] The calculations were performed using a user-friendly Excel workbook.[84] This program allows the user to select mixtures of up to 15 components.

RESULTS

The physico-chemical properties and the predicted percentage evaporated values of each fragrance raw material in all five mixtures are summarized in Table 7.1. The experimental and predicted values of headspace concentration along with the activity coefficients for each ingredient in the composition at time zero are reported in Tables 7.2-7.6. Comparisons between observed and predicted values are shown in Figs. 7.1-7.6.

DISCUSSION

In all cases except Shalimar (Fig. 7.1), the predicted headspace concentrations correlated reasonably well (r^2 = 0.70-0.76) with experimental values.[70] There was a weak correlation (r^2 = 0.32) between the observed and predicted percentage evaporated values in Shalimar. However, once limonene was removed from the analysis, a stronger correlation was obtained (r^2 = 0.57). The correlation in Unisex Fragrance was also improved when limonene was excluded from the plot (r^2 = 0.87). In both cases, the model overestimated the headspace concentration of limonene, which is a relatively low molecular weight fragrance raw material with high vapor pressure. A similar result was also found with benzyl acetate and ethyl acetoacetate, which have

similar physical properties to limonene. We noted that each perfume in the study contained one or more fragrance fixative(s) such as galaxolide and musk xylol. The mechanism for the fixative activity of these materials is depression of the volatility of the low to moderate boiling point components of the final perfume. This, in turn, extends the duration of the fragrance intensity by reducing the rate at which the fragrance components evaporate from the skin. In general, the fragrance fixative should have an affinity for the more volatile fragrance molecules (top notes), so that the odor of the perfume is more consistent throughout its life. The fixative activity is not explicitly accounted for in the current model, although the parameters used for the calculation were developed for a fixed fragrance mixture. Based on the present analysis, we found that the current model generally overpredicted the evaporation of the top note ingredients while it often underpredicted the evaporation of the fragrance fixatives, which are the least volatile compounds in the mixture. Compounds having intermediate volatilities were, in general, better predicted.

The linear regression data show that, on average, the model predicted the experimental data to within a factor of 1 to 4. However, examination of the data in Tables 7.2-7.6 shows that about half of the ingredients in the list were not accurately predicted by the model. In the worst case, the observed values deviated from the predicted values by a factor of 340. The discrepancies could be related to a number of factors. First, the constants used for estimating evaporation and absorption rate constants were obtained from experiments conducted under different conditions. Second, the values of vapor pressure used in the analysis were estimated values only, as we could not find well-documented experimental values. These estimations may introduce significant errors. Third, there may be some experimental errors associated with the data, e.g.,

Table 7.2. Shalimar fragrance: oil and headspace composition

	Component	Oil Conc (%)	Headspace Conc (%)			Activity	Ratio	Ratio
			Obs	Pred	Pred[a]	Coefficient	(Pred/Obs)	(Pred[a]/Obs)
I	Limonene	30	20.4	53.5	50.8	1.0480	2.6	2.5
II	Linalool	1.7	17.9	2.0	4.4	2.4141	0.1	0.2
III	Linalyl acetate	9.9	21.6	14.9	15.1	1.1209	0.7	0.7
IV	Ethyl vanillin	0.2	1.6	0.005	0.03	7.9705	0.003	0.02
V	Coumarin	1.7	7.8	0.1	0.2	2.6334	0.01	0.02
VI	Methyl ionone	1.1	2.1	1.2	1.2	1.0469	0.6	0.6
VII	Musk xylol	trace	0.3	NA	NA	NA		
	Total	44.6						

Table 7.3. Amarige fragrance: oil and headspace composition

	Component	Oil Conc (%)	Headspace Conc (%)			Activity	Ratio	Ratio
			Obs	Pred	Pred[a]	Coefficient	(Pred/Obs)	(Pred[a]/Obs)
I	Linalool	1.7	17.9	10.9	12.2	1.4154	0.6	0.7
II	Benzyl acetate	4.9	22.7	40.6	29.9	0.9274	1.8	1.3
III	Styrallyl acetate	1.2	9.7	9.7	7.1	0.9209	1.0	0.7
IV	Cashmeran	NA	0.5	NA	NA	NA	NA	NA
V	Bacdanol	0.2	0.5	0.005	0.006	1.5900	0.01	0.01
VI	Hedione	29.9	4.9	4.5	2.9	0.7954	0.9	0.6
VII	Cedramber	1.5	4.9	3.4	15.1	5.6342	0.7	3.1
VIII	Iso E Super	7.1	12.1	3.4	4.3	1.6187	0.3	0.4
IX	Ambrox	0.2	0.1	0.3	0.8	3.7889	2.6	7.7
X	Benzyl salicylate	32.5	1.1	0.7	0.6	0.9726	0.7	0.5
XI	Muskalactone	0.9	0.4	0.8	1.3	2.1764	1.9	3.3
	Total	80.1						

Table 7.4. Unisex fragrance: oil and headspace composition

	Component	Oil Conc (%)	Headspace Conc (%)			Activity	Ratio	Ratio
			Obs	Pred	Pred[a]	Coefficient	(Pred/Obs)	(Pred[a]/Obs)
I	Ethyl linalool	0.7	2.8	0.5	0.5	1.3087	0.2	0.2
II	Linalyl acetate	10.4	36	26.6	23.7	1.1220	0.7	0.7
III	Floralozone	0.1	0.3	0.03	0.01	0.4703	0.1	0.0
IV	Cyclogalbaniff	0.2	0.7	0.2	0.2	1.0986	0.2	0.2
V	Dihydromyrcenol	5.8	10.6	13.9	15.6	1.4127	1.3	1.5
VI	Linalool	7.7	11.5	15.5	16.8	1.3633	1.3	1.5
VII	Limonene	4.5	1.4	13.6	14.9	1.3715	9.7	10.6
VIII	beta-Ionone	2.5	6.2	4.7	3.9	1.0359	0.8	0.6
IX	Polysantol	0.2	0.4	0.003	0.003	1.3042	0.01	0.01
X	Iso E Super	4.8	4.8	0.7	0.6	1.0393	0.1	0.1
XI	Ambrox	0.7	0.4	0.3	0.4	1.6991	0.7	1.0
XII	Hedione	25.9	5	1.2	1.0	1.0366	0.2	0.2
XIII	Galaxolide	5.5	0.6	0.1	0.1	1.2741	0.2	0.2
XIV	Tonalid	3.3	0.1	3.5	3.1	1.1163	34.8	30.9
	Total	72.3						

[a] Corrected with activity coefficient parameter at time zero

Table 7.5. Feminine fragrance: oil and headspace composition

	Component	Oil Conc (%)	Headspace Conc (%)		Ratio
			Obs	Pred	(Pred/Obs)
I	Aldehyde AA	0.1	0.8	NA	NA
II	Methyl phenyl acetate	0.02	0.2	0.5	2.4
III	Ethyl linalool	5.0	30	21.2	0.7
IV	Diphenyl ether	0.01	0.04	0.03	0.7
V	Cyclogalbaniff	0.2	0.9	0.8	0.8
VI	Methyl ionone	2.5	9.5	17.7	1.9
VII	Ethyl acetoacetate	1.8	3.4	9.8	2.9
VIII	Iso E Super	2.6	2.1	0.3	0.1
IX	Ambrox	0.2	0.1	0.04	0.4
X	Hedione	18.0	2.4	0.1	0.05
XI	Cyclopentadecanolide	4.8	1.2	0.3	0.3
XII	Galaxolide	14.0	0.9	0.01	0.02
	Total	49.2			

Table 7.6. Women's fragrance: oil and headspace composition

	Component	Oil Conc (%)	Headspace Conc (%)		Ratio
			Obs	Pred	(Pred/Obs)
I	Lolitol	NA	0.1	NA	NA
II	Passionfruit compound	NA	0.01	NA	NA
III	Methyl octin carbonate	NA	0.1	NA	NA
IV	Givescone	0.10	1.2	0.3	0.2
V	Floralazone	0.01	0.1	0.01	0.1
VI	alpha-Damascone	0.1	0.5	0.3	0.6
VII	beta-Damascone	0.04	0.2	0.1	0.5
VIII	Ethyl linalool	1.4	6	2.9	0.5
IX	Undecavertol	0.3	1.0	0.3	0.3
X	Linalyl acetate	2.0	7.8	8.0	1.0
XI	cis-Jasmone	0.1	0.2	0.2	1.2
XII	Methyl ionone	2.0	4.6	7.4	1.6
XIII	Cyclopentadecanolide	0.9	0.2	1.6	8.2
XIV	Galaxolide	8.0	1	1.7	1.7
	Total	15.0			

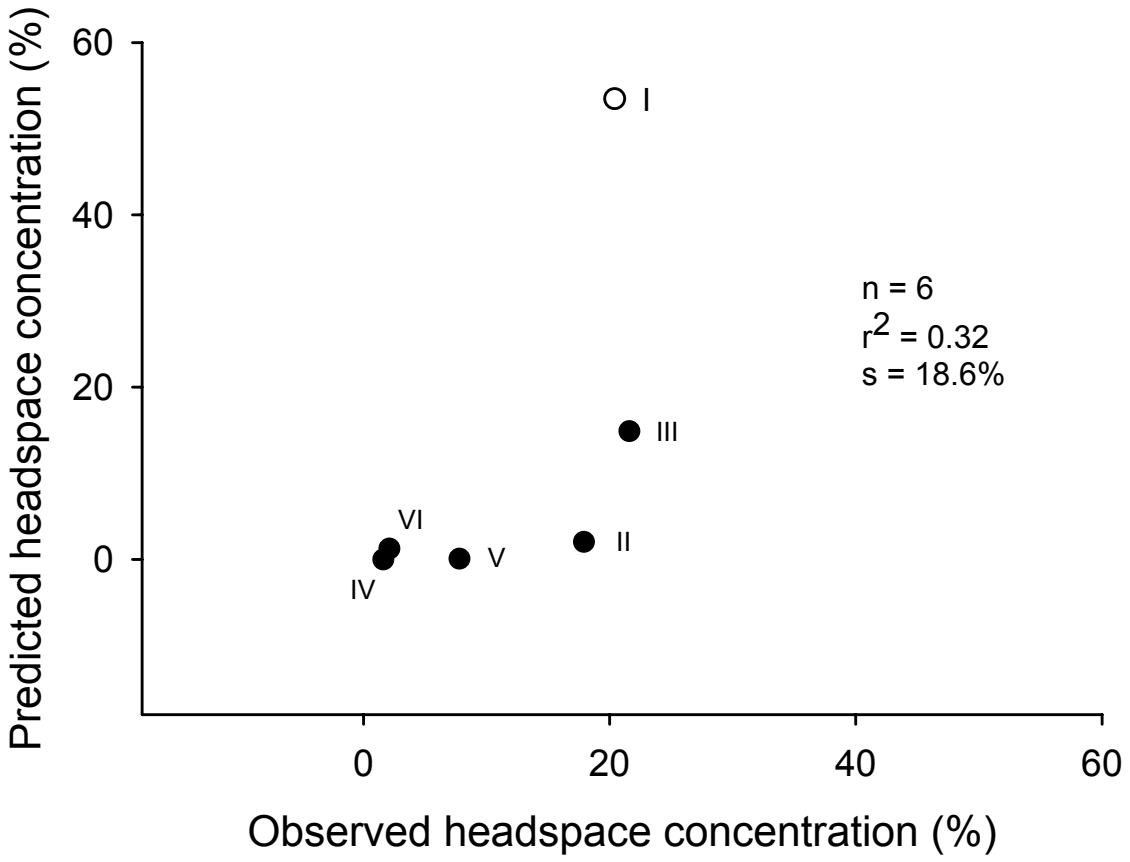

Figure 7.1. Shalimar Fragrance: by excluding limonene (I) from analysis, $r^2 = 0.57$ and s = 4.8%.

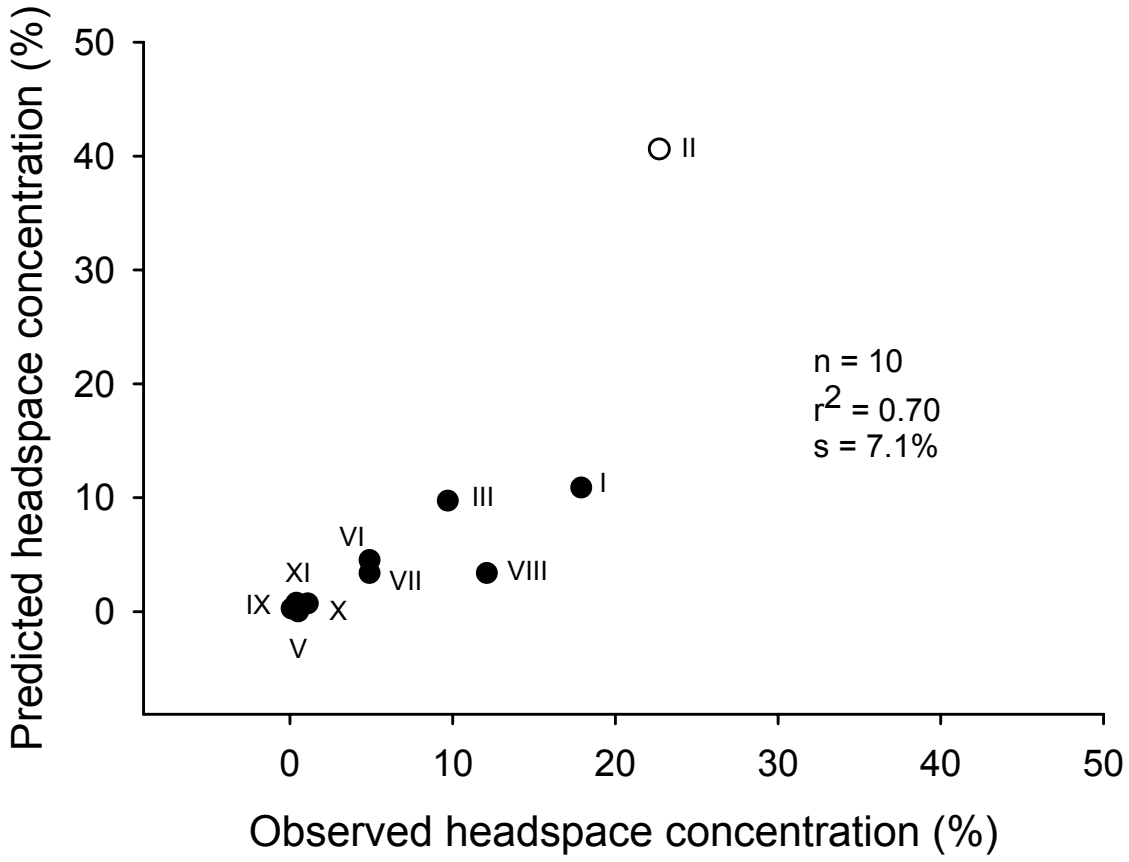

Figure 7.2. Amarige Fragrance: by excluding benzyl acetate (II) from analysis, $r^2 = 0.75$ and s = 2.2%.

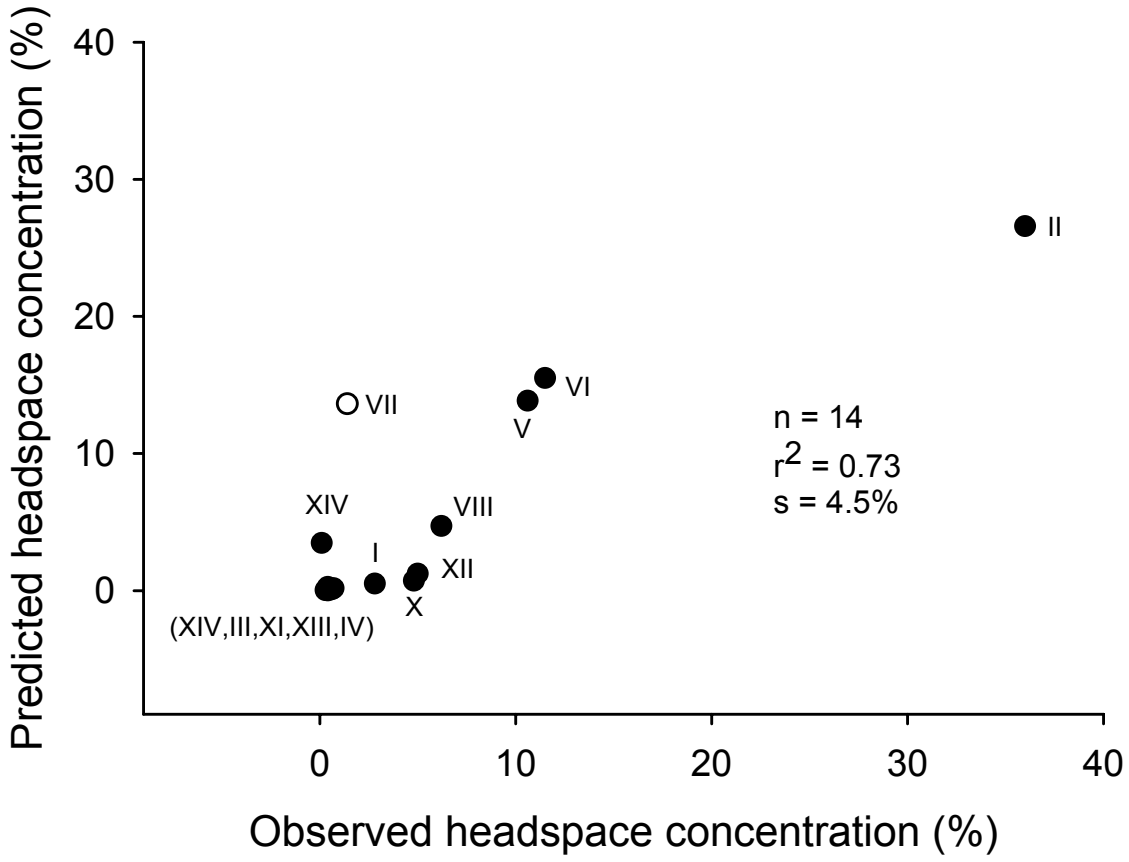

Figure 7.3. Unisex Fragrance: by excluding limonene (VII) from analysis, $r^2 = 0.87$ and s = 3.1%.

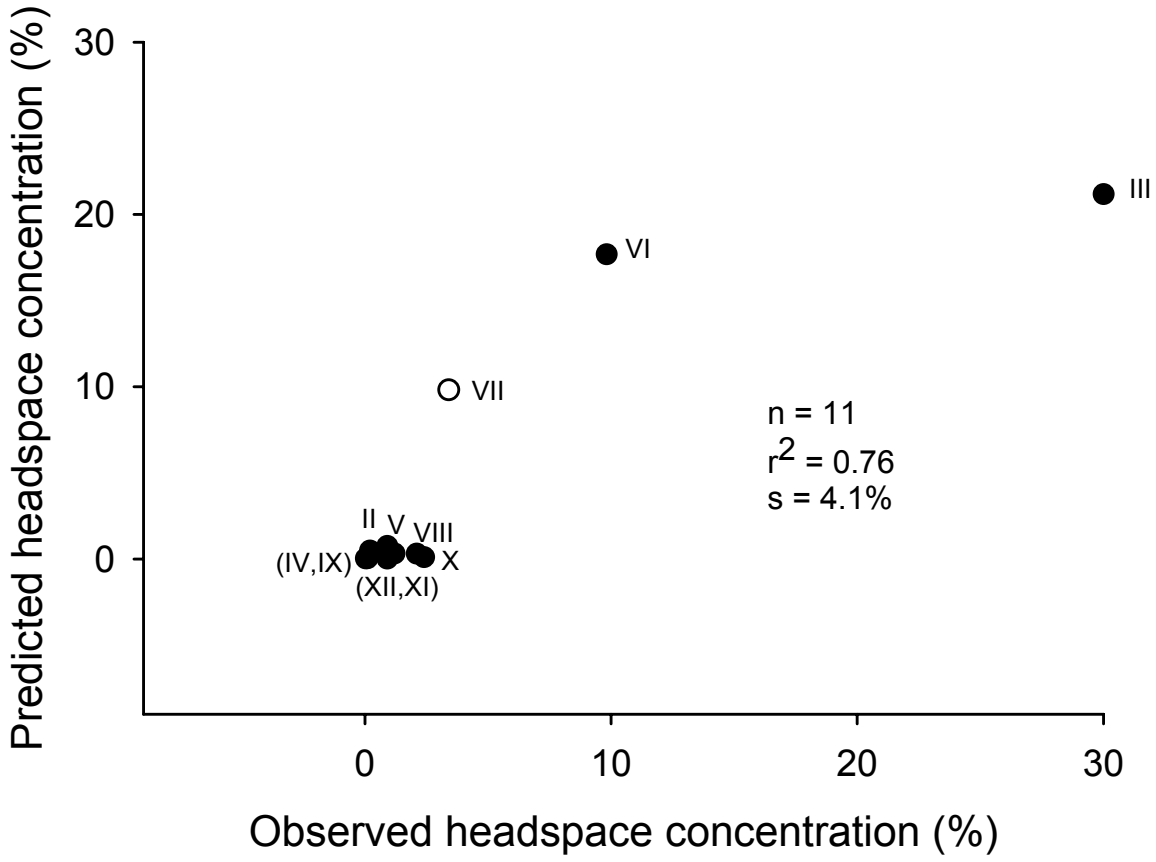

Figure 7.4. Feminine Fragrance: by excluding ethyl acetoacetate (VII) from analysis $r^2 = 0.81$ and s = 3.7%.

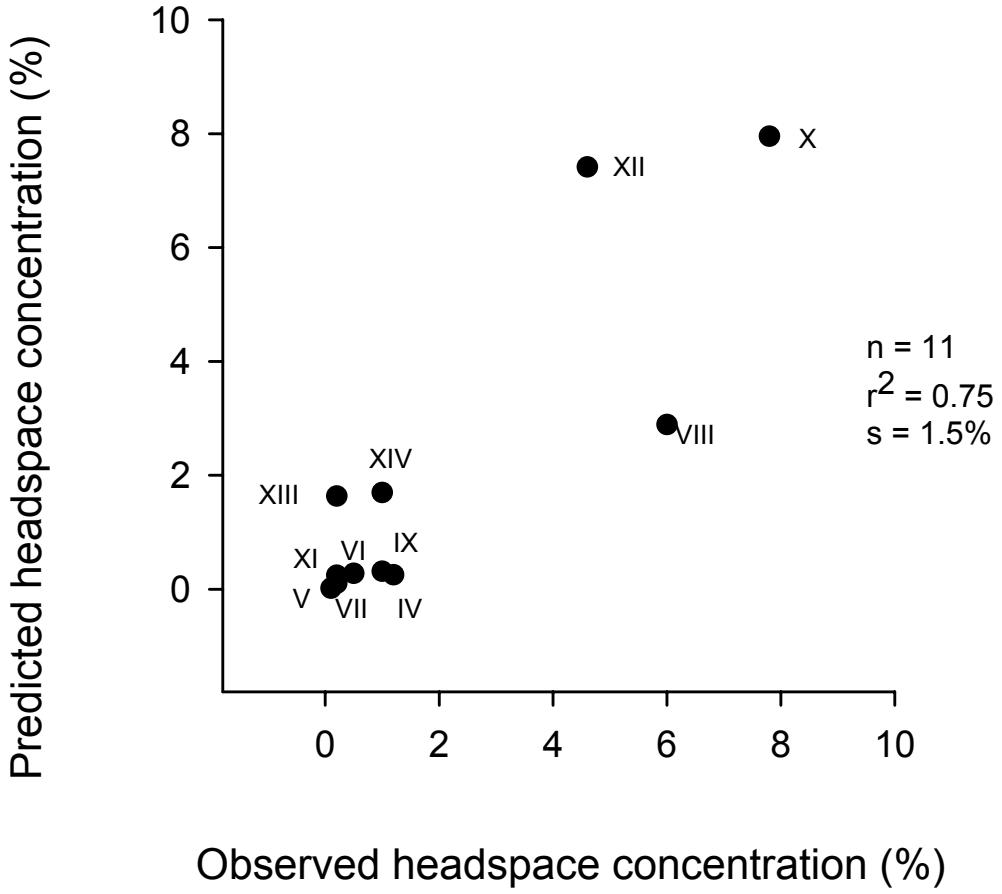

Figure 7.5. Women's Fragrance

the sampling efficiency may differ between compounds. More documentation of the SPME method[70] would be helpful in addressing this question.

There are several underlying assumptions in the model as discussed in Ref. 72. One of these assumptions is related to the ingredient interactions. The current model assumes no interactions

among ingredients in the fragrance mixture. If this is really the case, one would expect an ingredient to behave similarly regardless of the mixture in which it is applied. The present analysis shows that relative headspace concentrations of some materials (e.g., cyclopentadecanolide, galaxolide and methyl ionone) varied from one mixture to another. These findings may imply a significant effect of ingredient interactions in perfume mixtures. An additional parameter, the activity coefficient, may need to be incorporated into the calculation to account for these effects. The activity coefficient is a fractional number that, when multiplied by the mole fraction of a substance in solution, yields the thermodynamic activity. It is a measure of deviation from the ideal state.

The activity coefficients reported in Tables 7.2-7.4 were calculated using the UNIFAC method,[65] one of the best methods currently available. The concept of this method is that a liquid mixture may be considered to be a solution of the structural units (subgroups) from which the molecules are formed, rather than a solution of the molecules themselves. The fact that not all the components in the mixtures were reported (or even known) could lead to some errors in the calculations. Hence, the calculated activity coefficients are subject to this uncertainty. We could not obtain the activity coefficients of ingredients in Feminine and Women's Fragrances, as parameters for the carbonyl subgroup present in alpha- and beta- damascone and the phenoxyl subgroup present in diphenyl ether are not yet available.

No significant improvements were observed in any of the three perfumes when rate constants were multiplied by initial activity coefficients. It must be noted that these calculations were performed using activity coefficients calculated for the initial mixtures only. A more accurate

calculation would require that activity coefficients be re-evaluated regularly as the composition of the mixture remaining on the skin evolves over time. Our experience has not supported the use of activity coefficients in this manner, as add ons to a kinetic model.[81,85] However, this does not rule out their possible value when incorporated into an appropriate diffusion/evaporation model based on solution of the diffusion equation rather a compartmental approximation.

CONCLUSIONS

In most cases headspace concentrations predicted using a previously developed first-order kinetic model correlated reasonably well with experimental values from Ref. 70. The model employed in the analysis assumed independent absorption and evaporation of each fragrance ingredient. Further work is required to mechanistically understand the retention activity of the fragrance fixative especially on top note chemicals. Development of a diffusion model incorporating thermodynamic activity coefficients to represent the ingredient interactions appears to be warranted.

CHAPTER 8

SUMMARY AND FUTURE DIRECTIONS

SUMMARY

- Published *in vivo* mixture studies

  - Skin disposition of fragrance raw materials in a controlled *in vivo* study can be satisfactorily correlated with key physico-chemical properties including molecular weight, skin lipid solubility and vapor pressure.

  - The one-compartment kinetic approach provides a satisfactory description of the evaporated fractions. By adding a vehicle compartment to account for the initial dry-down process, further details of the evaporation rate profiles can be described.

  - Fragrance fixative agents such as musk are found to affect the evaporation kinetics of other fragrance components in the system both qualitatively and quantitatively.

  - The predicted headspace concentrations calculated using the simple first-order kinetic model correlated reasonably well with experimental data for several complex fragrance mixtures in an independent study. This was the first time test of the predictive power of the developed models.

- Laboratory studies (benzyl alcohol experiments)

    - Environmental factors such as surface airflow can significantly influence the skin disposition of fragrance raw materials.

    - The one-compartment kinetic approach provides a satisfactory description of the evaporated and absorbed fractions. By adding a vehicle compartment to account for the initial dry-down process, further details of the absorption and evaporation rate profiles can be described.

    - *In vitro* fragrance evaporation under controlled conditions appears to follow the same kinetics as fragrance evaporation *in vivo*.

FUTURE DIRECTIONS

- Construct a one-dimensional evaporation/diffusion model based on Fick's Law.

- Add ingredient interactions into the evaporation/diffusion model through UNIFAC/UNIQUAC approach in order to maximize its predictive power.

- Examine influence of exposure variables such as wind velocity, temperature, body site, and skin condition on fragrance disposition.

- Extend model to complex formulations.

- Calibrate versus typical *in vivo* exposures.

REFERENCES

1. Schueller R, Romanowski P. 1996. Common "Scents": Fragrance in personal care products. Cosmetics & Toiletries 111:1996.

2. Hostynek JJ. 1997. Safeguards in the use of fragrance chemicals. Cosmetics & Toiletries 112:47-54.

3. Robinson MK, Gerberick GF, Ryan CA, McNamee P, White I, Basketter DA. 2000. The importance of exposure estimation in the assessment of skin sensitization risk. Contact Dermatitis 42:251-259.

4. Gerberick GF, Robinson MK, Felter SP, White IR, Basketter DA. 2001. Understanding fragrance allergy using an exposure-based risk assessment approach. Contact Dermatitis 45:333-340.

5. Potts RO, Guy RH. 1992. Predicting skin permeability. Pharmaceutical Research 9:663-669.

6. Kasting GB. 2001. Kinetics of finite dose absorption 1. Vanillylnonanamide. Journal of Pharmaceutical Sciences 90:202-212.

7. Jimbo Y, Ishihara M, Osamura H, Takano M, Ohara M. 1983. Penetartion of fragrance compounds through human epidermis. The Journal of Dermatology 10:229-239.

8. Bronaugh RL, Stewart RF, Storm JE. 1989. Extent of cutaneous metabolism during percuaneous absorption. Toxicology and Applied Pharmacology 99:534-543.

9. Ford RA, Hawkins DR, Schwarzenbach R, Api AM. 1999. The systemic exposure to the polycyclic musks, AHTN and HHCB, under conditions of use as fragrance ingredients: evidence of lack of complete absorption from a skin reservoir. Toxicology Letters 111:133-142.

10. Barry BW, Harrison SM, Dugard PH. 1985. Vapour and liquid diffusion of model penetrants through human skin; correlation with thermodynamic activity. Journal of Pharmacy and Pharmacology 37:226-235.

11. Bronaugh RL, Wester RC, Bucks DAW, Maibach HI, Sarason R. 1990. *In vivo* percutaneous absorption of fragrance ingredients in rhesus monkeys and humans. Food and Chemical Toxicology 28:369-373.

12. Chidgey MA, Kennedy JF, Caldwell J. 1987. Studies on benzyl acetate. III. The percutaneous absorption and disposition of [methylene-14C]benzyl acetate in the rat. Food and Chemical Toxicology 25:521-525.

13. Hotchkiss SAM, Miller JM, Caldwell J. 1992. Percutaneous absorption of benzyl acetate through rat skin *in vitro*. 2. Effect of vehicle and occlusion. Food and Chemical Toxicology 30:145-153.

14. Garnett A, Hotchkiss SAM, Caldwell J. 1994. Percutaneous absorption of benzyl acetate through rat skin *in vitro*. 3. A comparison with human skin. Food and Chemical Toxicology 32:1061-1065.

15. Ballard BE, Menczel E. 1967. Subcutaneous absorption kinetics of benzyl alcohol. Journal of Pharmaceutical Sciences 56:1476-1485.

16. Menczel E, Maibach HI. 1970. *In vitro* human percutaneous penetration of benzyl alcohol and testosterone: epidermal-dermal retention. The Journal of Investigative Dermatology 54:386-394.

17. Jimbo Y, Ishihara M, Osamura H, Takano M, Ohara M. 1983. Influence of vehicles on penetration through human epidermis of benzyl alcohol, isoeugenol and methyl isoeugenol. The Journal of Dermatology 10:241-250.

18. Bronaugh RL, Stewart RF, Wester RC, Bucks D, Maibach HI, Anderson J. 1985. Comparison of percutaneous absorption of fragrances by humans and monkeys. Food and Chemical Toxicology 23:111-114.

19. Weibel H, Hansen J. 1989. Penetration of the fragrance compounds, cinnamaldehyde and cinnamyl alcohol, through human skin *in vitro*. Contact Dermatitis 20:167-172.

20. Yourick JJ, Bronaugh RL. 1997. Percutaneous absorption and metabolism of coumarin in human and rat skin. Journal of Applied Toxicology 17:153-158.

21. Hotchkiss SAM, Beckley-Kartey SAJ. 1995. Disposition of ^{14}C-coumarin after topical application to human skin *in vitro*. 104:687.

22. Hotchkiss SAM, Chidgey MAJ, Rose S, Caldwell J. 1990. Percutaneous absorption of benzyl acetate through rat skin *in vitro*. 1. Validation of an *in vitro* model against *in vivo* data. Food and Chemical Toxicology 28:443-447.

23. Ford RA, Hawkins DR, Mayo BC, Api AM. 2001. The *in vivo* dermal absorption and metabolism of [4-^{14}C]coumarin by rats and by human volunteers under simulated conditions of use in fragrances. Food and Chemical Toxicology 39:153-162.

24. Hawkins DR, Elsom LF, Kirkpatrick D, Ford RA, Api AM. 2002. Dermal absorption of musk ambrette, musk ketone and musk xylene in human subjects. Toxicology Letters 131:147-151.

25. Hood HL, Wickett RR, Bronaugh RL. 1996. In vitro percutaneous bsorption of the fragrance ingredient musk xylol. 1996 34:483-488.

26. Wilschut A, ten Berge WF, Robinson PJ, McKone TE. 1995. Estimating skin permeation. The validation of five mathematical skin penetration models. Chemosphere 30:1275-1296.

27. Cleek R, Bunge A. 1993. A new method for estimating dermal absorption from chemical exposure. 1. General approach. Pharmaceutical Research 10:497-506.

28. Reifenrath WG. 1995. Volatile substances. Cosmetics & Toiletries 110:85-93.

29. Guy RH, Maibach HI. 1984. Correction factors for determining body exposure from forearm percutaneous absorption data. Journal of Applied Toxicology 4:26-28.

30. Scott RC, Corrigan MA, Smith F, Mason H. 1991. The Influence of Skin Structure on Permeability: An Intersite and Interspecies Comparison with Hydrophilic Penetrants. Journal of Investigative Dermatology 96:921-925.

31. Feldmann RJ, Maibach HI. 1967. Regional variations in percutaneous penetration of 14C-cortisol in man. Journal of Investigative Dermatology 48:181-183.

32. Maibach HI, Feldmann RJ, Milby TH, Serat WF. 1971. Regional variations in percutaneous penetration in man. Archives of Environmental Health 23:208-211.

33. Wester RC, Maibach HI, Bucks DAW. 1984. In vivo percutaneous absorption of paraquat from hand, leg, and forearm of humans. Journal of Toxicology and Environmental Health 14:759-762.

34. Scheuplein RJ. 1978. Skin permeation. In The Physiology and Pathophysiology of the Skin. Vol. 5. A. Jarrett, editor. Academic Press, New York. 1693-1730.

35. Blank IH, Moloney J, Emslie AG, Simon I, Apt C. 1984. The diffusion of water across the stratum corneum as a function of its water content. Journal of Investigative Dermatology 82:183-194.

36. Scheuplein RJ, Ross LW. 1974. Mechanism of percutaneous absorption V. Percutaneous absorption of solvent deposited solids. Journal of Investigative Dermatology 62:353-360.

37. Reifenrath WG, Spencer TS. 1989. Evaporation and penetration from skin. In Percuatneous absorption. H.I. Maibach, editor. Marcel Dekker, New York. 313-334.

38. Reifenrath WG, Hawkins DR, Kurtz MS. 1991. Percutaneous penetartion and skin retention of topically applied compounds: An in vitro-in vivo study. Journal of Pharmaceutical Sciences 80:526-532.

39. Zatz JL. 1991. Modification of skin permeation by surfactants. Cosmetics & Toiletries 106:89-94.

40. Rhein LD. 1997. Review of properties of surfactants that determine their interactions with stratum corneum. Journal of the Society of Cosmetic Chemists 48:253-274.

41. Friberg SE. 1997. Vapor pressure of some fragrance ingredients in emulsion and microemulsion formulations. International Journal of Cosmetic Science 19:75-86.

42. Friberg SE, Szymula M, Fei L, Barber J, Al-bawab A. 1997. Vapour pressure of a fragrance ingredient during evaporation in a simple emulsion. International Journal of Cosmetic Science 19:259-270.

43. Langlois BRC, Friberg SE. 1993. Evaporation from a complex emulsion system. Journal of the Society of Cosmetic Chemists 44:23-34.

44. Friberg SE, Langlois B. 1992. Evaporation from emulsions. J Dispers Sci Technol 13:223-243.

45. Basketter DA. 1998. Skin sensitization: risk assessment. International Journal of Cosmetic Science 20:141-150.

46. Kimber I, Gerberick GF, Basketter DA. 1999. Thresholds in contact sensitization: theoretical and practical considerations. Food and Chemical Toxicology 37:553-560.

47. Sanderson DM, Earnshaw CG. 1991. Computer prediction of possible toxic action from chemical structure; the DEREK system. Human and Experimental Toxicology 10:261-273.

48. Vuilleumier C, Flament I, Sauvegrain P. 1995. Headspace analysis study of evaporation rate of perfume ingredients applied onto skin. International Journal of Cosmetic Science 17:61-76.

49. Kasting GB, Smith RL, Anderson BD. 1992. Prodrugs for dermal delivery: solubility, molecular size, and functional group effects. In Prodrugs: Topical and Ocular Drug Delivery. K.B. Sloan, editor. Marcel Dekker, New York. 117-161.

50. Anderson BD, Raykar PV. 1989. Solute structure-permeability relationships in human stratum corneum. Journal of Investigative Dermatology 93:280-286.

51. Thomas RG. 1982. Volatilization from soil. In Chemical Property Estimation Methods. D.H. Rosenblatt, editor. McGraw-Hill, New York. 16-11 to 16-50.

52. Mehta SC, Afouna MI, Ghanem A-H, Higuchi WI, Kern ER. 1997. Relationship of skin target site free drug concentration (C*) to the in vivo efficacy: an extensive evaluation of

the predictive value of the C* concept using acyclovir as a model drug. Journal of Pharmaceutical Sciences 86:797-801.

53. Meylan W. 1999. MPBPVP. Syracuse Research Corporation, North Syracuse.

54. Lyman WJ, Reehl WF, Rosenblatt DH. 1982. Handbook of Chemical Property Estimation. McGraw-Hill, New York.

55. Hansch C, Leo A. 1999. MEDCHEM database and CLOGP. BioByte, Inc.

56. Yalkowski SH, Valvani SC, Roseman TJ. 1983. Solubility and partitioning. Part 6. Octanol solubility and octanol-water partition coefficients. Journal of Pharmaceutical Sciences 72:866-870.

57. Yalkowski SH. 1993. AQUASOL database. University of Arizona, Tucson.

58. Gibaldi M, Perrier D. 1982. Pharmacokinetics. Marcel Dekker, New York.

59. Bevington PR. 1969. Data Reduction and Error Analysis for the Physical Sciences. McGraw-Hill, New York.

60. Guy RA, Hadgraft J. 1983. Physicochemical interpretation of the pharmacokinetics of percutaneous absorption. Journal of Pharmacokinetics and Biopharmaceutics 11:189-203.

61. Kubota K. 1991. A compartment model for percutaneous drug absorption. Journal of Pharmaceutical Sciences 80:502-504.

62. McCarley K, Bunge AL. 1999. Chapter 6. Dermal absorption of solvent deposited chemicals. In Department of Chemical Engineering. Colorado School of Mines.

63. Kasting GB. 1997. Finite dose diffusion in skin -- When is the applied dose infinite? Pharmaceutical Research 14:S313.

64. Hellewegen PG, van Bergen TJ. 2000. personal communication.

65. Reid RC, Prausnitz JM, Poling BE. 1987. The Properties of Liquids and Gases. McGraw Hill, New York.

66. USEPA. 1992. Guidelines for Exposure Assessment. Risk Assessment Forum, U.S. Environmental Protection Agency, Washington, DC.

67. Peck KD, Ghanem A-H, Higuchi WI. 1995. The effect of temperature upon the permeation of polar and ionic solutes through human epidermal membrane. Journal of Pharmaceutical Sciences 84:975-982.

68. Blank IH, Scheuplein RJ, MacFarlane DJ. 1967. Mechanism of percutaneous absorption III. The effect of temperature on the transport of non-electrolytes across the skin. Journal of Investigative Dermatology 49:582-589.

69. Johnson ME, Blankschtein D, Langer R. 1997. Evaluation of solute permeation through the stratum corneum: lateral bilayer diffusion as the primary transport mechanism. Journal of Pharmaceutical Sciences 86:1162-1172.

70. Mookherjee BD, Patel SM, Trenkle RW, Wilson RA. 1998. A novel technology to study the emission of fragrance from the skin. Perfumer & Flavorist 23:1-11.

71. Gerberick GF, Robinson MK. 2000. A skin sensitization risk assessment approach for evaluation of new ingredients and products. American Journal of Contact Dermatitis 11:65-73.

72. Kasting GB, Saiyasombati P. 2001. A physico-chemical properties based model for estimating evaporation and absorption rates of perfumes from skin. International Journal of Cosmetic Science 23:49-58.

73. Saiyasombati P, Kasting GB. In Submission. Disposition of Benzyl Alcohol Following Topical Application to Human Skin *In Vitro*. Journal of Pharmaceutical Sciences.

74. Barry BW, Harrison SM, Dugard PH. 1985. Correlation of thermodynamic activity and vapour diffusion through human skin for the model compound, benzyl alcohol. Journal of Pharmacy and Pharmacology 37:84-90.

75. Consumers TSCoCPaN-fPIf. 1999. Fragrance allergy in consumers: A review of the problem.

76. McCarley KD, Bunge AL. 2001. Pharmacokinetic Models of Dermal Absorption. Journal of Pharmaceutical Sciences 90:1699-1719.

77. Wagner JG. 1979. Fundamentals of Clinical Pharmacokinetics. Drug Intelligence Publications, Hamilton, Illinois.

78. Merritt EW, Cooper ER. 1984. Diffusion apparatus for skin penetration. Journal of Controlled Release 1:161-162.

79. Kasting GB, Filloon TG, Francis WR, Meredith MP. 1994. Improving the sensitivity of in vitro skin penetration experiments. Pharmaceutical Research 11:1747-1754.

80. Tse G, Blankschtein D, Shefer A, Shefer S. 1999. Thermodynamic prediction of active ingredient loading in polymeric microparticles. Journal of Controlled Release 60:77-100.

81. Saiyasombati P, Kasting GB. In Press. Disposition of Benzyl Alcohol Following Topical Application to Human Skin *In Vitro*. Journal of Pharmaceutical Sciences.

82. Supelco. 2000. Supelco 2000 Catalog.

83. IFF. 1996. Spray Technology & Marketing 26.

84. Randhol P, Engelien H. 2000. *xlUNIFAC*. Norwegian University of Science and Technology, Norway.

85. Saiyasombati P, Kasting GB. In preparation for submission. Two-stage kinetic analysis of fragrance evaporation and absorption rates of perfumes from skin.

APPENDIX A

EXAMPLE OF DATA FILE

```
BA In Vitro 40 ml/min - Trial 1
2      ,     14     ,     1,    15         NCOMPOUNDS, NPTS, NAIRFLOW, NF
EtOH   ,     BA                            COMPOUND1, COMPOUND2
46.06  ,     108.14                        MW1      , MW2
80.9   ,     0.0847                        Pvp1     , Pvp2
812.8  ,     562.7                         Soct1    , Soct2
10000  ,     126.6                         Dose1    , Dose2
40
0      ,     0      ,     0
0.08   ,     0      ,     0.4594
0.25   ,     0      ,     0.7484
0.5    ,     1      ,     0.0610
1      ,     1      ,     0.1264
1.25   ,     0      ,     0.8006
2      ,     1      ,     0.1611           Evaporation and absorption data
2.25   ,     0      ,     0.8072           0 = evaporation
4      ,     1      ,     0.1724           1 = absorption
4.25   ,     0      ,     0.8107
6      ,     1      ,     0.1743
6.25   ,     0      ,     0.8126
8      ,     1      ,     0.1751
8.25   ,     0      ,     0.8137
1      ,     0
1      ,     0
0      ,     0
0      ,     0
0      ,     0
0      ,     0
0      ,     0
0      ,     0
0      ,     0
0      ,     5
0      ,     0
0      ,     0
0      ,     1
0      ,     0
1      ,     1
0      ,     0
0      ,     0
0      ,     0
0      ,     0
0      ,     0
0      ,     0
0      ,     0
0      ,     0
0      ,     0
0      ,     0
0      ,     0                           UNIFAC parameters
0      ,     0
0      ,     0
0      ,     0
0      ,     0
0      ,     0
0      ,     0
0      ,     0
0      ,     0
0      ,     0
0      ,     0
0      ,     0
0      ,     0
0      ,     0
0      ,     0
0      ,     0
0      ,     0
0      ,     0
0      ,     0
0      ,     0
0      ,     0
0      ,     0
0      ,     0
0      ,     0
0      ,     0
0      ,     0
```

0	,	0	
0	,	0	
0	,	0	
0	,	0	
0	,	0	
0	,	0	
0	,	0	
0	,	0	
0	,	0	
0	,	0	
0	,	0	
0	,	0	
0	,	0	
0	,	0	
0	,	0	
0	,	0	
0	,	0	
0	,	0	
0	,	0	
0	,	0	
0	,	0	UNIFAC parameters
0	,	0	
0	,	0	
0	,	0	
0	,	0	
0	,	0	
0	,	0	
0	,	0	
0	,	0	
0	,	0	
0	,	0	
0	,	0	
0	,	0	
0	,	0	
0	,	0	
0	,	0	
0	,	0	
0	,	0	
0	,	0	
0	,	0	

APPENDIX B

BASIC COMPUTER CODE FOR UNIFAC/UNIQUAC ACTIVITY COEFFICIENT CALCULATIONS

```
'--------==========---------=============================----------==
'        subroutine unifac
'calculations parameters for uniquac equation by unifac method
'
'Penpan Saiyasombati, College of Pharmacy, University of Cincinnati
'August 16 - October 15, 2001; Modified June 2002
'
'glossary:
'
'       Temp            temperature in K
'       NCOMPOUNDS      number of species in the system
'       II              species
'       IJ              dummy index running all over species
'       IK              subgroup
'       IM              dummy index running all over subgroups
'       NF              Maximum no. of fragments in test compounds
'       Nk              number of subgroup k
'       Ri              relative molecular volume
'       Rk              relative volume of subgroup k
'       Qi              relative molecular surface area
'       Qk              relative surface area of subgroup k
'       Amk             group interaction parameter
'       Amain           main group interaction parameter
'       EE              parameter for computer programming
'       Tau             parameter for computer programming
'       BBBeta          parameter for computer programming
'
'
'
'--------==========---------=============================----------==
'input parameters:
'
'temperature
'
15000   PRINT : PRINT "Enter activity coefficient mode:"
       PRINT "(1) Unit activities; (2) UNIFAC activities"
       INPUT ModeG: PRINT
       TempC = 30!
       Temp = TempC + 273.15
       ON ModeG GOTO 21300, 21400
21300   RETURN
21400   PRINT : PRINT "Temperature (deg C) = "; TempC
'
'----'----==========---------=============================----------==
'
'values for Rk(I)
'
       A$ = "c:\Rk.txt"
       OPEN "I", 1, A$
       FOR I = 1 TO NF
              INPUT #1, Rk(I)
              NEXT I
       CLOSE 1
'
'values for Qk(I)
'
              A$ = "c:\Qk.txt"
       OPEN "I", 1, A$
       FOR I = 1 TO NF
              INPUT #1, Qk(I)
              NEXT I
       CLOSE 1
'
'----'----==========---------=============================----------==
'calculations for Ri(I) and Qi(I)
       FOR I = 1 TO NCOMPOUNDS
              Ri(I) = 0!
              Qi(I) = 0!
              FOR K = 1 TO NF
                     Ri(I) = Ri(I) + Nk(K, I) * Rk(K)
                     Qi(I) = Qi(I) + Nk(K, I) * Qk(K)
                     NEXT K
```

```
            NEXT I
'
'calculations for EE(K,I)
      FOR I = 1 TO NCOMPOUNDS
            FOR K = 1 TO NF
                  EE(K, I) = Nk(K, I) * Qk(K) / Qi(I)
                  NEXT K
            NEXT I
'
'----'----------==========----------==========----------==
'values for Amk(M,K)
'
'interaction parameters 'Amain'
'from Table 8-22, P. 324, The Proeprties of Gases and Liquids
'Reid & Prauznitz
'
      A$ = "c:\Amain.txt"
      OPEN "I", 1, A$
      FOR I = 1 TO 47
            FOR J = 1 TO 47
                 INPUT #1, ARRAY(I, J)      'ARRAY used in place of AMAIN
                  NEXT J                   'to save space
            NEXT I
      CLOSE 1
'
       FOR I = 1 TO NF
            FOR K = 1 TO NF
                  Tau(I, K) = ARRAY(FNu%(I), FNu%(K))
                  NEXT K                     'TAU used in place of Amk
            NEXT I                            'to save space
'
'----'----------==========----------==========----------==
'calculations for Tau(IM,K)
'
      FOR IM = 1 TO NF
            FOR K = 1 TO NF
                  Tau(IM, K) = EXP(-Tau(IM, K) / Temp)
                  NEXT K
            NEXT IM
'
'calculations for BBeta(I,K)
'
      FOR I = 1 TO NCOMPOUNDS
            FOR K = 1 TO NF
                  BBeta(I, K) = 0!
                  FOR IM = 1 TO NF
                        BBeta(I, K) = BBeta(I, K) + EE(IM, I) * Tau(IM, K)
                        NEXT IM
                  NEXT K
            NEXT I
'
      RETURN
      END
'
'----'----------==========----------==========----------==
'        subroutine uniquac(MF!,Gamma)
'calculations of activity coefficients from uniquac equation
'
'Penpan Saiyasombati, College of Pharmacy, University of Cincinnati
'August 16 - October 15, 2001; Modified June 2002
'
'glossary:
'
'       Gamma           activity coefficient
'       NCOMPOUNDS      number of species in the system
'       Mi!             number of moles for each species
'       MTotal!         total number of micromoles
'       MF!             mole fraction
'       II              species
'       IJ              dummy index running all over species
'       IK              subgroup
'       IM              dummy index running all over subgroups
```

```
'       Ri              relative molecular volume
'       Qi              relative molecular surface area
'       EE              parameter for computer programming
'       Tau             parameter for computer programming
'       BBeta           parameter for computer programming
'       Theta           parameter for computer programming
'       Sk              parameter for computer programming
'       Vk              parameter for computer programming
'       Pi              parameter for computer programming
'       Li!             parameter for computer programming
'       lgammaC!        parameter for computer programming
'       lgammaR!        parameter for computer programming
'
'
'
'----'----------=========-------------------=========----------==
'calculations for Mole Fraction MF!(II)
'
21000   ON ModeG GOTO 21100, 21200
21100   FOR II = 1 TO NCOMPOUNDS
              Gamma(II) = 1!
              NEXT II
        RETURN
'
21200   MTotal! = 0!
        FOR II = 1 TO NCOMPOUNDS
              JJJ = 3 * II
              Mi!(II) = Y(1, JJJ) / MW!(II)
              MTotal! = MTotal! + Mi!(II)
              NEXT II
'
        FOR II = 1 TO NCOMPOUNDS
              MF!(II) = ABS(Mi!(II) / MTotal!)
              NEXT II
'
'----'----------=========-------------------=========----------==
'calculations for Theta(IK)
'
        FOR IK = 1 TO NF
              Vk(IK) = 0!
              FOR IJ = 1 TO NCOMPOUNDS
                    Vk(IK) = Vk(IK) + (MF!(IJ) * Qi(IJ))
                    NEXT IJ
              NEXT IK
'
        FOR IK = 1 TO NF
              Theta(IK) = 0!
              FOR II = 1 TO NCOMPOUNDS
                    Theta(IK) = Theta(IK) + (MF!(II) * Qi(II) * EE(IK, II))
                    NEXT II
              Theta(IK) = Theta(IK) / Vk(IK)
              NEXT IK
'
'----'----------=========-------------------=========----------==
'calculations for Sk(IK)
'
        FOR IK = 1 TO NF
              Sk(IK) = 0!
              FOR IM = 1 TO NF
                    Sk(IK) = Sk(IK) + Theta(IM) * Tau(IM, IK)
                    NEXT IM
              NEXT IK
'
'----'----------=========-------------------=========----------==
'calculations for Pi(II)
'
        FOR II = 1 TO NCOMPOUNDS
              Pi(II) = 0!
              FOR IJ = 1 TO NCOMPOUNDS
                    Pi(II) = Pi(II) + Ri(IJ) * MF!(IJ)
                    NEXT IJ
              Pi(II) = Ri(II) / Pi(II)
```

```
            NEXT II
'
'calculations for Li!(II)
'
      FOR II = 1 TO NCOMPOUNDS
            Li!(II) = 0!
            FOR IJ = 1 TO NCOMPOUNDS
                  Li!(II) = Li!(II) + Qi(IJ) * MF!(IJ)
                  NEXT IJ
            Li!(II) = Qi(II) / Li!(II)
            NEXT II
'
'----'----==========---------=========----------=========----------==
'calculations for lgammaC!(II)
'
      FOR II = 1 TO NCOMPOUNDS
            lgammaC!(II) = 1! - Pi(II) + LOG(Pi(II)) - 5! * Qi(II) * (1! - Pi(II) /
Li!(II) + LOG(Pi(II) / Li!(II)))
            NEXT II
'
'calculations for lgammaR!(II)
'
      FOR II = 1 TO NCOMPOUNDS
            lgammaR!(II) = 1!
            FOR IK = 1 TO NF
                  IF (Sk(IK) <> 0! AND BBeta(II, IK) <> 0!) THEN
                        lgammaR!(II) = lgammaR!(II) - Theta(IK) * BBeta(II, IK) /
Sk(IK) + EE(IK, II) * LOG(BBeta(II, IK) / Sk(IK))
                  END IF
                  NEXT IK
            lgammaR!(II) = lgammaR!(II) * Qi(II)
            NEXT II
'
'----'----==========---------=========----------=========----------==
'calculations for Gamma(II)
'
      FOR II = 1 TO NCOMPOUNDS
            Gamma(II) = EXP(lgammaC!(II) + lgammaR!(II))
            'PRINT "Gamma("; II; ") = "; Gamma(II)
            'INPUT B$
            NEXT II
'
      RETURN
      END
'
'
'
```

APPENDIX C

EVAPORATION RATE OF FRAGRANCE RAW MATERIALS FROM THE HUMAN *IN VIVO* STUDY: a) Vector A Trial 1; b) Vector A Trial 2; c) Vector B Trial 1 and d) Vector B Trial 2 (cf. CHAPTER 5)

Compound I-Linalool

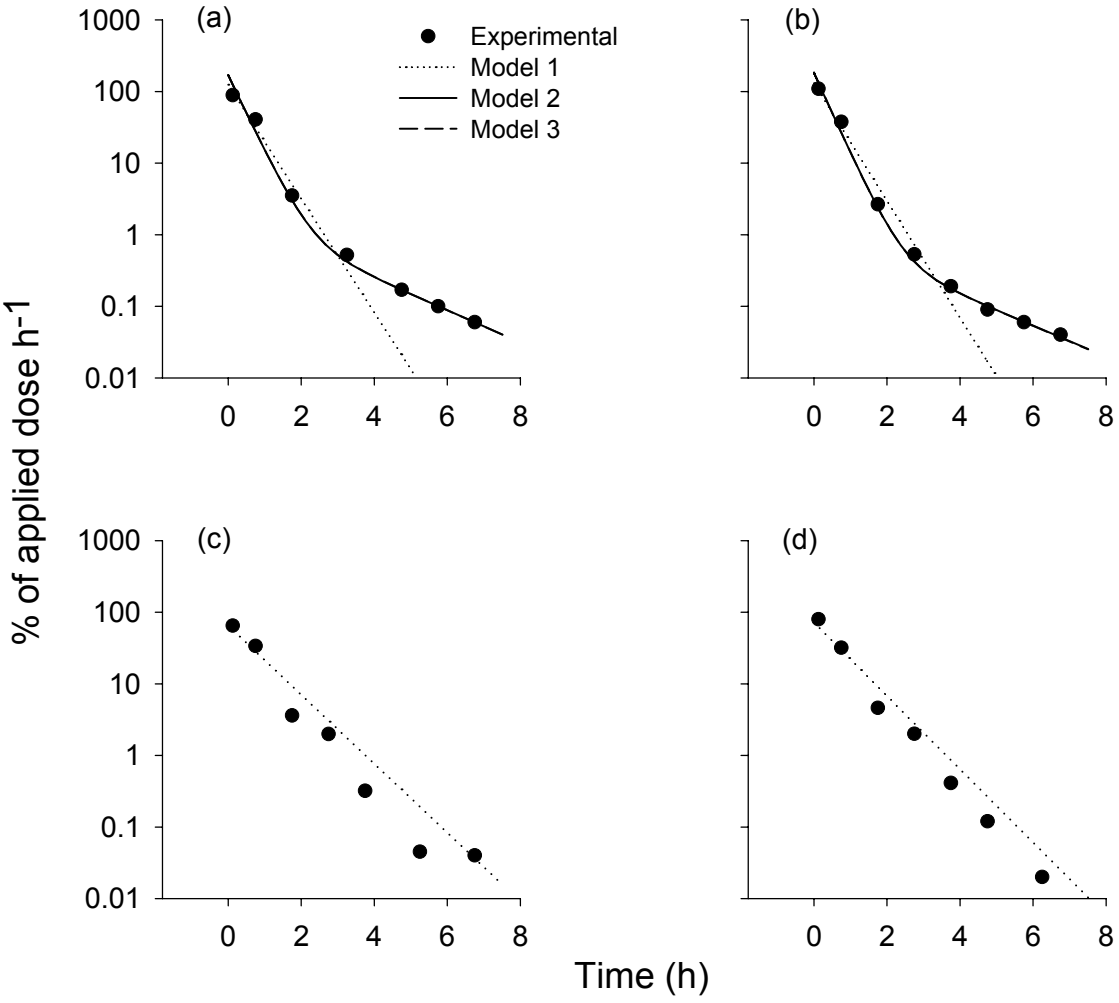

Compound II-dihydromyrcenol

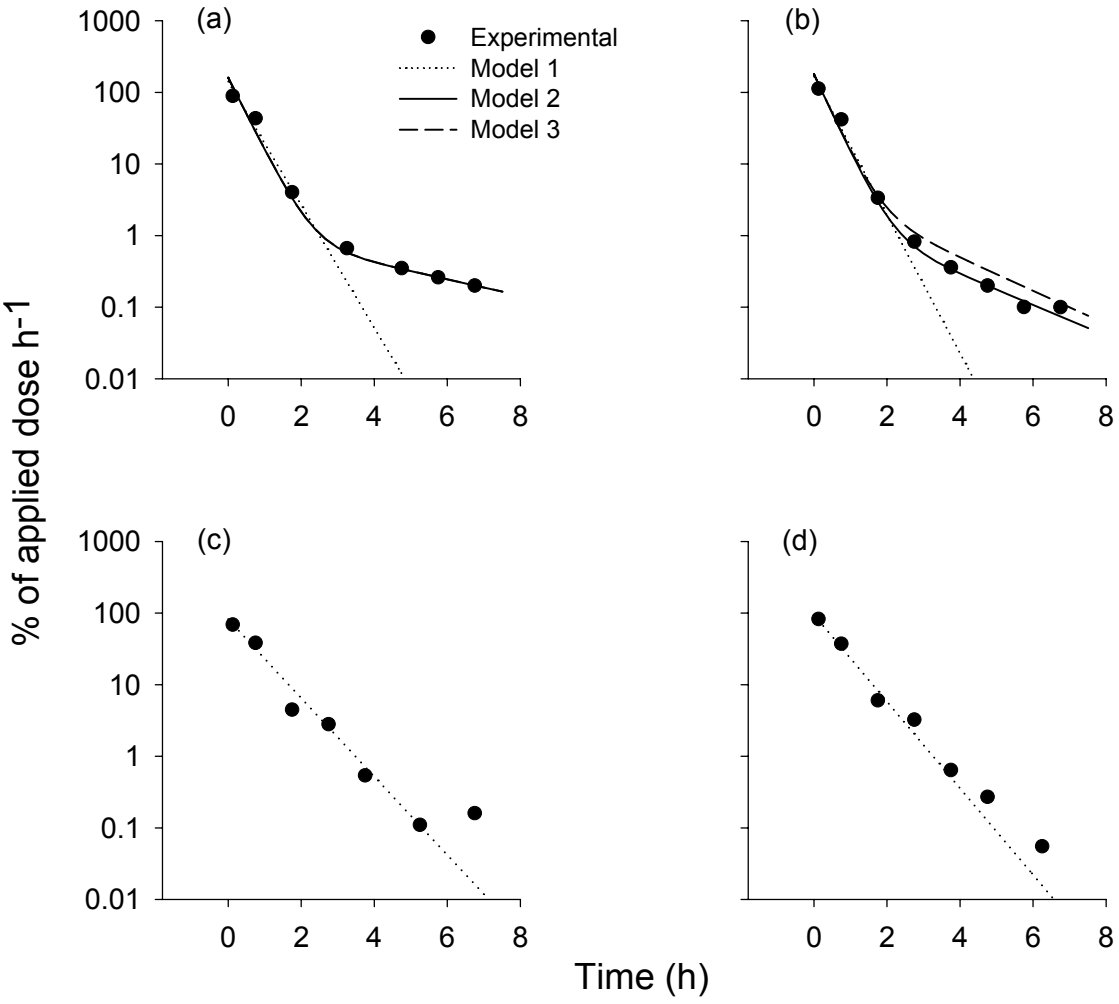

Compound III-Undecanal

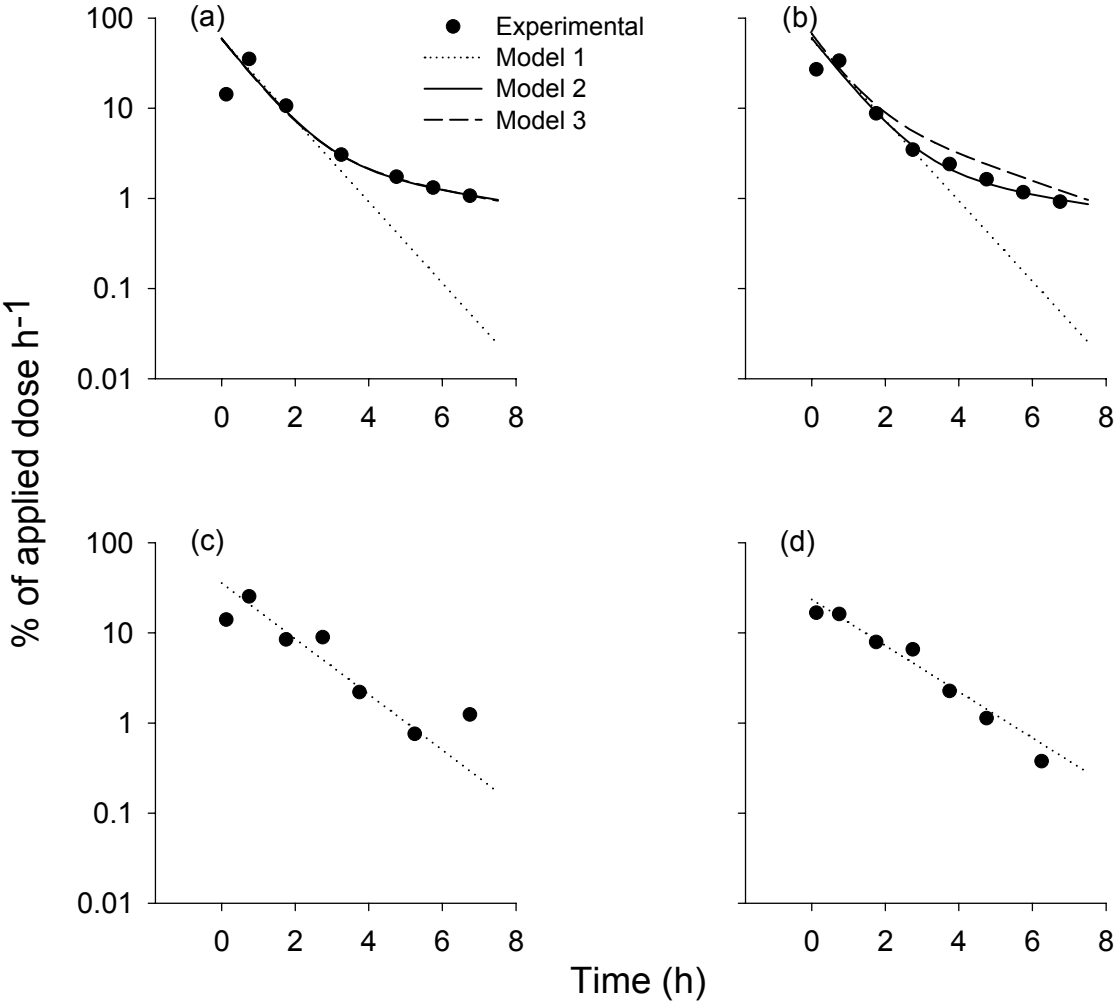

Compound IV-Citronellol

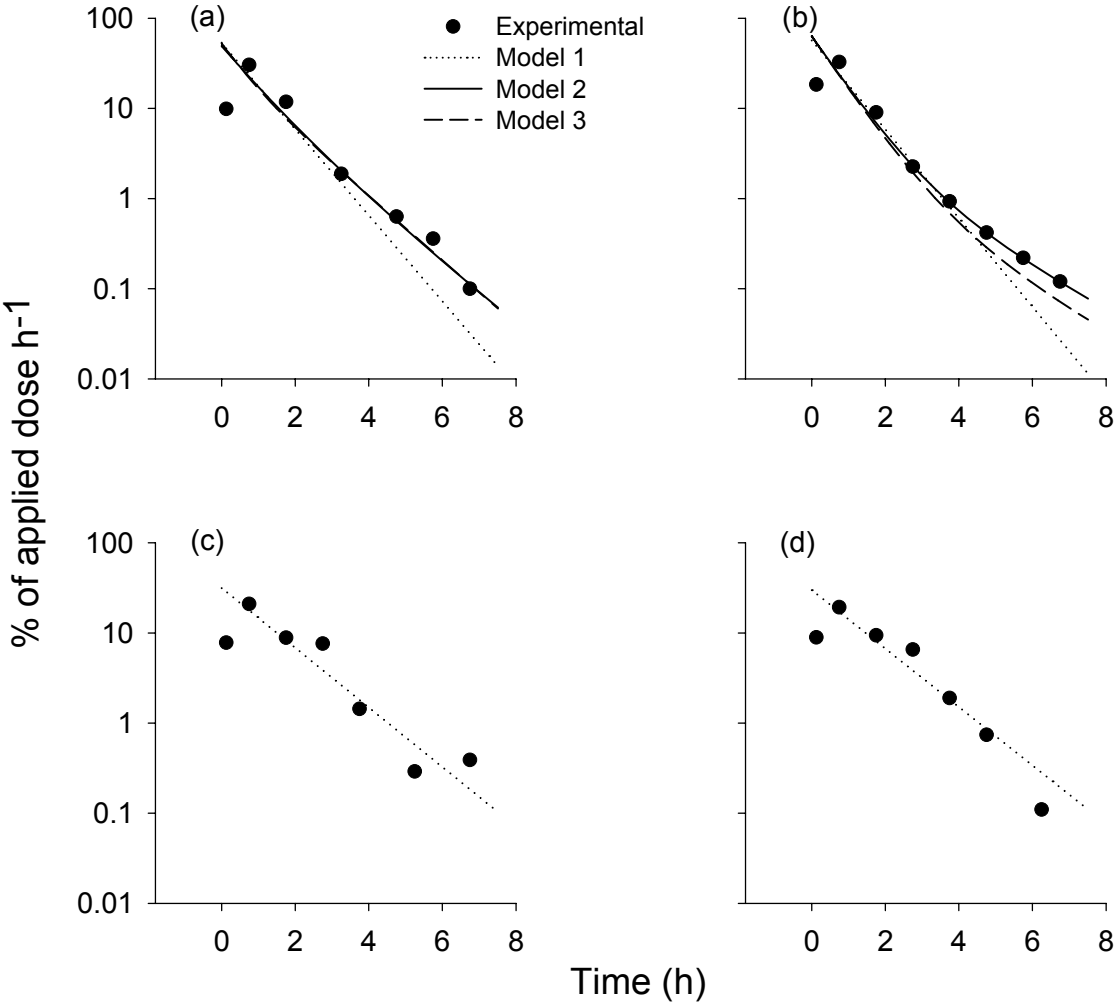

Compound V-2-Phenyl-1-ethanol

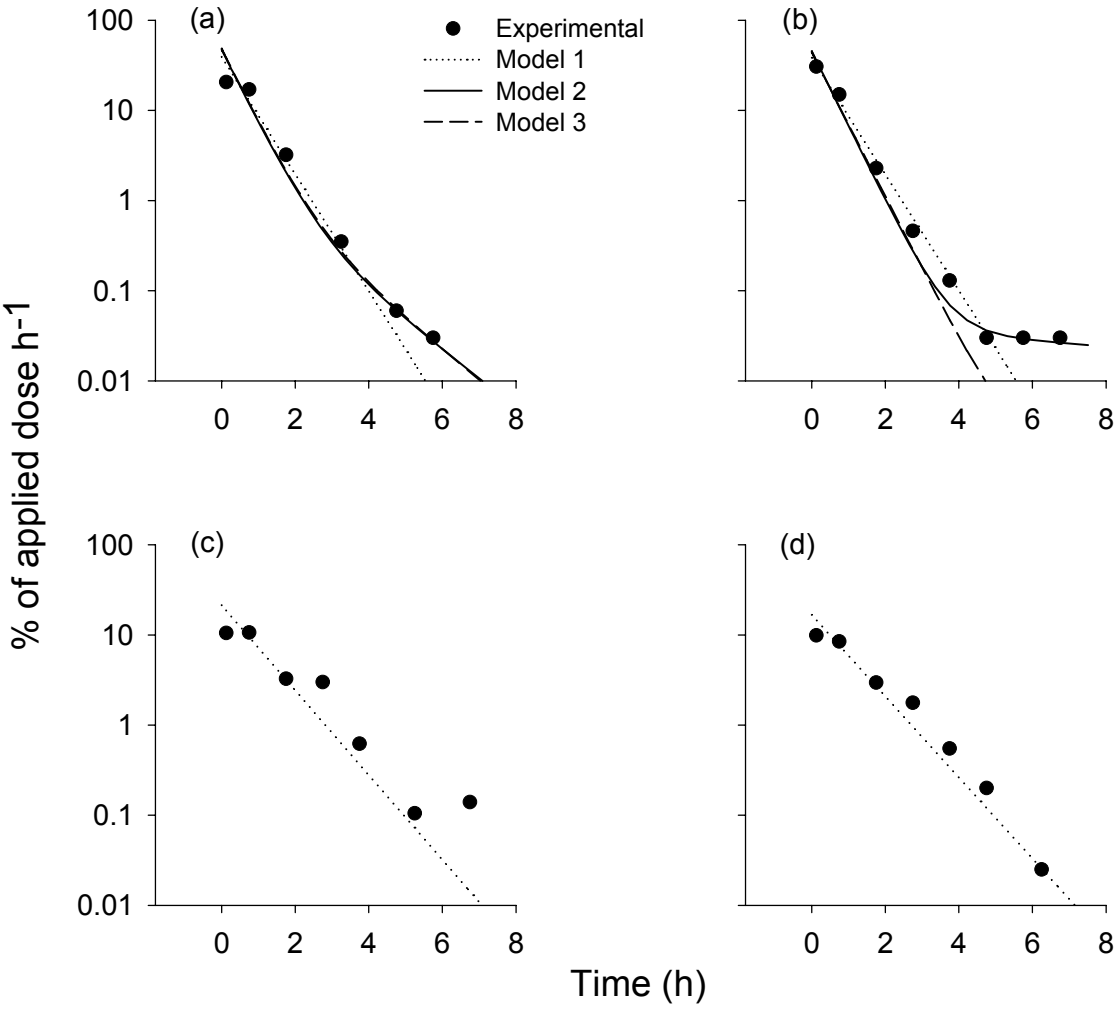

Compound VI-(E)-Cinnamic alcohol

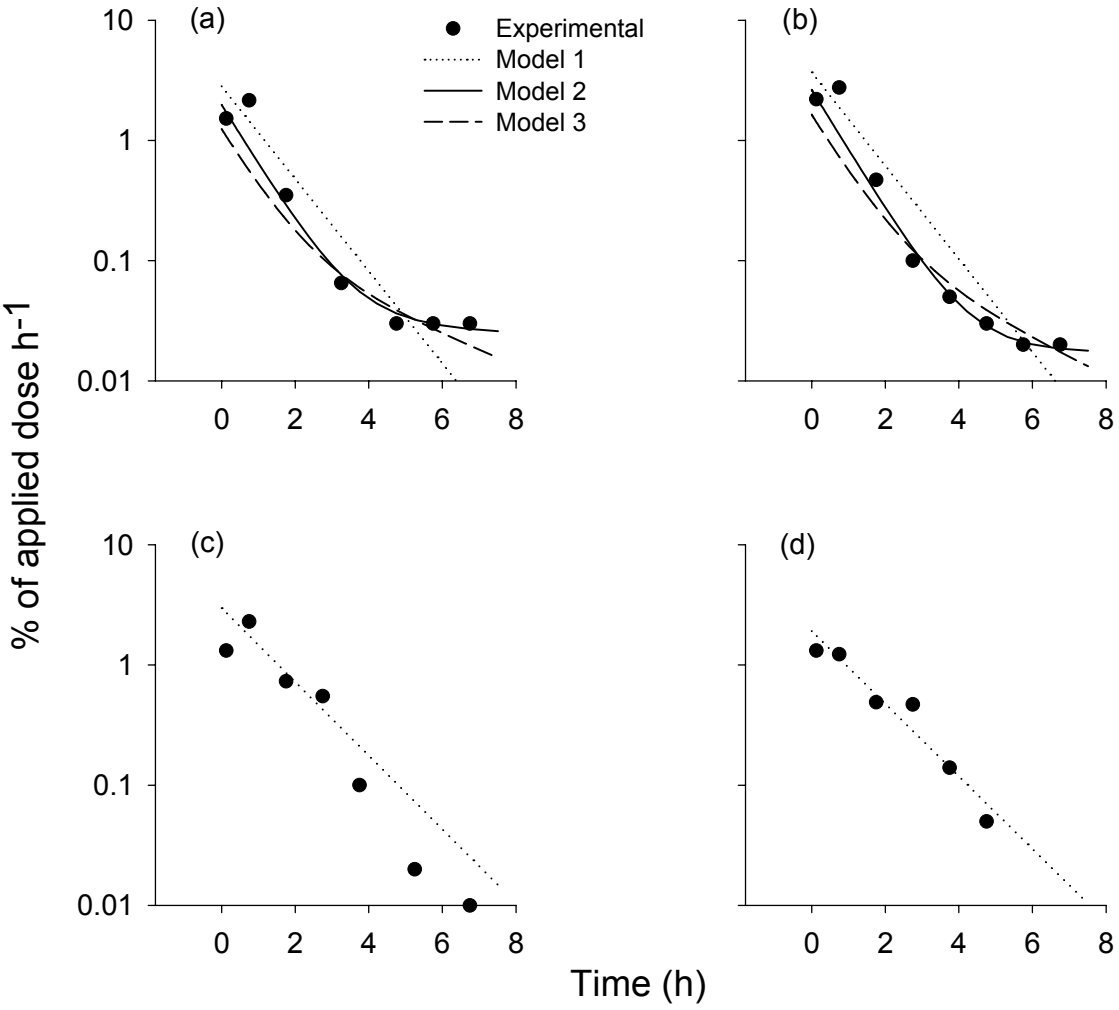

Compound VII-α-Damascone

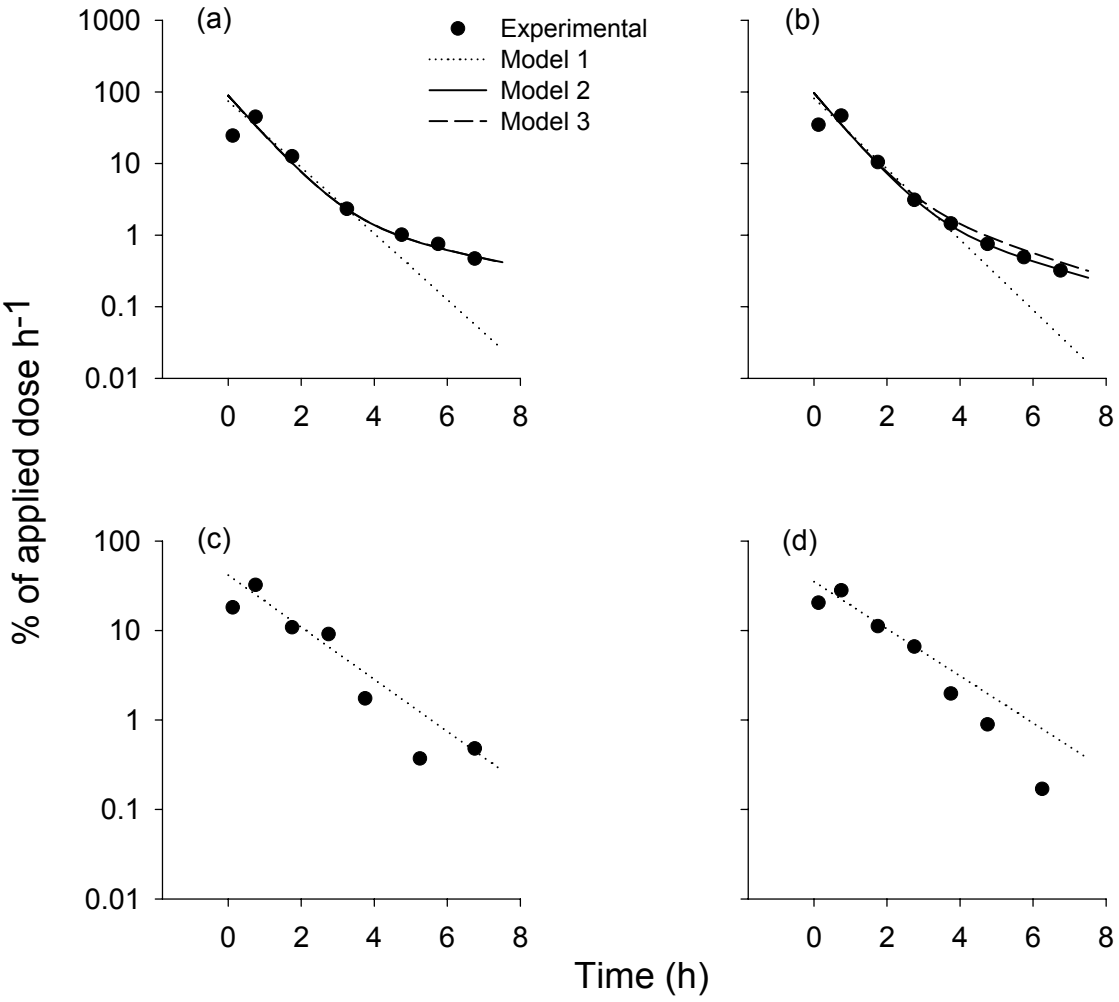

Compound VIII-Cis-7-p-Menthanol

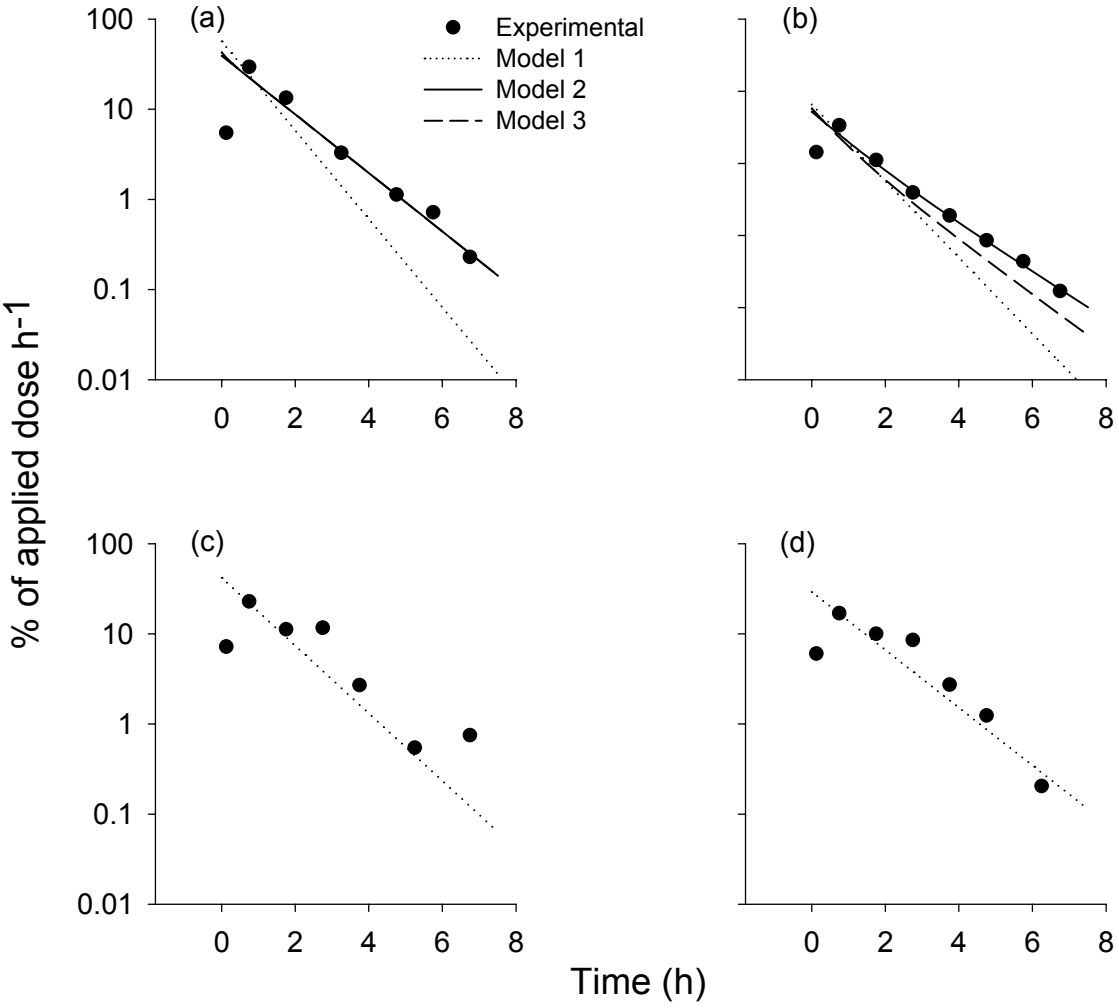

Compound IX-2,2,2-Trichloro-1-phenylethylacetate

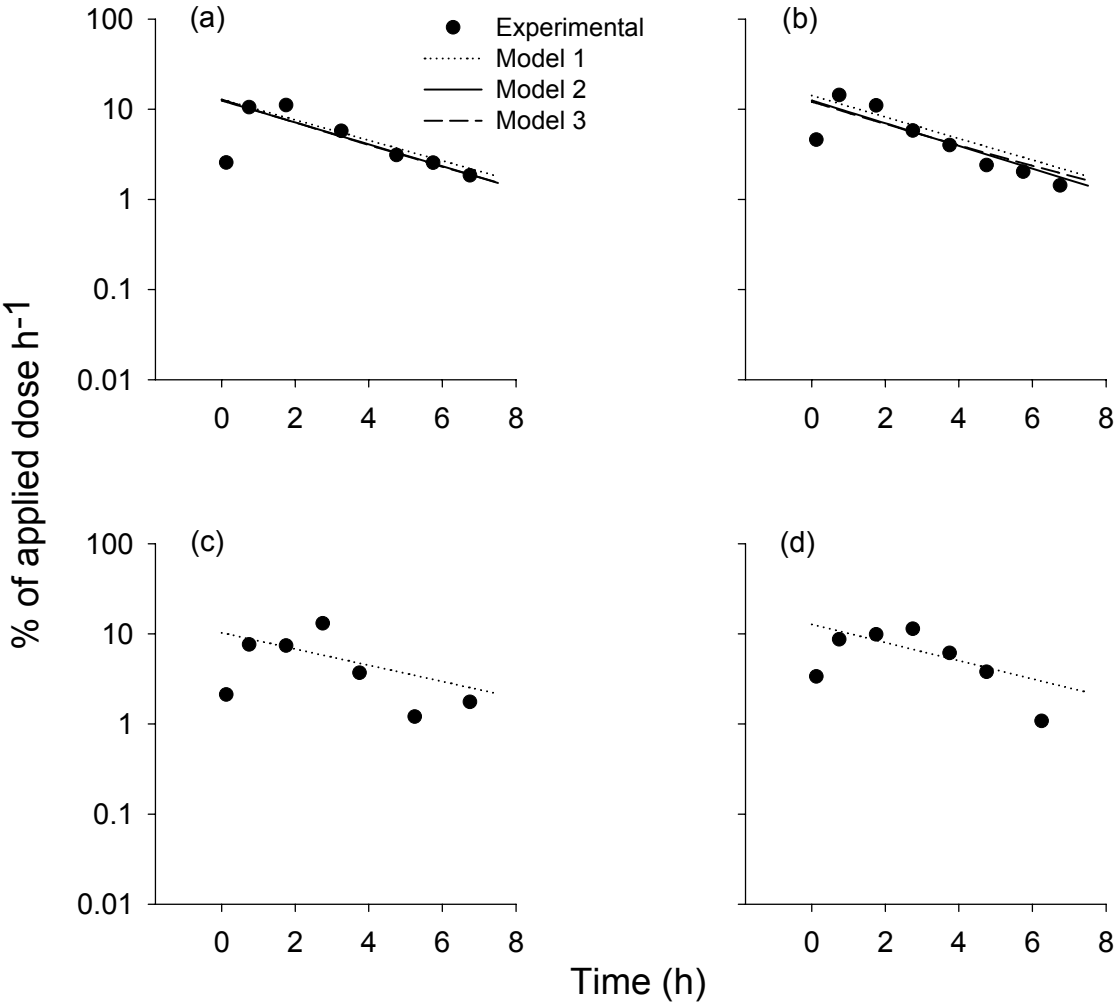

Compound X-M.P.C.C.

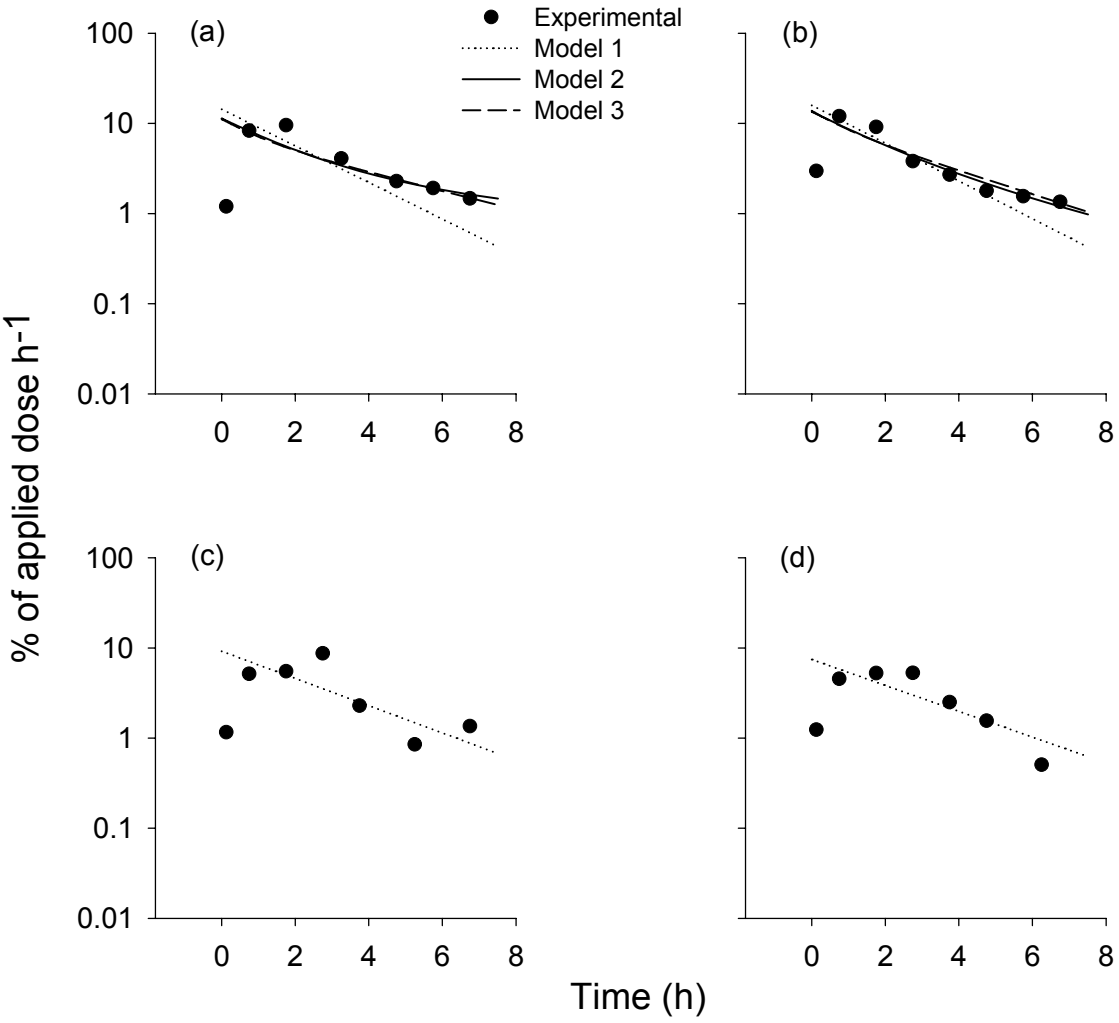

APPENDIX D

EVAPORATION RATE OF ^{14}C-BENZYL ALCOHOL FROM THE HUMAN *IN VITRO* STUDY AT DIFFERENT AIRFLOW VELOCITIES: a) Trial 1, Evaporation rate; b) Trial 1, Absorption rate; c) Trial 2, Evaporation rate and d) Trial 2, Absorption rate

(cf. CHAPTER 5)

10 mL/min

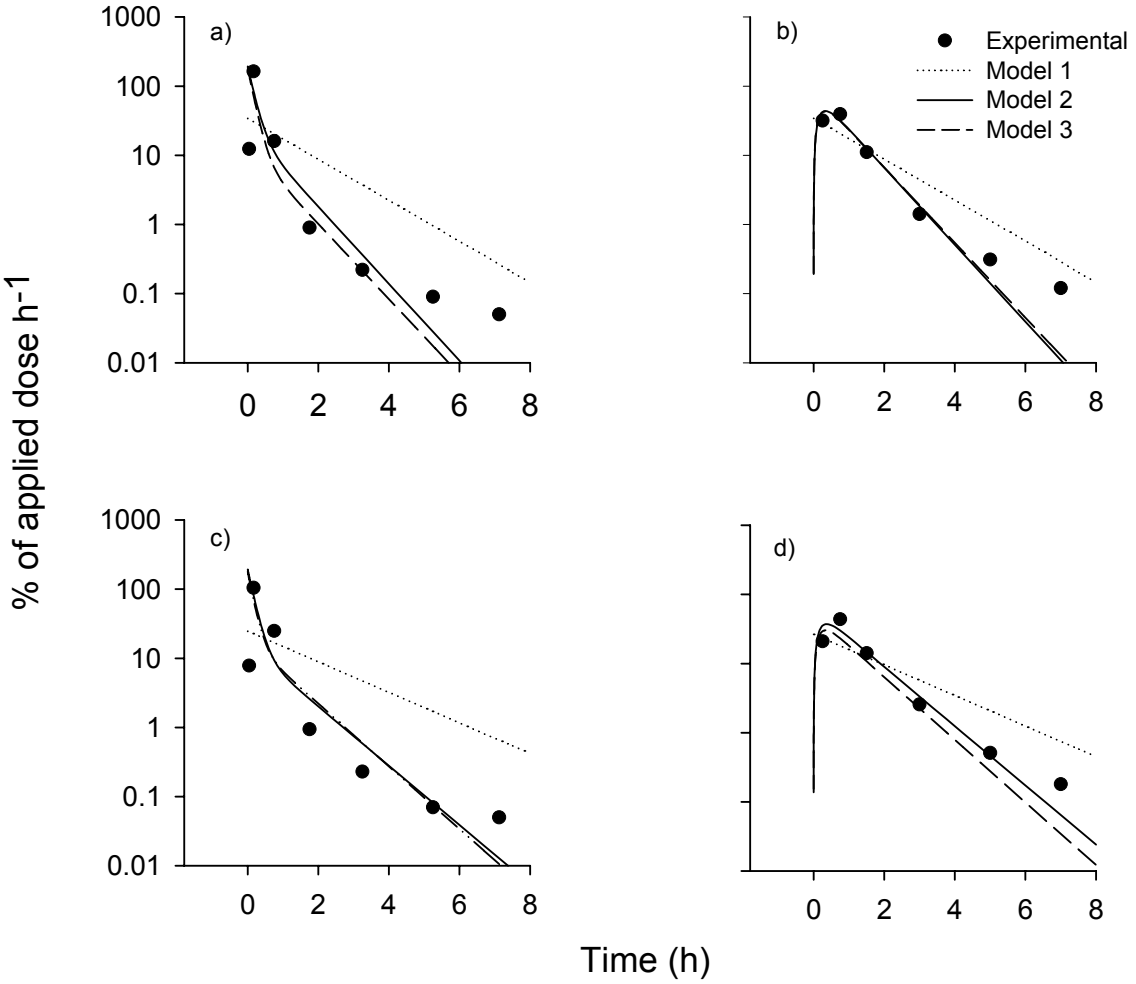
a)
b)
c)
d)
Experimental
Model 1
Model 2
Model 3
% of applied dose h-1
Time (h)
1000
100
10
1
0.1
0.01
0
2
4
6
8

20 mL/min

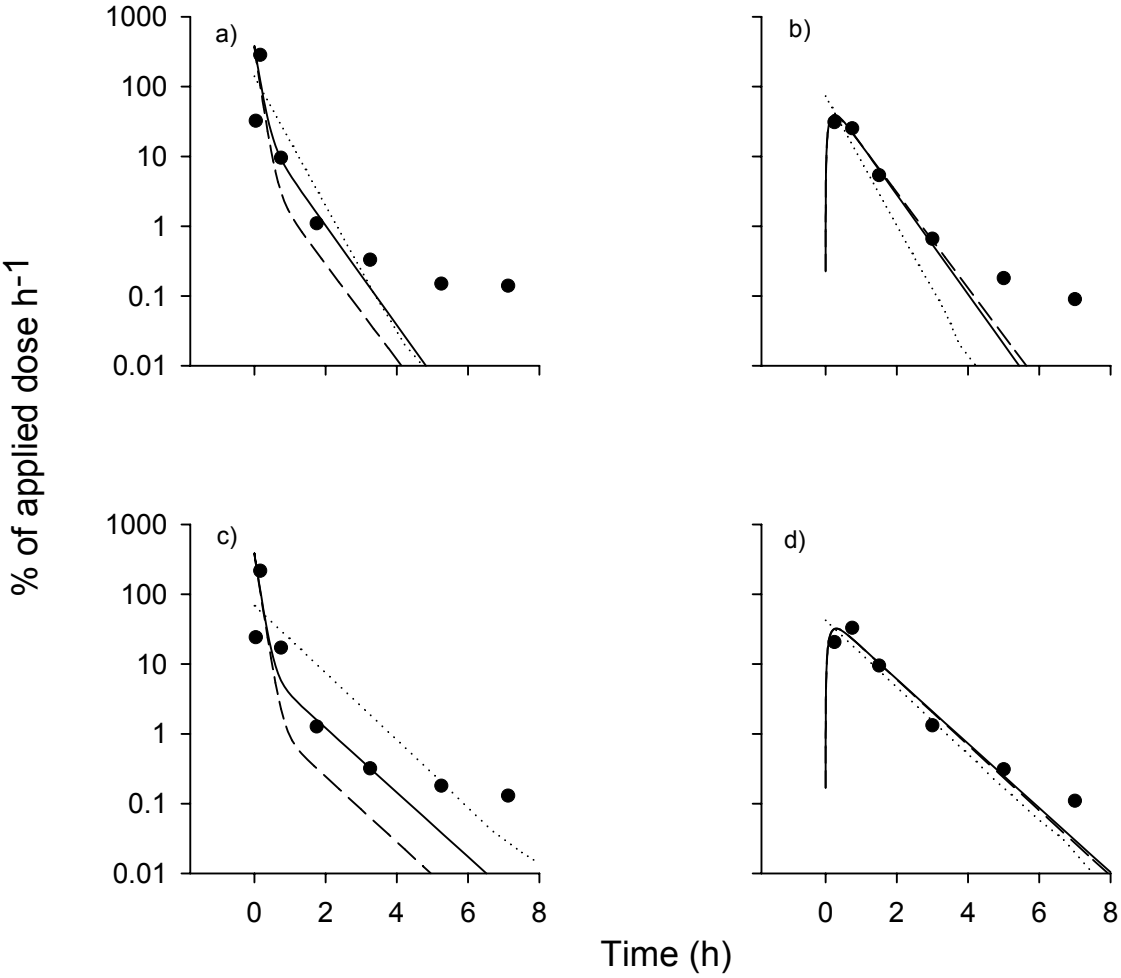

30 mL/min

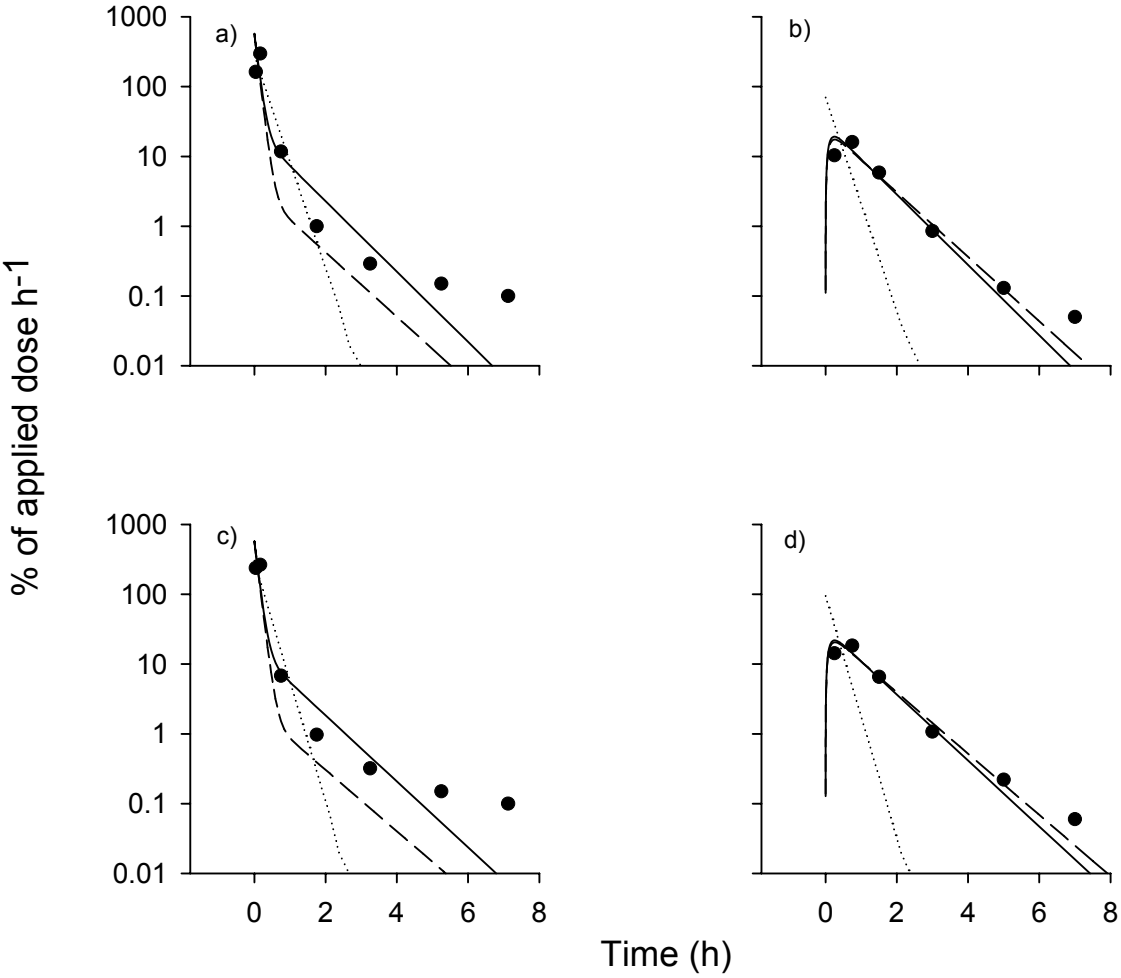

40 mL/min

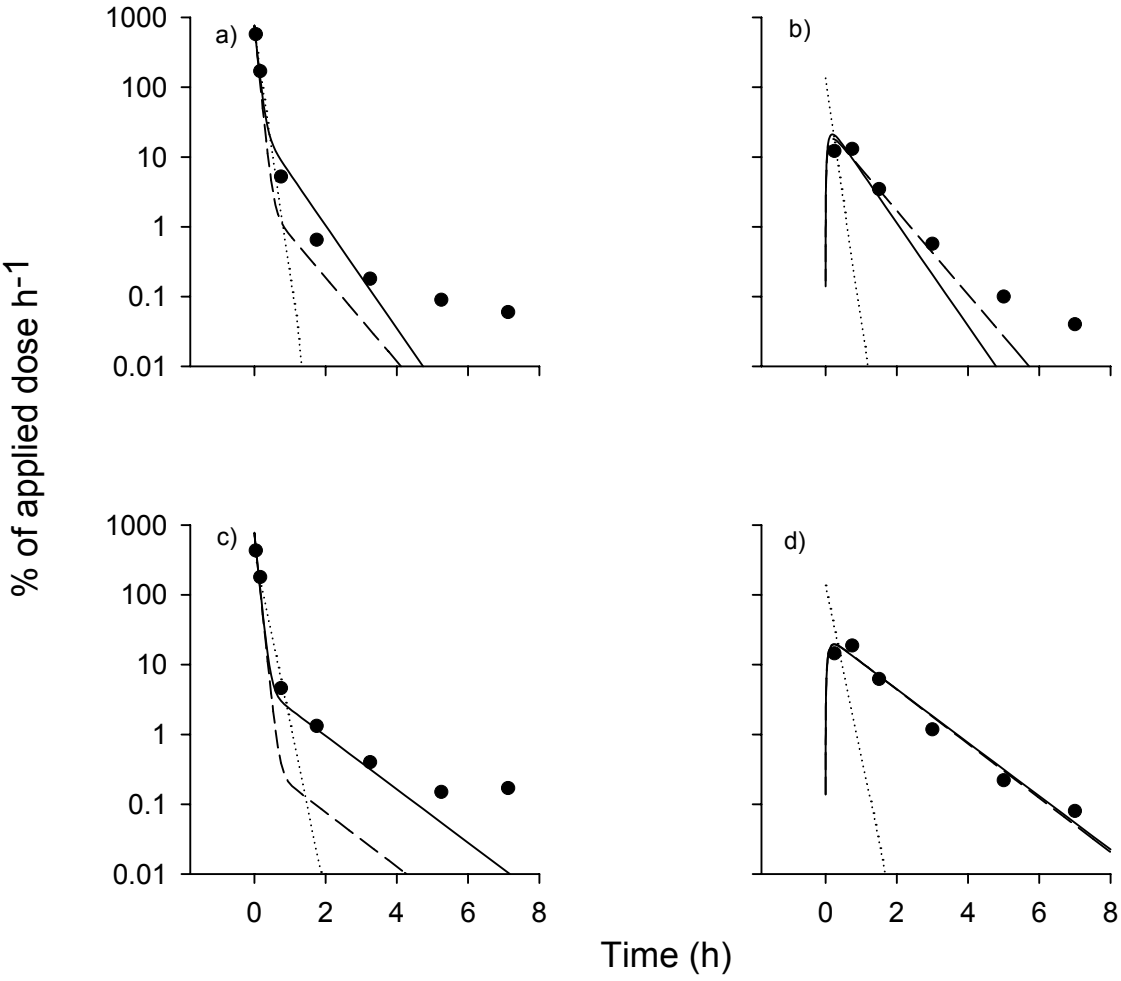

50 mL/min

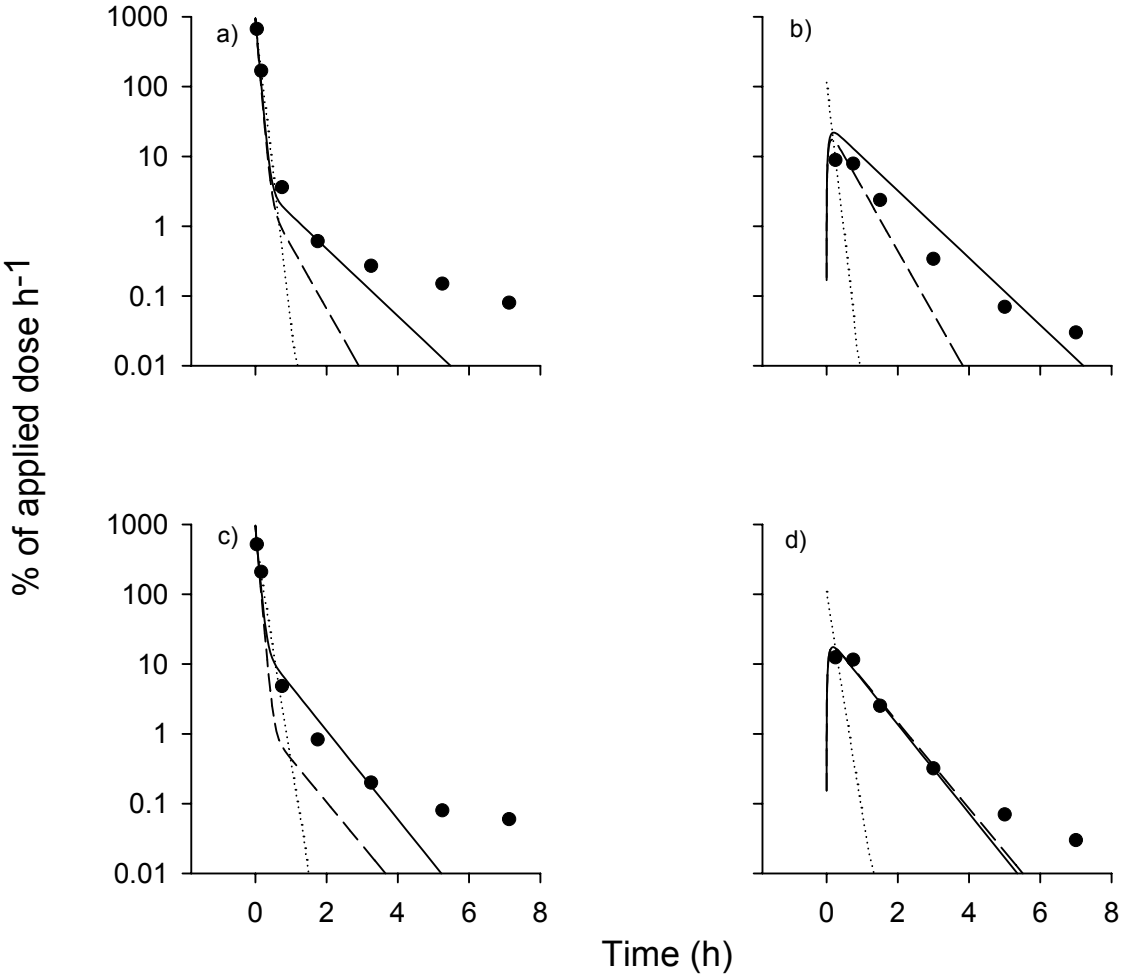

65 mL/min

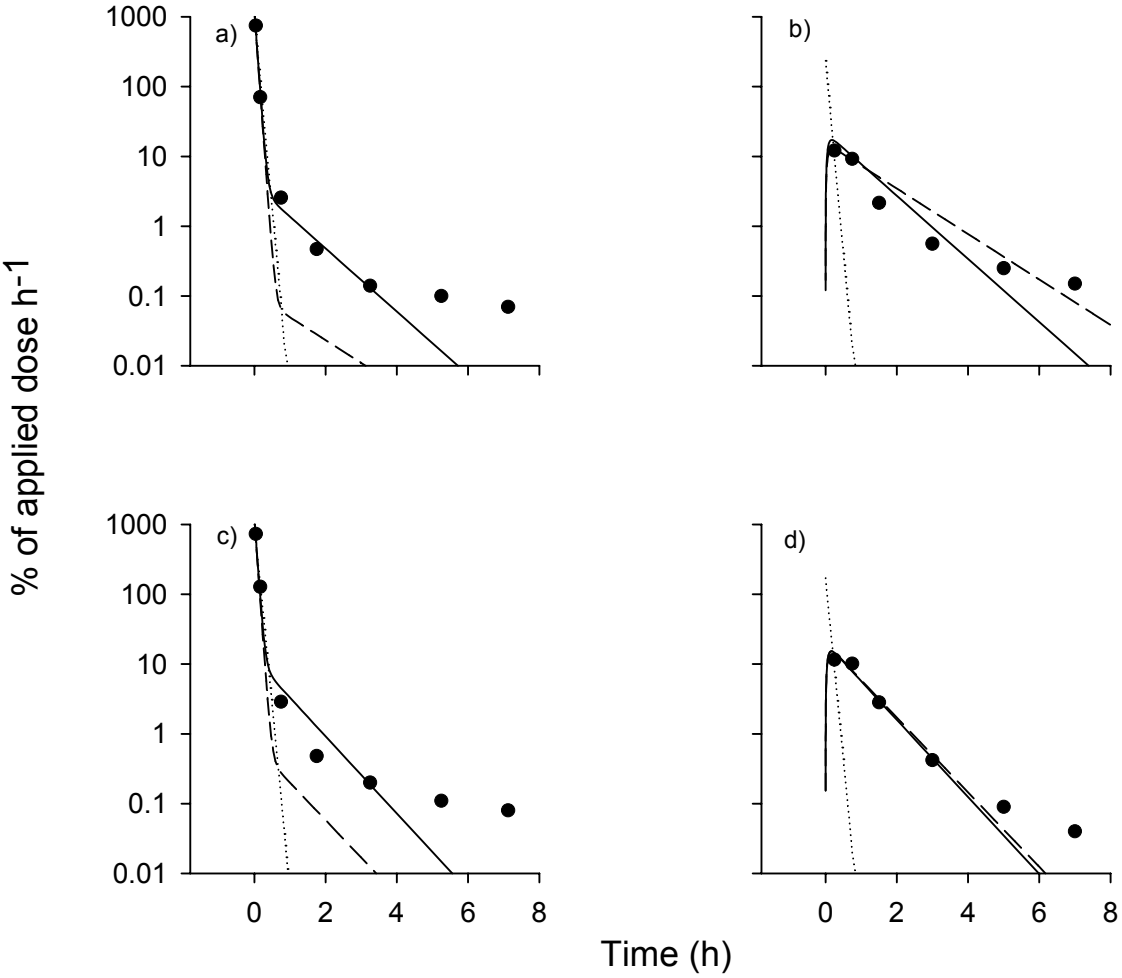

80 mL/min

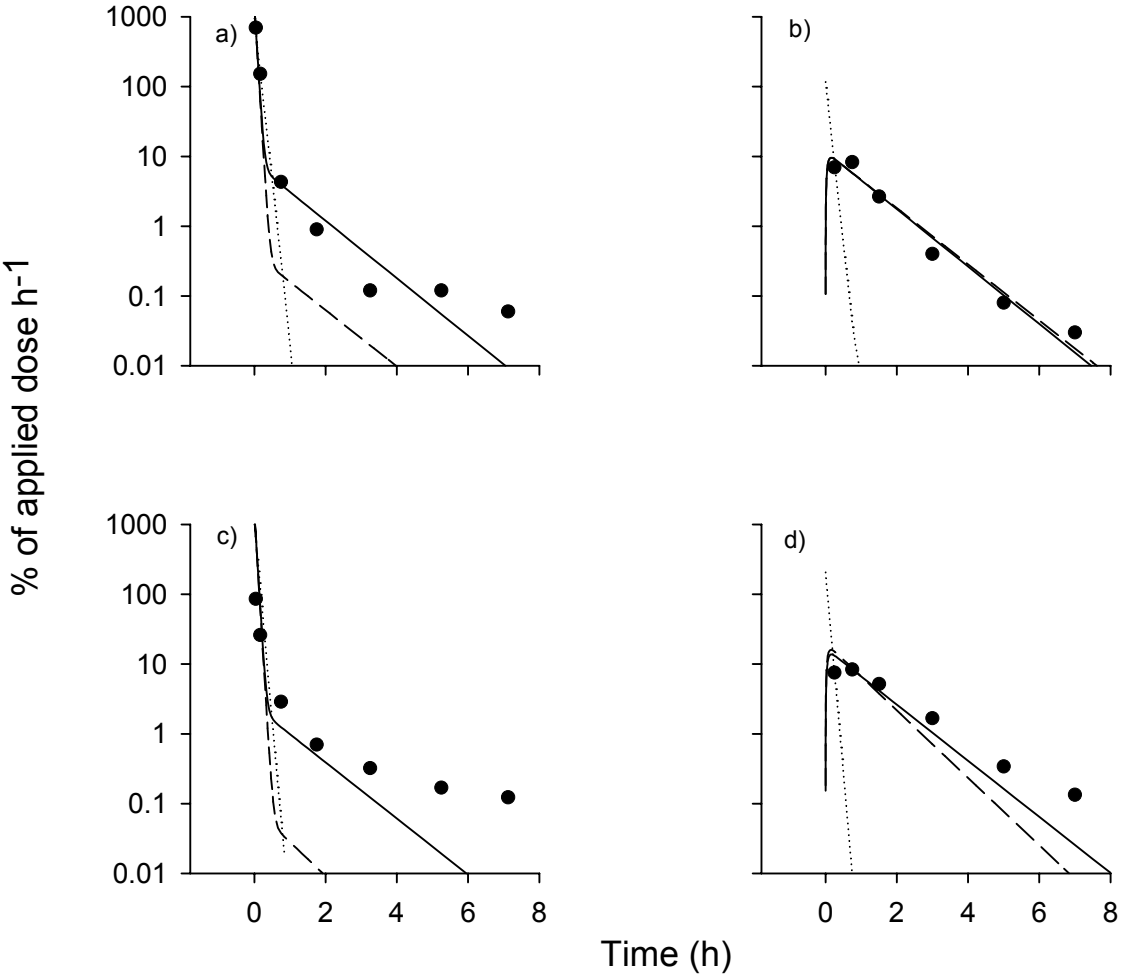

100 mL/min

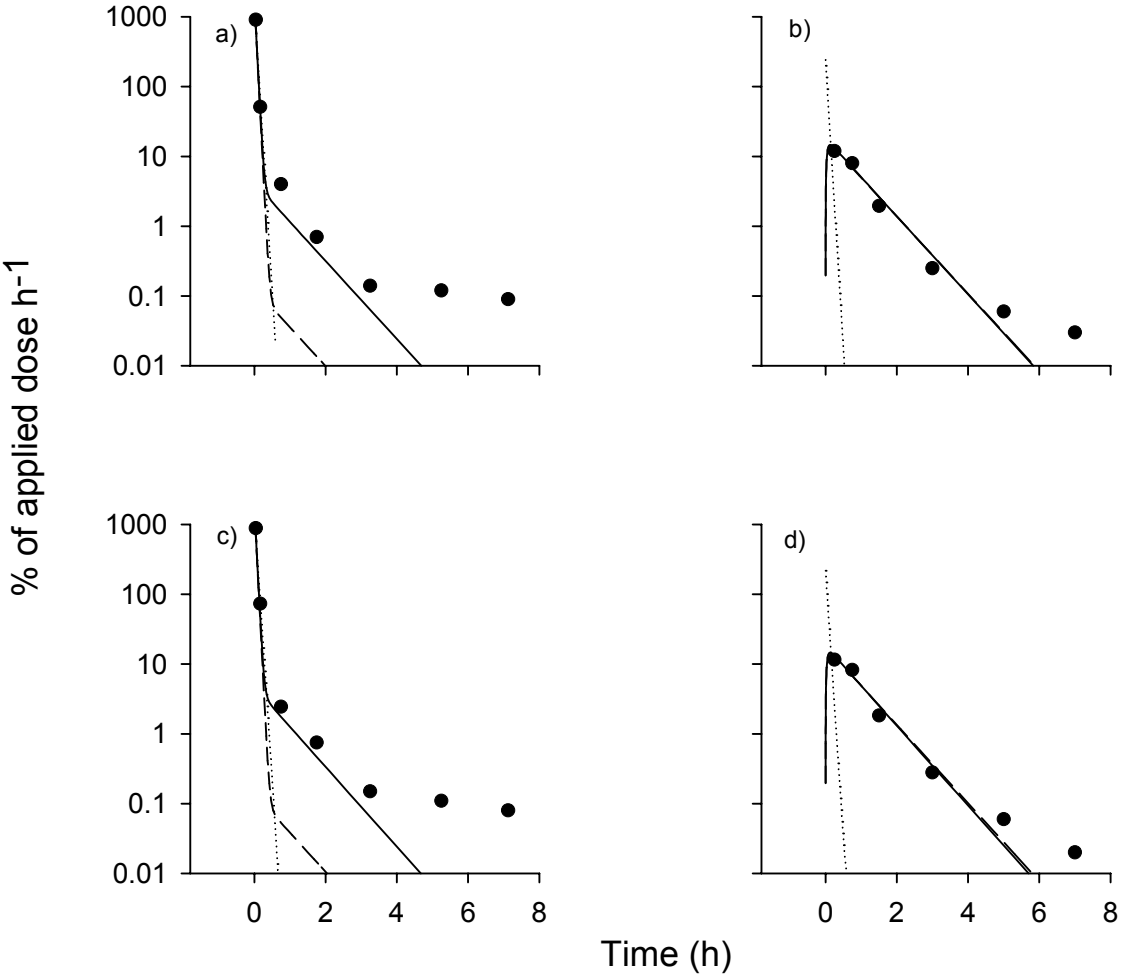

APPENDIX E

EVAPORATION OF BENZYL ALCOHOL FROM HUMAN *IN VIVO* STUDY AT DIFFERENT AIRFLOW VELOCITIES: a) Cumulative evaporated fraction and b) Evaporation rate (cf. CHAPTER 6)

20 mL/min

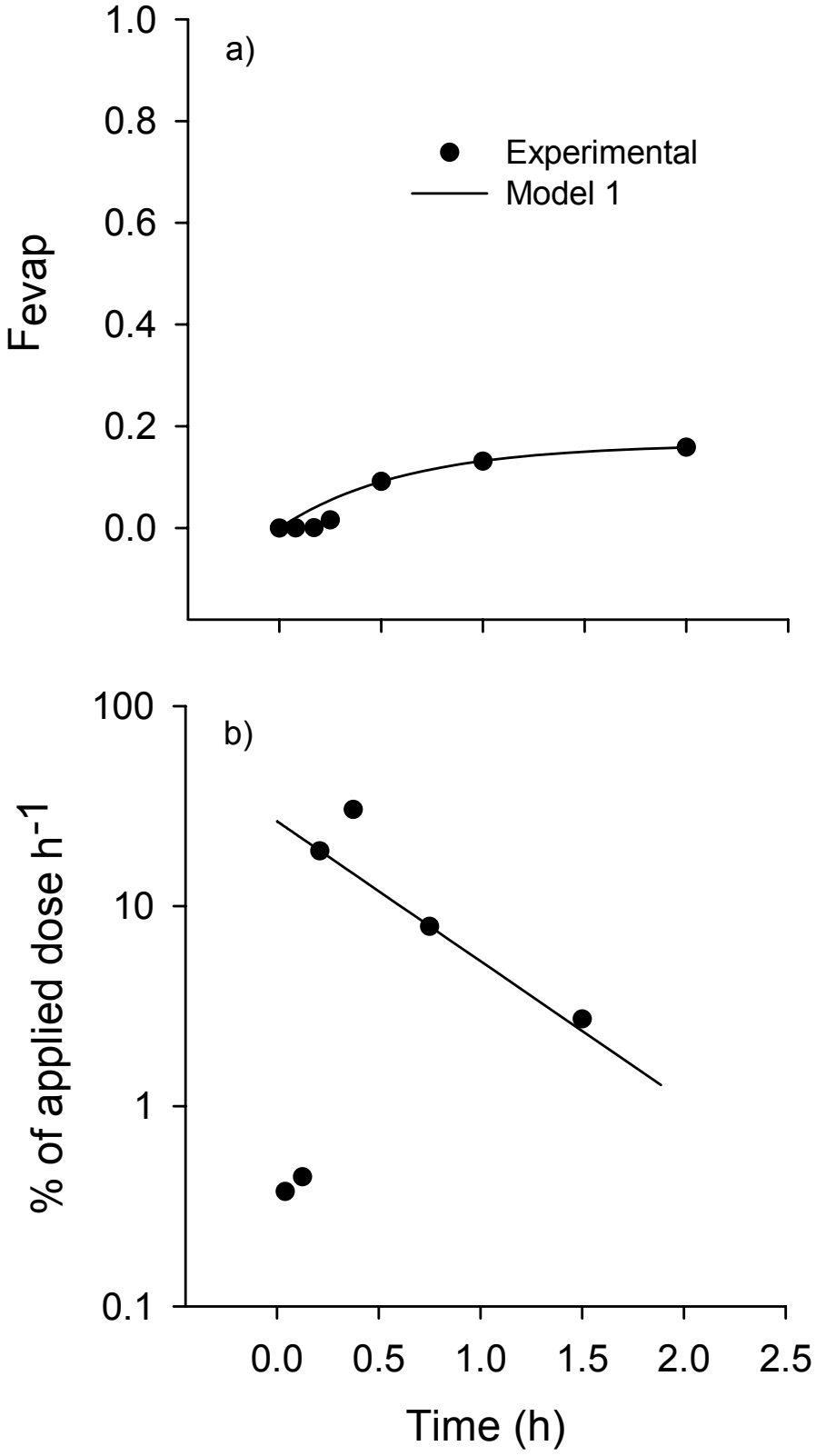
a)
Experimental
Model 1
Fevap
1.0
0.8
0.6
0.4
0.2
0.0
b)
% of applied dose h-1
100
10
1
0.1
0.0
0.5
1.0
1.5
2.0
2.5
Time (h)

40 mL/min

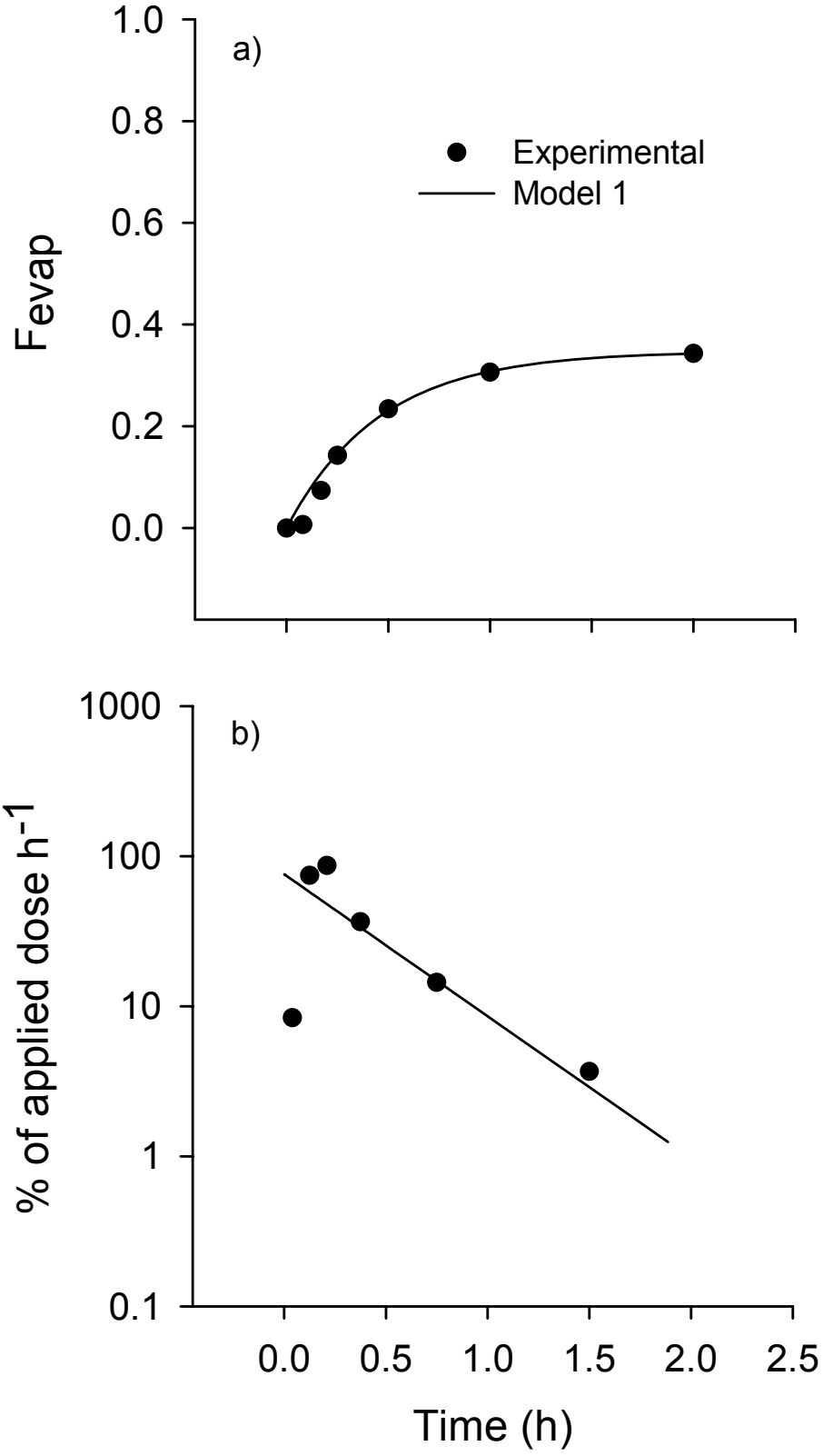
a)
Experimental
Model 1
Fevap
1.0
0.8
0.6
0.4
0.2
0.0
b)
% of applied dose h-1
1000
100
10
1
0.1
0.0
0.5
1.0
1.5
2.0
2.5
Time (h)

60 mL/min

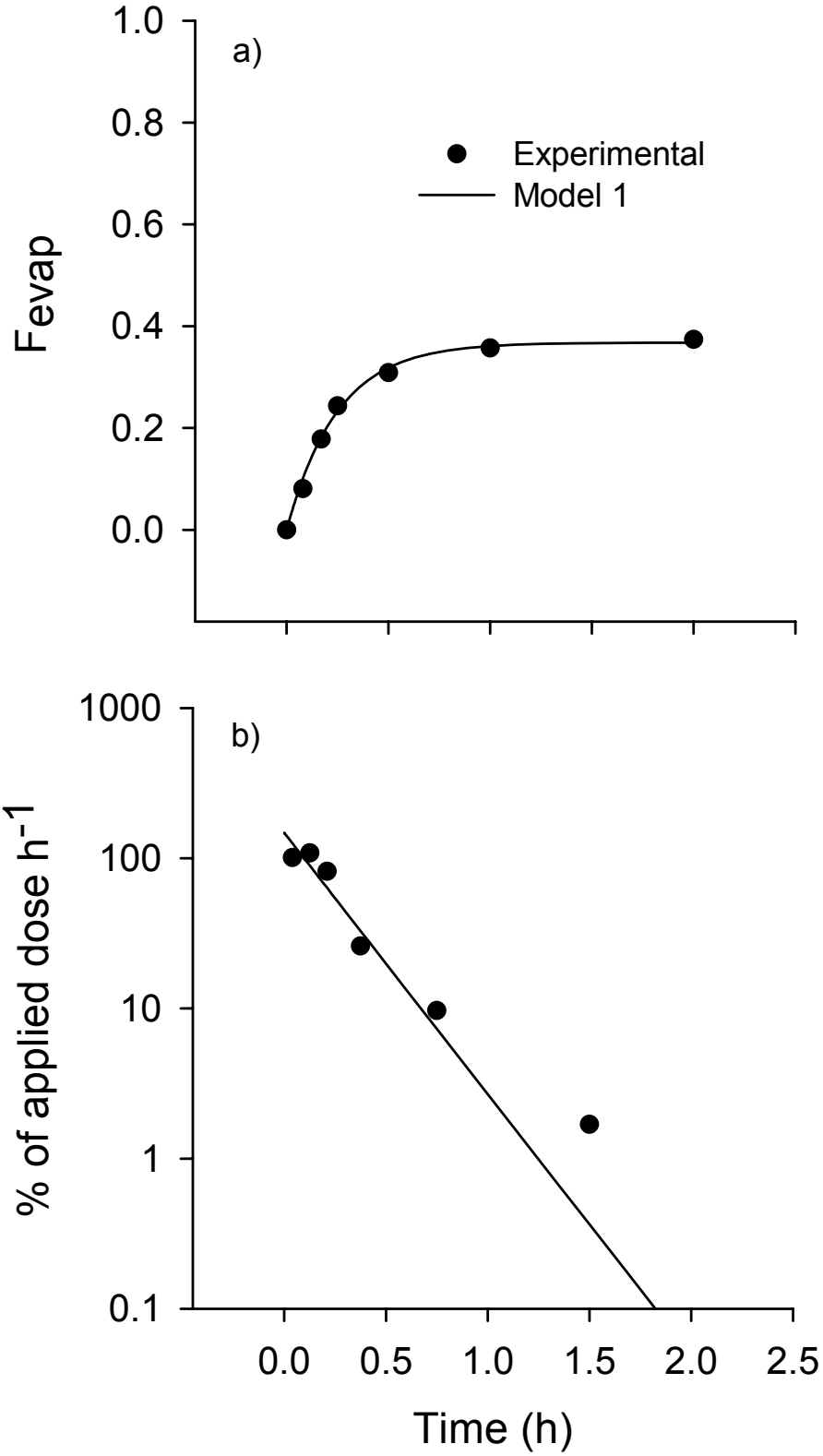
a)
Experimental
Model 1
Fevap
1.0
0.8
0.6
0.4
0.2
0.0
b)
% of applied dose h-1
1000
100
10
1
0.1
0.0
0.5
1.0
1.5
2.0
2.5
Time (h)

80 mL/min

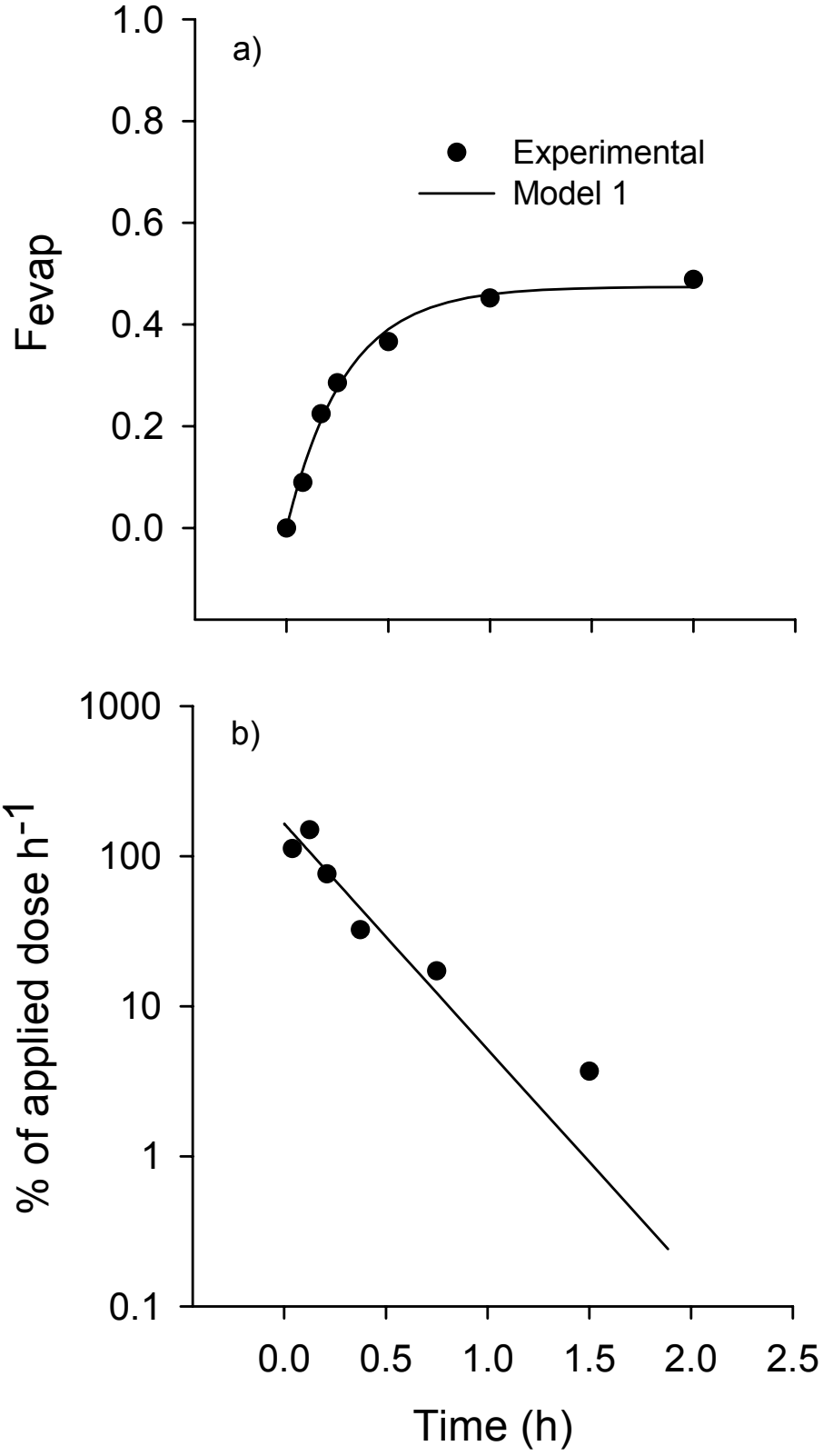
a)
Experimental
Model 1
Fevap
1.0
0.8
0.6
0.4
0.2
0.0
b)
% of applied dose h-1
1000
100
10
1
0.1
0.0
0.5
1.0
1.5
2.0
2.5
Time (h)

100 mL/min

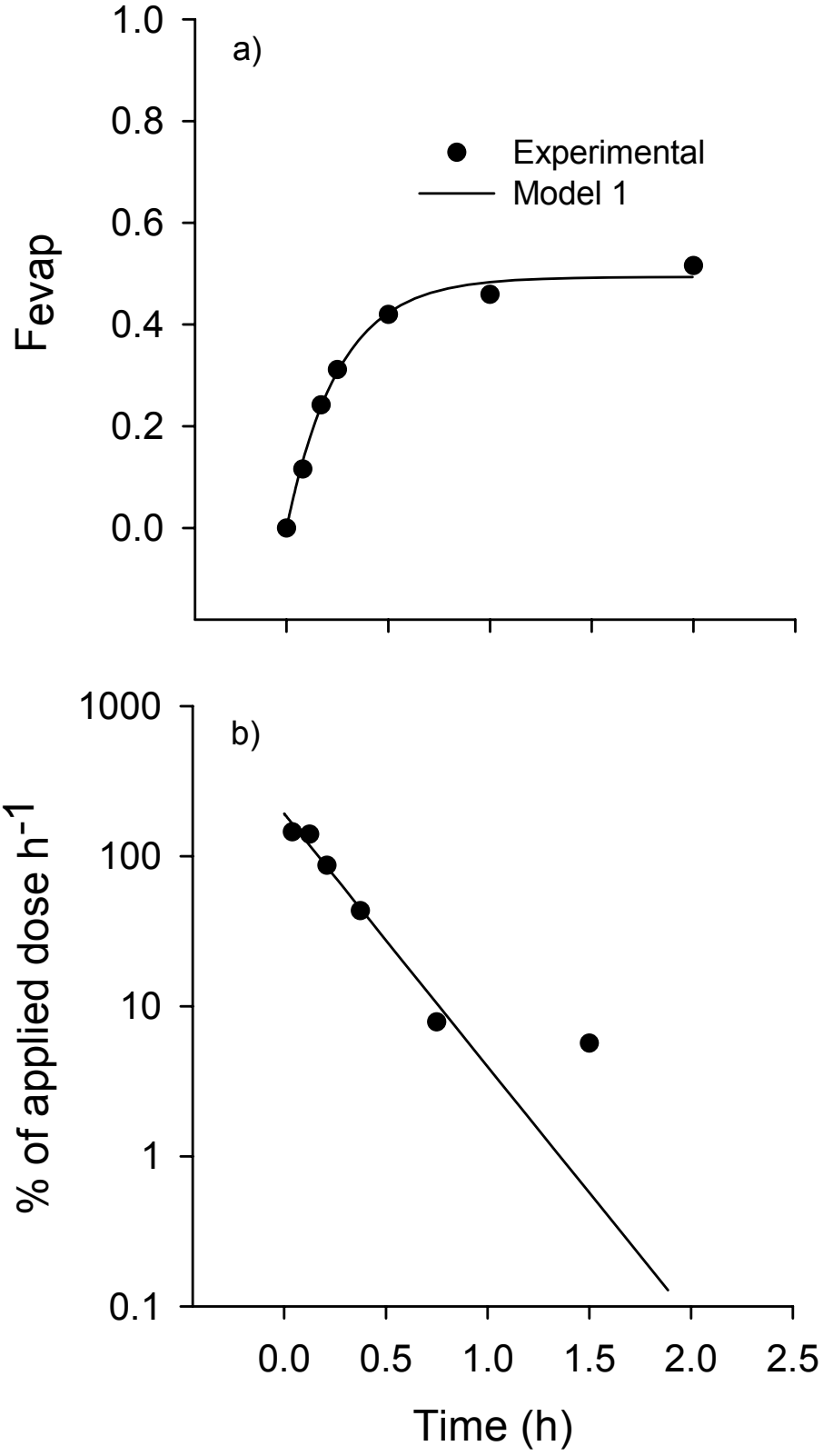
a)
Experimental
Model 1
Fevap
1.0
0.8
0.6
0.4
0.2
0.0
b)
% of applied dose h-1
1000
100
10
1
0.1
0.0
0.5
1.0
1.5
2.0
2.5
Time (h)

APPENDIX F

PHYSICAL PROPERTIES OF FRAGRANCE RAW MATERIALS STUDIED BY MOOKHERJEE ET AL. (cf. REF. 70, CHAPTER 7)

	Compound	MW (Da)	BP (deg C)	Type	Pvp (mm Hg)	MP (deg C)	Type	Log P	Type	Del S.F.	Soct (mg/ml)	Sw (mg/ml)
1	Aldehyde AA											
2	Allyl amyl glycolate	186	218	EST	0.22	-4.7	EST	2.72	EXP	13.5	812.8	1.5
3	Ambrox	236	277	EST	0.0069	74	EST	5.40	EST	13.5	421.1	0.0017
4	Bacdanol	208	298	EST	0.00015	60	EST	4.54	EXP	13.5	506.6	0.015
5	Benzyl acetate	150	213	EXP	0.28	-51	EXP	1.96	EXP	13.5	812.8	8.9
6	Benzyl acetone	148	234	EXP	0.099	-13	EXP	1.74	EST	13.5	812.8	15
7	Benzyl salicylate	226	320	EXP	3.7E-05	131	EXP	3.76	EXP	13.5	137.8	0.024
8	C10 aldehyde	156	208	EXP	0.35	-5.0	EXP	4.01	EST	28.5	812.8	0.079
9	Carveol	152	228	EXP	0.022	5.7	EST	2.27	EST	13.5	812.8	4.4
10	Caryophyllene	204	257	EST	0.048	25	EXP	6.45	EST	13.5	812.8	0.00029
11	Cashmeran	206	206	EST	0.0071	71	EST	4.62	EXP	13.5	418.4	0.010
12	Cedramber	236	265	EST	0.016	62	EST	6.16	EXP	13.5	513.9	0.00036
13	Cedrene	204	262	EXP	0.00012	48	EST	6.13	EST	13.5	617.8	0.00046
14	Cedrol	222	280	EST	0.00025	86	EXP	4.53	EST	13.5	329.3	0.010
15	Citral	152	227	EXP	0.14	-10	EXP	4.33	EST	13.5	812.8	0.038
16	Citronellol	156	224	EXP	0.028	-12	EST	3.25	EST	16.0	812.8	0.46
17	Citronellyl acetate	198	229	EXP	0.12	-7.4	EST	4.20	EST	21.0	812.8	0.051
18	Coumarin	146	302	EXP	0.0012	71	EXP	1.39	EXP	13.5	347.0	14
19	Cyclogalbaniff	198	255	EST	0.033	23	EST	2.86	EXP	13.5	812.8	1.1
20	Cyclopentadecanolide	240	280	EXP	0.0085	32	EXP	5.35	EST	13.5	793.1	0.0035
21	alpha-Damascone	192	259	EST	0.032	43	EST	3.62	EST	13.5	660.7	0.16
22	beta-Damascone	192	263	EST	0.022	52	EST	3.77	EST	13.5	563.4	0.10
23	Dihydromyrcenol	156	191	EST	0.19	-13	EST	2.99	EXP	16.0	812.8	0.83
24	Dimethyl octyl acetate	200	237	EST	0.083	1.9	EST	4.72	EST	23.5	812.8	0.015
25	Diphenyl ether	170	258	EXP	0.029	27	EXP	4.21	EXP	13.5	812.8	0.050
26	Ethyl acetoacetate	130	181	EXP	1.3	-45	EXP	0.24	EXP	18.5	812.8	468
27	Ethyl linalool	168	223	EST	0.029	-0.13	EST	3.08	EST	13.5	812.8	0.68
28	Ethyl myristate	256	295	EXP	0.0041	12	EXP	7.06	EST	43.5	812.8	7.1E-05
29	Ethyl vanillin	166	294	EXP	0.00056	78	EXP	1.58	EXP	13.5	326.6	8.6
30	Floralozone	190	274	EST	0.0088	46	EST	3.60	EXP	13.5	624.4	0.16
31	Galaxolide	258	325	EST	0.00017	103	EST	6.06	EST	13.5	265.4	0.00023
32	Geranyl acetate	196	245	EXP	0.055	-6.1	EST	3.72	EST	13.5	812.8	0.15
33	Givescone	210	259	EST	0.020	42	EST	4.34	EST	13.5	684.8	0.031

	Compound	MW (Da)	BP (deg C)	Type	Pvp (mm Hg)	MP (deg C)	Type	Log P	Type	Del S.F.	Soct (mg/ml)	Sw (mg/ml)
34	Hedione	226	309	EST	0.00077	74	EST	2.42	EST	13.5	415.8	1.6
35	Helional	192	295	EST	0.0033	39	EXP	1.37	EXP	13.5	705.9	30
36	cis-3-Hexenol	100	156	EXP	1.4	-38	EST	1.40	EST	13.5	812.8	32
37	cis-3-Hexyl methyl carbonate											
38	beta-Ionone	192	239	EXP	0.069	52	EST	4.00	EXP	13.5	563.4	0.056
39	Iso E Super	234	297	EST	0.0020	86	EST	5.23	EXP	13.5	341.1	0.0020
40	cis-Jasmone	164	258	EXP	0.036	40	EST	2.64	EST	13.5	674.8	1.5
41	Lilial	204	258	EXP	0.020	46	EST	3.86	EST	13.5	634.6	0.088
42	Limonene	136	178	EXP	2.0	-95	EXP	4.57	EXP	13.5	812.8	0.022
43	Linalool	154	197	EXP	0.13	25	EXP	2.97	EXP	13.5	812.8	0.87
44	Linalyl acetate	196	220	EXP	0.20	-2.1	EST	3.50	EST	13.5	812.8	0.26
45	Lolitol											
46	8-para-Menthane thiol	172	218	EST	0.22	-7.6	EST	4.72	EST	13.5	812.8	0.015
47	Methyl ionone	206	238	EXP	0.062	59	EST	4.23	EST	13.5	511.8	0.030
48	gamma-Methyl ionone	206	230	EXP	0.12	45	EST	4.02	EST	13.5	646.5	0.062
49	Methyl octin carbonate	168	220	EXP	0.16	38	EST	3.10	EST	16.0	693.8	0.55
50	Methyl phenyl acetate	150	216	EXP	0.23	-0.50	EST	1.83	EXP	13.5	812.8	12
51	Musk xylol	297	412	EST	1.4E-06	110	EXP	4.04	EST	13.5	254.5	0.023
52	Neryl acetate	196	231	EXP	0.11	-6.1	EST	3.72	EST	13.5	812.8	0.15
53	Oxyphenolon	164	280	EST	0.0013	72	EST	1.07	EST	13.5	359.3	31
54	Patchouli alcohol	222	280	EST	0.00048	56	EXP	4.53	EST	13.5	555.5	0.016
55	2-Pentadecanone	226	294	EXP	0.0063	40	EXP	6.14	EST	38.5	549.1	0.00040
56	Phenyl ethyl acetate	164	233	EXP	0.10	-31	EXP	2.26	EXP	13.5	812.8	4.5
57	Phenyl ethyl alcohol	122	218	EXP	0.04	-27	EXP	1.36	EXP	13.5	812.8	35.5
58	Polysantol	222	288	EST	0.00025	64	EST	4.61	EST	13.5	490.0	0.012
59	alpha-Santalol	220	302	EXP	6.9E-05	83	EST	3.91	EST	13.5	343.5	0.042
60	beta-Santalol	220	309	EXP	0.00014	25	EST	4.23	EST	13.5	812.8	0.048
61	Styrallyl acetate	164	214	EXP	0.26	-0.17	EST	2.27	EST	13.5	812.8	4.4
62	4-Terpineol	154	209	EXP	0.068	15	EST	2.75	EST	13.5	812.8	1.4
63	alpha-Terpineol acetate	196	220	EXP	0.20	21	EST	3.59	EXP	13.5	812.8	0.21
64	Tonalid	258	248	EXP	0.032	46	EXP	6.25	EST	13.5	667.7	0.00038
65	2-Tridecanone	198	263	EXP	0.034	31	EXP	5.08	EST	33.5	798.1	0.007
66	Undecavertol	170	240	EST	0.010	-2.9	EST	3.69	EST	16.0	812.8	0.17